ORNL/TM-2023/3094

Feasibility Studies and Downselection of New Materials and Manufacturing Technologies for Nuclear Applications

T. S. Byun
D. A. Collins
Y. Lin
K. O. Hanson
et al.

September 2023

M2CT-23OR1304062

OAK RIDGE National Laboratory

ORNL IS MANAGED BY UT-BATTELLE LLC FOR THE US DEPARTMENT OF ENERGY

ORNL/TM-2023/3094

Advanced Materials and Manufacturing Technologies Program

FEASIBILITY STUDIES AND DOWNSELECTION OF NEW MATERIALS AND MANUFACTURING TECHNOLOGIES FOR NUCLEAR APPLICATIONS

TS Byun*
David A. Collins*
Yan-Ru Lin*
Kevin O. Hanson*
Bryant A. Kanies**
Robin A. Montoya**
Michael J. Brand**
Erofili Kardoulaki**
Miles F. Beaux II**
A. David Andersson**
Mohan Sai Kiran Kumar Yadav Nartu***
Subhashish Meher***
Isabella van Rooyen***
Shalini Tripathi***
Nathan Canfield***

* Oak Ridge National Laboratory
** Los Alamos National Laboratory
***Pacific Northwest National Laboratory

September 2023

M2CT-23OR1304062

Prepared by
OAK RIDGE NATIONAL LABORATORY
Oak Ridge, TN 37831
managed by
UT-BATTELLE, LLC
for the
US DEPARTMENT OF ENERGY
under contract DE-AC05-00OR22725

CONTENTS

LIST OF FIGURES

LIST OF TABLES

ACKNOWLEDGEMENTS

This research was sponsored by the US Department of Energy Office of Nuclear Energy's Advanced Materials and Manufacturing Technologies Program under contract DE-AC05-00OR22725 with UT-Battelle, LLC. The authors thank Dr. Maxim Gussev and Dr. Sebastien Dryepondt for their thoughtful review of this report before publication.

ABBREVIATIONS

AD	as-deposited
ALD	atomic layer deposition
AM	additive manufacturing
AMMT	Advanced Materials and Manufacturing Technologies
ASME	American Society of Mechanical Engineers
ATF	accident-tolerant fuel
bcc	body-centered cubic
C/C	carbon fiber–reinforced carbon
CMC	ceramic matrix composite
CTE	coefficient of thermal expansion
CVD	chemical vapor deposition
CVI	chemical vapor infiltration
DED	directed energy deposition
dpa	displacements per atom
EBAM	electron beam additive manufacturing
EDS	energy dispersive spectroscopy
fcc	face-centered cubic
FIB	focused ion beam
GFR	gas-cooled fast reactor
HEA	high-entropy alloy
HT	heat treatment
HTGR	high-temperature gas reactor
HTR	high-temperature reactor
INL	Idaho National Laboratory
LANL	Los Alamos National Laboratory
LDRD	Laboratory Directed Research and Development
LENS	laser engineered net shaping
LFR	lead-cooled fast reactor
LPBF	laser powder bed fusion
LWR	light-water reactor
MBS	miniature fracture bend bar side-grooved
MI	melt infiltration
Mo/C-C	molybdenum-coated carbon fiber–reinforced carbon
Mo/SiC-SiC	molybdenum-coated SiC fiber–reinforced SiC
MSR	molten salt reactor
NFA	nanostructured ferritic alloy
NITE	nanopowder infiltration and transient eutectic
NRC	US Nuclear Regulatory Commission
ODS	oxide dispersion–strengthened
ORNL	Oak Ridge National Laboratory
PLC	Portevin–Le Chatlier
PNNL	Pacific Northwest National Laboratory
PVD	physical vapor deposition
RT	room temperature
SEBM	selective electron beam melting
SEM	scanning electron microscopy
SFR	sodium-cooled fast reactor
ShAPE	Shear Assisted Processing and Extrusion

SiC/SiC	SiC fiber–reinforced SiC
SLM	selective laser modeling
SS	stainless steel
STEM	scanning transmission electron microscopy
TE	total elongation
TEM	transmission electron microscopy
TMP	thermomechanical processing
TMT	thermomechanical treatment
TPB	three-point bend
TRIP	transformation-induced plasticity
TRISO	tristructural-isotropic
TRL	technology readiness level
TWIP	twinning-induced plasticity
UE	uniform elongation
UTS	ultimate tensile strength
VHTR	very high-temperature reactor
VLM	vacuum levitation melting
W/C-C	tungsten-coated carbon fiber–reinforced carbon
W/SiC–SiC	tungsten-coated SiC fiber–reinforced SiC
WAAM	wire arc additive manufacturing
YS	yield strength
Zr/C–C	zirconium-coated carbon fiber–reinforced carbon
Zr/SiC-SiC	zirconium-coated SiC fiber–reinforced SiC

EXECUTIVE SUMMARY

This report is intended to present the results of multilaboratory collaborative studies on the feasibility and downselection of the structural materials that are newly considered for applications to future nuclear energy technologies. The Advanced Materials and Manufacturing Techniques (AMMT) Program has been implemented to develop crosscutting technologies in support of a broad range of nuclear reactor technologies and to maintain US leadership in materials and manufacturing technologies for nuclear energy applications. In line with these program objectives, this collaborative study aims to explore new materials using advanced manufacturing technologies.

The FY 2023 research scope consists of the feasibility studies on new materials and relevant advanced manufacturing technologies, a collection of materials properties data and knowledge through experiments and literature survey, and the development and application of decision criteria matrix for downselecting candidate materials and manufacturing technologies. The three-laboratory effort for FY 2023 has focused on the three new material groups, including oxide dispersion–strengthened (ODS) materials, refractory composites and alloys, and high-entropy alloys (HEAs), which were investigated by Oak Ridge National Laboratory (ORNL) (work package: CT-23OR130406), Los Alamos National Laboratory (LANL) (CT-23LA130403), and Pacific Northwest National Laboratory (PNNL) (CT-23PN130408), respectively. The execution of this multilab research aimed to provide the AMMT Program with a merit-based feasibility study identifying an accelerated development path for these materials. A collaborative approach for achieving this goal was to develop a common materials evaluation criteria matrix and apply to all new candidate materials for the evaluation and prioritization of new materials using advanced manufacturing processes. The created decision criteria matrix is a matrix of criteria that a prospective material is scored against. The evaluation criteria are divided into four categories: application space, environmental compatibility, physical and mechanical properties, and manufacturability. Materials are given a score from 1 to 5 for each criterion, with the highest score (5) essentially meaning that a material has the most near-term potential for application. Application of the decision criteria matrix will provide guidance to future research on new materials.

ORNL has performed a merit-based feasibility study to identify an accelerated development path for ODS alloys by creatively combining additive manufacturing (AM) technologies with the recent advances in ODS materials and traditional manufacturing technologies. The primary tasks were to develop a combined processing route of AM and postbuild treatment for ODS ferritic (Fe–Cr alloy or 14YWT alloy) and austenitic (Fe–Cr–Ni alloys or stainless steel 316L and 316H) alloys and to perform basic characterization to provide feedback for the materials development and downselection. Key mechanical test results, including tensile strength, tensile ductility, and fracture toughness data, are reported and are used as inputs in the downselection process. Higher strength was measured from the ferritic ODS alloys, whereas higher ductility and fracture toughness were measured from the austenitic ODS alloys. Many of the decision criteria were scored the same for the additively manufactured ferritic and austenitic ODS alloys; however, the austenitic alloys generally have higher corrosion resistance and significantly better ductility. Although these scores are not significantly different enough to make them highly discernable, the austenitic ODS alloys were downselected to be the primary materials group in the future research on ODS materials in the AMMT Program.

LANL has identified and evaluated several composite materials and refractory alloys with high thermal and radiation resistances that should be pursued through the AMMT Program. Composite considerations were limited to a carbon fiber–reinforced carbon (C/C) or SiC fiber-reinforced SiC (SiC/SiC) composite backbone in conjunction with a metallic (Mo, Zr, or W) liner. Ultimately, tungsten-coated SiC/SiC (W/SiC-SiC) has the highest score (95/135) of all coated composites. The scoring for each coated composite was extremely close, with the scores varying by only three points. The W/SiC-SiC will

maintain its structural integrity at elevated temperatures, is thought to have satisfactory neutronics properties and sufficient compatibility liquid metal coolants (Pb, Li) and coolants used in molten salt reactors and gas-cooled fast reactors. It is seen as a candidate material for in-core and out-of-core structural components. Refractory materials considered included WTa, WNiFe, and C-103. The C-103 scored the highest on the decision criteria matrix with a score 105/135 and has been used in other industries, such as the aerospace industry. It is anticipated to have superior creep performance, fatigue, fracture toughness, and neutronics compatibility compared with those of WTa and WNiFe. Based on the results of the evaluation using the decision criteria matrix, it is recommended that W/SiC-SiC be pursued for further development under the AMMT Program. Because of their similar scoring, should time and resources allow, continued pursuit of all refractory-coated composites would also be beneficial. It is also recommended that the AMMT Program pursue the development of AM C-103 for advanced nuclear reactor use.

PNNL focused on understanding the nuclear energy–relevant HEAs through a detailed literature survey, selected experimental work, and development of a decision matrix with criteria for the identification of HEAs that may have the most effect and value for further examination. HEAs have the potential to serve in extreme environments of next generation nuclear reactors for temperatures up to 1,000°C for nearly 100,000 hours due to their unique phase transformation pathways and nanoscale and mesoscale microstructures. The HEA classification used in this review and the elaborate literature survey presented in this report provide insights into the processing, microstructure, and properties of the several HEAs reported, targeting different applications. Based on the literature survey, six HEAs were identified as promising for the nuclear industry, focusing on the high-temperature properties with cobalt as an alloying element in two of these alloys [$(Ni_2Co_2FeCr)_{92}Al_4Nb_4$; $Al_{0.3}Ti_{0.2}Co_{0.7}CrFeNi_{1.7}$]. GRX-810, developed by NASA, shows creep performance two to three orders of magnitude better than the current high-temperature alloys and is best classified as a medium-entropy alloy or an ODS alloy because of the presence of Y_2O_3 particles. Therefore, this report recommends pursuing this material as part of a different AMMT work package. Although the decision matrix is not fully developed yet for the six candidate HEAs, the literature survey provides the technical justification to downselect two HEAs ($Al_{0.3}Ti_{0.2}Co_{0.7}CrFeNi_{1.7}$ and $Al_{10}Cr_{12}Fe_{35}Mn_{23}Ni_{20}$) for detailed experimental work under this work package. This work package also investigated an advanced processing route for fabricating functionally graded HEAs using directed energy deposition and off-the-shelf metal alloy powders. This advanced processing methodology for functionally graded HEAs would open avenues for rapidly assessing new HEA compositions at significantly cheaper costs. Based on the literature review, the preliminary experiments performed, and engineering rationale, a preliminary rating was performed on the two downselected alloys. HEA $Al_{10}Cr_{12}Fe_{35}Mn_{23}Ni_{20}$ performed marginally better than HEA $Al_{0.3}Ti_{0.2}Co_{0.7}CrFeNi_{1.7}$ with a rating of 62.5 vs. 56.5. Most of the HEA research reviewed, used arc (73%) and vacuum melting (15%) processes as a fabrication method, with only 11% of the papers reviewed used laser based additive manufactured processes. Solid state manufacturing processes were only reported in less than 5% of the instances. The literature survey shown therefore the opportunity to explore solid phase processes as a manufacturing technique due to the grain refinement and decreased segregation properties during processes.

1. INTRODUCTION

1.1 BACKGROUND AND OBJECTIVE

The structural materials used in advanced nuclear reactors designed for high thermal and economic efficiencies will be subject to high-temperature, high-dose neutron irradiations. Materials challenges are keeping the next generation of nuclear power (generation IV, small modular reactors, advanced light-water reactors [LWRs], and microreactors) from being widely embraced, constructed, and operated. Several of these advanced reactors, such as the sodium-cooled fast reactor (SFR) and molten salt reactor (MSR), will operate at high temperatures (>500°C) and irradiation doses as high as 200 displacements per atom (dpa) to achieve higher thermal and economic efficiencies [1, 2]. Many of these reactors will also use more corrosive and reactive coolants compared with water. Furthermore, new emphasis has been placed on developing passive safety systems and accident-tolerant fuels (ATFs) in response to the Fukushima-Daiichi accident [2]. These operational environments require materials to be reliable and withstand harsh environments, including accident scenarios such as loss of coolant accidents. Exposing a material to such extreme conditions will significantly modify the material's microstructure and local chemistry and thus degrade its mechanical, chemical, and physical properties [3]. Therefore, the reactor core components for any high-performance reactor will require excellent high-temperature mechanical properties, high radiation resistance, and high corrosion/oxidation resistance in addition to a feasible manufacturing process. Design and selection of key structural materials for such high-performance reactors or extreme conditions will require considerable research on feasible manufacturing routes and significantly enhanced materials property databases.

The AMMT Program aims to develop crosscutting technologies in support of a broad range of nuclear reactor technologies and to maintain US leadership in materials and manufacturing technologies for nuclear energy applications. The overarching vision of the AMMT Program is to accelerate the development, qualification, demonstration, and deployment of advanced materials and manufacturing technologies to enable reliable and economical nuclear energy. Through advanced manufacturing techniques, new materials can be created for many applications in nuclear reactors. These materials can further the development of advanced reactors where properties such as improved high-temperature strength, improved corrosion resistance, or improved radiation tolerance are needed. A successful development of such a new structural material with an extreme damage tolerance can provide a safety improvement through larger safety margins, economic benefit for higher efficiency during operation, and a cost reduction through more cost-effective manufacturing processes and less waste.

To achieve the common goal, this multilaboratory collaborative research pursued accelerated approaches to develop and understand potential candidate alloys and to downselect materials and feasible processing routes [4, 5, 6]. The accelerated approach also harnesses existing knowledge for the candidate materials and feasible manufacturing technologies in the decision-making process by incorporating a selection criteria matrix. For FY 2023, the multilaboratory efforts have focused on the advanced manufacturing techniques applied to three new material groups: oxide dispersion–strengthened (ODS) materials [4], refractory composites and alloys [5], and high-entropy alloys (HEAs) [6].

1.2 ADDITIVE MANUFACTURING OXIDE DISPERSION–STRENGTHENED ALLOYS

To achieve the required reactor materials performance—in particular, high thermal and radiation resistances—the candidate metallic alloys are typically processed to have the fine-grained microstructures that can be stabilized using various strong and thermally stable nanoparticles, such as oxides, carbides, and nitrides [3, 7, 8, 9, 10, 11, 12]. In the past two decades, highly stable nanoparticles such as fine oxides or oxygen-enriched nanoclusters have become the most important constituent in the future fission and fusion reactor materials. For example, the 14YWT nanostructured ferritic alloy (NFA) is an advanced

ODS ferritic alloy that can deliver excellent high-temperature strength and creep properties, as well as high radiation tolerance because of its unique microstructure of ultrasmall grains and high concentration (~[5–10] × 10^{23} m^{-3}) of nanoscale (~2–5 nm) Ti–Y–O-rich nanoclusters [13, 14]. The nanoclusters show remarkable high-temperature stability—up to approximately 1,400°C for short times and 825°C for around 7 years in creep testing [15, 16]. The large interfacial area associated with these microstructural features provides the high point defect sink strength that is beneficial to radiation tolerance. Results of recent ion irradiation studies show that the 14YWT alloy has the lowest void swelling for doses up to 500 dpa in the temperature range of 400°C–500°C compared with various steels and other ODS alloys [17]. Several helium-ion irradiation studies have also demonstrated that these microstructures trap helium atoms and form high-density nanoscale bubbles rather than coarse bubbles at grain boundaries.

Despite all the advances established for the 14YWT NFA and its variants, so far, the only viable processing path for producing the advanced ODS alloys is high-energy mechanical alloying, which involves days or a week of high-energy ball milling a gas-atomized alloy powder with a small quantity (~0.3 wt %) of yttria (Y_2O_3) powder followed by an extrusion path to produce solid products. The Ti–Y–O-rich nanoparticles precipitate during this consolidation process. However, using this processing route might have a prohibitively high cost for mass production of any component, and the long process route is not practical for commercial applications. Without a breakthrough innovation to resolve this issue, the enormous merits of the distribution of highly stable nanoparticles in metallic materials will be missing in the future of advanced reactor technologies. Lately, the additive manufacturing (AM) method based on laser melting was proposed as an alternative manufacturing route for the ODS alloys. This AM method is feasible for producing ODS alloys because the local cooling rate after the laser melting is so high that some oxygen content can be retained in a solid solution state and later can be precipitated into oxide particles in a controlled thermomechanical condition.

AM technologies can provide many opportunities and challenges if they are used to build a nuclear reactor structure. These technologies offer enormous flexibility in designing and building complex components that can be cost-prohibitive with traditional manufacturing methods. Indeed, recent research efforts confirmed that the austenitic steels are highly suitable for AM of complex-shaped reactor components [18, 19, 20]. This suitability likely comes from the fast cooling that occurs during the AM process, preventing the formation of the high-temperature ferrite (i.e., δ-ferrite) phase in austenitic steels during cooling. Phase decomposition and segregation occurring in this metastable phase cause degradation at high temperatures. Examples of key AM technologies that might be relevant to manufacturing nuclear reactor structures include the laser powder bed fusion (LPBF) and laser directed energy deposition (DED) methods. In principle, the microstructures—and, thus, the mechanical properties—of additively manufactured alloys can be tailored by changing the processing parameters, such as scan speed, laser power, powder feedstock purity, and powder layer thickness [21, 22, 23]. In particular, the size and orientation of the fine-grained dislocation cell structure in metallic materials can be controlled by changing processing parameters [24, 25, 26] or applying postbuild heat treatments [22].

Although an optimized LPBF process can produce a very fine and desirable metastable microstructure owing to the fast cooling and solidification, many unknowns and adverse effects remain regarding the microstructural and chemical stability of additively manufactured materials in high-temperature, corrosion, and irradiation environments. The as-printed materials usually display increased room temperature (RT) yield strength (YS) but less work hardening because of the characteristic microstructure of fine grains and dislocation cells formed during the localized rapid solidification [24, 27, 28, 29]. Recent test results indicate that these fine-grained structures with mobile dislocations can shorten the high-temperature creep life [18, 19, 25]. Furthermore, the fracture toughness of additively manufactured materials could be reduced by the increased porosity from the build process, structural anisotropy relative to the build direction, and inclusions from impurities in the feedstock powder [20, 30]. Neutron or ion irradiation could also significantly affect the behaviors (i.e., shortened creep life and reduced fracture

toughness) observed in additively manufactured alloys [20, 31, 32, 33]. Some of these property degradation mechanisms can be more pronounced in ferritic alloys and ferritic–martensitic steels [34, 35]. The ferritic alloys usually have relatively lower initial ductility compared with the austenitic alloys, and thus, the reduction of ductility owing to any causes mentioned previously can significantly embrittle the alloy. Furthermore, the complex but often incomplete phase transformations that occur during the repeated reheating of deposited layers can make the microstructural evolution of the ferritic or ferritic–martensitic steels significantly more complex compared with other single-phase alloy systems such as the nickel-based alloys [34, 35].

Because the combination of some embrittling features from AM processing—such as the high porosity, incomplete transformation (residual δ-ferrite), and metastable state with high residual stress—can result in significantly degraded properties, the manufacturing process for reactor components may require a postbuild process to obtain a high-performance alloy. This postbuild process may include a controlled thermomechanical treatment (TMT). Therefore, the AM-based production of a component will require a processing route that combines multiple materials processing methods. This research project focuses on understanding potential candidate ODS alloys, as well as downselecting specific alloys and processing routes that would provide significant benefit when fabricated using advanced manufacturing technologies.

1.3 COMPOSITES AND REFRACTORY ALLOYS

Composite materials are made by combining two or more distinct phases of constituent materials to form one material. Composites may be made through many processes; some example fabrication methods include layering, mixing, chemical vapor infiltration (CVI), and melt infiltration (MI). The advantage of composites is the beneficial combination of properties from the constituent materials. Composite materials can be tailored to have improved properties compared with those of the individual constituent materials. For example, a ceramic coating layer may be applied to a metal substrate (or vice versa), forming a layered composite. Ceramics maintain their properties at elevated temperatures and are often chemically inert and corrosion-resistant, but monolithic ceramics can be brittle and flaw- sensitive [36, 37, 38]. Metals are used as structural materials but can often be susceptible to corrosion and irradiation and lose their structural stability at high temperatures. By combining a refractory metal layer with a ceramic matrix composite substrate, a composite material can be obtained with characteristics such as higher toughness, improved corrosion resistance and chemical compatibility, and the ability to retain its structural properties at high temperatures [39]. Therefore, composites are anticipated to greatly benefit the nuclear industry as generation IV, modular, space, and microreactor concepts are developed and implemented.

The proposed composite matrix materials—carbon (graphite) and SiC—have been investigated and used broadly by the nuclear industry for some time. Carbon in the form of graphite was used in the first nuclear reactor: the Chicago Pile 1 [40]. The compound SiC was first used to form tristructural-isotropic (TRISO) fuels in the 1960s, and since the 1970s, its performance after irradiation has been the subject of many studies [41]. More recently, fiber-reinforced composites of these materials (carbon fiber–reinforced carbon [C/C] and SiC fiber–reinforced SiC [SiC/SiC]) have gained traction because they increase the overall strength and toughness of the ceramic matrix material and maintain these properties at elevated temperatures (>1,000°C). Since the 1990s, SiC/SiC has been seen as a candidate for fusion applications [41]. Furthermore, composites could be revolutionary when applied as claddings or casings for heat pipes, fuel, and even structural core components because of their combination of beneficial properties. In practice, historical efforts of manufacturing composites have suffered from the difficulty of coating tubes of practical length while maintaining high performance.

Composites enable the separation of material functionalities (i.e., a strength-bearing material in conjunction with a hermetic and chemical compatibility layer). A carbon or SiC composite backbone in

conjunction with a metallic (e.g., Mo, Zr, or W) coating can be produced by depositing the refractory metal coating using advanced manufacturing techniques. Refractory metal coatings deposited on a carbon or SiC backbone will increase the compatibility of these backbone materials with liquid metals. Refractory metals are attractive because they have high temperature stability, high wear resistance, good compatibility with liquid metal coolants (such as those expected to be used in advanced nuclear reactors), and good thermal conductivity—even at elevated temperatures. The difficulty in conventional manufacturing and shaping of these types of alloys can be overcome by developing AM techniques.

1.4 HIGH-ENTROPY ALLOYS AND ADVANCED MANUFACTURING TECHNOLOGIES

Structural materials need to sustain against creep and void swelling and exhibit reasonably high mechanical strength and fracture toughness under irradiation at high temperatures (>300°C). Three main strategies are commonly used for improving the radiation tolerance in materials: (a) designing radiation-resistant matrix phases, (b) immobilizing the vacancies and interstitials, and (c) enhancing the sink strength of the material [42]. Among the new materials, HEAs are shown to address all three design strategies [43] and thus form an integral part of the advanced materials development portfolio and provide a reason for further exploration under the current work package.

HEAs with significantly higher configurational entropy than conventional alloys exhibit unusual lattice distortion and sluggish diffusion, which could potentially immobilize the radiation-induced defects and result in undesired swelling and segregation. This consequence is detrimental to mechanical and functional properties [44, 45, 46, 47, 48, 49, 50, 51, 52]. The high levels of transmutation in conventional alloys may already produce compositionally complex alloys locally resembling HEAs [43, 52].

Although the first two strategies mentioned previously, (a) and (b), can only augment the radiation resistance of the HEAs to a limited extent, the third strategy, (c), enhancing the sink strength of the material, can show multifold improvement in the radiation resistance [53, 54, 55]. One of the ways to improve the sink strength of the HEAs is to have multiple interfaces either by secondary-phase precipitation or by a multimodal distribution of grain sizes, including nanostructured grains. HEAs offer significant potential for inducing such microstructural heterogeneities, but conventional casting is tedious and time-consuming [53, 56, 57, 58]. For instance, the microstructure of a transformation-induced plasticity (TRIP)-enabled HEA has been innovatively engineered by Agrawal et al. for enhanced radiation resistance [53]. The processing route involved a preliminary homogenization annealing of the cast HEA followed by a hot rolling to eliminate the cast defects. The rolled HEA was eventually descaled, heat-treated at 500°C (desired phase field), and then warm-rolled to obtain a massively interfaced alloy.

Considering this process, AM methods such as DED [42, 59, 60, 61] can be beneficial because materials with significantly better properties than the conventionally cast counterparts can be obtained [62, 63, 64, 65, 66]. Moreover, straightforward, one-step annealing approaches can be designed by exploiting the residual stresses in these AM techniques to successfully engineer microstructures with multiple interfaces desired for nuclear applications [67, 68]. The DED process can also enable the fabrication of functionally graded materials that possess applications across different industries, including nuclear. Additionally, the functionally graded materials produced via DED can rapidly assess the material's properties [42, 59, 60, 61, 69, 70, 71, 72], reducing the overall cost of downselecting in a given compositional space, especially HEAs [73, 74].Pacific Northwest National Laboratory's (PNNL's) Shear Assisted Processing and Extrusion (ShAPE) is another recently developed solid-state processing technique that produces parts with significantly finer and compositionally homogenous microstructures that result in enhanced functional and mechanical properties [75]. Therefore, it is worthwhile for the nuclear industry to investigate novel HEAs via advanced manufacturing processes.

1.5 FY 2023 WORK SCOPE

The three groups of nontraditional nuclear structural materials have been investigated, commonly focusing on activities including (1) the feasibility studies on new materials and application of relevant advanced manufacturing technologies, (2) collection of materials properties data and knowledge through experiments and literature survey, and (3) development and application of a decision criteria matrix for downselecting candidate materials and manufacturing technologies.

The research at Oak Ridge National Laboratory (ORNL) has focused on developing an AM and postbuild processing route for ODS ferritic and austenitic alloys and performing microstructural and mechanical characterizations to provide feedback on the materials and processing route design [4]. The key outcome of the research includes the ODS alloy processing routes combining AM processes and postbuild TMTs, mechanical and microstructural characteristics of the newly developed materials, and the application results of the decision criteria matrix for the AM ODS alloys—a downselected material and feasible processing route.

Los Alamos National Laboratory (LANL) exerted significant efforts for the first steps toward a longer-term effort to identify, vet, and develop the use of advanced manufacturing techniques to fabricate neutron-friendly composite materials and refractory alloys for nuclear energy applications [5]. The efforts focused on providing an assessment of new material development of composites and refractory alloys, excluding their use as nuclear fuels. This assessment is performed through a decision criteria matrix downselection evaluation. Recommendations on which composites and refractory alloys to use are given based on the matrix scores and preliminary feasibility studies.

The overall objective of PNNL's HEA work scope was to evaluate the current manufacturing techniques applied for HEAs, addressing challenges and needs for upscaling the current manufacturing processes, and to identify HEAs relevant to the nuclear industry [6]. To reach this goal, a comprehensive literature survey was performed for the current manufacturing techniques applied for HEAs and the current HEAs explored in research communities, as well as identifying HEAs relevant specifically for nuclear applications. Activities also included characterization and property measurement of the downselection of HEA compositions to aid decision-making criteria and bulk manufacturing experiments using liquid and solid-state manufacturing processes to determine the effectiveness of advanced techniques. All information collected was used for the completion of the decision matrix for HEAs for nuclear applications, drawing recommendations for future work to increase the technical readiness of bulk HEAs.

2. DEVELOPMENT OF DECISION CRITERIA MATRIX

2.1 APPROACH FOR CREATION OF DECISION CRITERIA

The assessment of the new materials will require an evaluation instrument with a set of systematic scoring criteria [76] to objectively evaluate the suitability and maturity of the new materials for nuclear applications. The structural materials used in nuclear reactors can be produced through various materials design and manufacturing processes and are exposed to various extreme conditions during reactor service. Creating an objective decision criteria matrix that is applicable to diverse, new materials should be a challenging task, especially considering the wide range of compositionally different materials and manufacturing routes. A variety of factors, ranging from manufacturing routes and parameters to service environments, need to be considered in the downselection process for the proposed new materials.

First of all, the neutron irradiation in the reactor may cause various radiation-induced effects such as hardening, swelling, transmutation, and embrittlement of materials. It also may cause radioactivation of some composition elements, which has implications on disposal, decommissioning, and reactor

operations. With regards to neutron economy, materials used in a reactor may (simplistically) reflect, absorb, or moderate neutrons. So, with a high resistance to radiation damage, a material must also be compatible with the fission reaction, not greatly affecting the delicate balance of criticality. Second, the reactor materials must also be chemically compatible with the coolant and other materials within the reactor. Advanced reactors may use liquid metals, molten salts, water, or high-temperature gases. These coolants should pose reactor-dependent corrosion, oxidation, and erosion concerns. Third, high service temperatures, up to 500°C−1,000°C, are expected for some reactor designs. Radiation enhances the diffusion of species in materials, accelerating various segregation and precipitation mechanisms and permeation of elements such as hydrogen and helium, which can cause swelling and embrittlement. Fourth, because all reactor structures have to be manufactured through usually multistep processes, there are questions of manufacturability for the reactor components. Advanced manufacturing techniques might be required to overcome the aforementioned materials challenges. To select a material and its manufacturing route for a reactor component, many aspects need to be considered, including consistency in production quality, cost-effective and cost-efficient processing methods, and the additional development needed for consistent performance and cost-effective manufacturability. Finally, different generation IV, small modular, and microreactor concepts will have very different operational parameters, ranging from the neutron spectrum to operation temperature and coolant material. The decision criteria matrix needs to be created in such a way that its criteria would broadly encompass the operational parameters of foreseen reactor concepts while also putting a premium on materials with high-temperature and high-dose stability, as well as versatile materials that may be compatible with multiple coolant types and used for multiple reactor components.

As mentioned previously, numerous variables can arise from the combination of different materials, manufacturing routes, properties, and service environments and need to be considered in the evaluation and selection of materials, thereby complicating the materials assessment process. These considerations form the basis for the criteria used in the decision criteria matrix. Collaborative work among ORNL, LANL, and PNNL has developed a common decision criteria matrix for the prioritization of new materials produced via various and combined advanced manufacturing processes [4, 5, 6]. The scoring items were categorized into four property criteria groups: application space, environmental compatibility, physical and mechanical properties, and manufacturability. The scores based on references, ranging from 1 (poor) to 5 (excellent), were also established to consider a variety of aspects of new materials. Applying these criteria primarily allows for reasonable evaluation of new materials based on the limited accumulation of property data and knowledge. The main conclusion from the application of the criteria matrix should be a recommendation on the downselected material with a feasible processing route.

2.2 DECISION CRITERIA MATRIX FOR NEW MATERIALS

Table 2-1 through Table 2-4 summarize the product of the multilaboratory collaborative work: the decision criteria matrix for the evaluation of the new materials.

Table 2-1. Decision criteria matrix and scoring criteria for the application space of new materials.

Category	Criteria	Evaluation	Score Reference				
			5	4	3	2	1
Application Space	**Applicability To Different Reactor Types**	Can the material be used in multiple reactor types, or is it only suitable for a few?	Potential application for material across all generation IV reactor types	Potential application for material in 4 to 5 of the generation IV reactor types	Potential application for material in 2 to 3 of the generation IV reactor types	Potential application of material in only one reactor type	No conceivable application for material in any reactor type
	Other Industry Experience	Do other industries use this material, and/or are other industries interested in this material?	Widespread use of this material in multiple industries	Material is used extensively in only a few other industries but has widespread interest in other industries	Material has only moderate use and interest in other industries	The material has limited use and interest in other industries	Other industries do not use or have any interest in the material
	Data Availability	The availability and comprehensiveness of data associated with a given material	Material has been extensively studied for use in nuclear energy, and data are published and available	One or two notable gaps exist in data; otherwise, material has been studied, and data are published and available	Several studies have been performed on material, and data are available, but there are still several notable gaps in data	Relatively few studies have been performed on material, with limited published data	Limited or no information or data available for specified material
	Code and Standards Availability	The availability of codes and standards, which govern the production, material quality/standards, and implementation of a material	Codes and standards are available for the material, its production, and its most likely application	Codes or standards are available for 4–5 of the areas	Codes or standards are only available for 3 of the areas	Codes or standards are only available for 2 of the areas	Codes and standards are only available for ≤1 area
	Component Versatility	The potential for a material to be used for different types of components	Material has potential for application in all types of components	Material has potential for application in 3/4 types of components	Material has potential for application in 2/4 types of components	Material has potential for application in 1/4 types of components	Material does not have potential for application in any type of components

Table 2-2. Decision criteria matrix and scoring criteria for the environmental compatibility of new materials.

Category	Criteria	Evaluation	Score Reference				
			5	4	3	2	1
Environmental Compatibility	**Radiation Resistance**	The ability of a material to maintain its shape, size, and properties after exposure to radiation	Material exhibits <1% volumetric change and limited mechanical property degradation at doses of ≥300 dpa	Material exhibits <1% volumetric change and limited mechanical property degradation at doses between 200 and 300 dpa	Material exhibits <1% volumetric change mechanical property degradation at doses between 100 and 200 dpa	Material exhibits <1% volumetric change and limited mechanical property degradation at doses between 50 and 100 dpa	Material exhibits <1% volumetric change and limited mechanical property degradation at doses ≤50 dpa
	Elemental Transmutation	Elemental stability of a material and impact of transmutation	Transmutation of elements in the material is not a concern	Transmutation of elements in the material results in at least one of the concerns or only causes concern when dose received is comparable with the reactor or material lifetime, meaning the material would be replaced before transmutation was cause for concern	Transmutation of elements in the material results in two of the concerns, or transmutation is only a concern in one neutron spectrum (either fast or thermal) but not the other	Transmutation of the elements in the material leads to premature material failure or three of the major concerns	Transmutation of constituent elements disqualifies the material from consideration or results in all of the major concerns
	High-Temperature Oxidation Resistance	The ability of a material to resist oxidation at high temperatures	Oxidation initiation occurs at temperatures ≥800°C	Oxidation initiation occurs at temperatures ≥600°C	Oxidation initiation occurs at temperatures ≥400°C	Oxidation initiation occurs at temperatures ≥200°C	Oxidation initiation occurs at temperatures <200°C
	Neutronics Compatibility	Degree of negative impact to the neutron economy of reactors	Material has a low thermal and fast neutron capture cross section and exhibits no detrimental reactions to either spectrum of neutrons	Material has moderately low thermal or fast neutron capture cross sections	Material has a low neutron capture cross section in one of either thermal or fast spectrums	Material has moderately high thermal or fast neutron capture cross sections, making it likely unsuitable for in-core applications	Material is a known neutron absorber or has a large neutron capture cross section at both fast and thermal energies
	Coolant Compatibility and Corrosion Resistance	Number of coolants, corrosion, erosion considerations The material's relative stability in a given coolant, including its resistance to corrosion, erosion, and other chemical reactions	Material is compatible with all types of coolants, showing no significant degradation	Material is compatible with 3/4 types of coolants, exhibiting good stability and inertness	Material is compatible with two types of coolants, exhibiting good stability in those coolants	Material is compatible in only one type of coolant, exhibiting significant instability in the other types of coolants	Material is not compatible with any of the coolant types, showing significant degradation in short periods of time

Table 2-3. Materials scoring criteria for the physical and mechanical properties of new materials.

Category	Criteria	Evaluation	Score Reference				
			5	4	3	2	1
Physical and Mechanical Properties	**Thermal Conductivity**	Capability (with high thermal conductivity) to increase the thermal efficiency of an energy system and reduce transitional thermal stress in the components	Maintain >100 W/(m·K) over lifetime	Maintain 50–100 W/(m·K) over lifetime	Maintain 10–50 W/(m·K) over lifetime	Falls to <10 W/(m·K) in the end of lifetime	Begins with a low thermal conductivity < 10 W/(m·K)
	Thermal Capacity	General thermal capacity such as melting point, softening point, phase stability across temperature range	Operation temperatures in all reactor types <0.4 T_M	Operation temperatures in most reactor types in 0.4–0.6 T_M	Operation temperatures in some reactor types in 0.4–0.6 T_M	Operation temperatures in some reactor types >0.6 T_M	Operation temperatures in most reactor types >0.6 T_M
	Tensile Properties	High-temperature tensile properties including strength, ductility, and type of failure	Yield strength >200 MPa; uniform ductility >2%; no brittle failure mode over lifetime	Yield strength >150 MPa; uniform ductility >2%; no brittle failure mode over lifetime	Yield strength >100 MPa; uniform ductility >2%; no brittle failure mode over lifetime	Yield strength >100 MPa; uniform ductility >2%; possibly brittle failure mode in lifetime	Yield strength >100 MPa; uniform ductility <2%; possibly brittle failure mode in lifetime
	Creep Performance	Risk of losing dimension stability in long-term service	No creep rupture expected in lifetime. No measurable creep strain (<0.001% in lifetime) in all reactor types	No creep rupture expected in lifetime. Little creep strain <0.01% in lifetime in most reactor types.	No creep rupture expected in lifetime. No creep strain <0.1% in lifetime in most reactor types.	No creep rupture expected in lifetime. Creep strain >0.1% in lifetime in some reactor types.	Possible creep rupture in lifetime. Creep strain >1% in lifetime in some reactor types.
	Fatigue	Risk of component failure owing to crack growth by cyclic loading	Load conditions in most reactor types are more than 20% below the fatigue limit	Load conditions in some reactor types are more than 20% below the fatigue limit	Load conditions in most reactor types are close but below the fatigue limit	Load conditions in some reactor types are above the fatigue limit	Load conditions in most reactor types are above the fatigue limit
	Fracture Toughness	Capability to avoid the most probable failure mode with aging and degradation	Fracture toughness >150 MPa√m over lifetime	Fracture toughness >100 MPa√m over lifetime	Fracture toughness >50 MPa√m over lifetime	Fracture toughness >50 MPa√m over most of lifetime	Fracture toughness <50 MPa√m over most of lifetime
	Microstructural Dependency	The sensitivity of material's properties to its microstructure	Properties are not sensitive to microstructure and processing route. Microstructure is highly stable in any service environment	Properties are not sensitive to microstructure and processing route. Microstructure is reasonably stable in most of service environments.	Properties are somewhat dependent on microstructure and processing route. Microstructure is reasonably stable in most of service environments.	Properties are sensitive to microstructure and processing route. Microstructure is reasonably stable in most of service environments.	Properties are sensitive to microstructure and processing route. Microstructure is not stable in some service environments.
	Scope For Microstructural Enhancement	The possibility of enhancing material properties by microstructural engineering through feasible processing routes	Microstructure is easily controlled for desirable properties within traditional and advanced processing means. No limitation in mass production and product size.	Microstructure is easily controlled for desirable properties within traditional and advanced processing means. Some limitations in mass production and product size.	Microstructure can be controlled for desirable properties through a few limited processing methods only	Microstructure can be controlled for desirable properties through a specially designed processing method only	Microstructure can be controlled for a few properties through a specially designed processing method only

Table 2-4. Materials scoring criteria for the manufacturability of new materials.

Category	Criteria	Evaluation	Score Reference				
			5	4	3	2	1
Manufacturability	**Reproducibility/ Consistency**	Degree of reproducibility and consistency in product quality for various manufacturing routes/methods of the same material (e.g., for the same material, 3D printing is not consistent, but casting is)	Number of critical parameters that need to be carefully monitored >1	Number of critical parameters that need to be carefully monitored >3	Number of critical parameters that need to be carefully monitored >5	Number of critical parameters that need to be carefully monitored >7	Number of critical parameters that need to be carefully monitored >9
	Process Complexity	Number of processing steps (when writing, provide post processing information)	If it involves: 0 preprocessing steps but a maximum of 1 postprocessing steps	If it involves: 0–1 preprocessing steps but a maximum of 2 postprocessing steps	If it involves: 0–2 preprocessing steps but a maximum of 3 postprocessing steps	If it involves: 0–3 preprocessing steps but a maximum of 4 postprocessing steps	If it involves: 0–4 preprocessing steps but a maximum of 5 postprocessing step
	Cost	Overall cost for production of components (considering the same concern as reproducibility/consistency)	If it the overall cost is 30%–50% lower than the current commercial processing method	If the overall cost is 10%–30% lower than the current commercial processing method	If the overall cost is comparable with the current commercial processing method	If the overall cost is 10%–30% higher than the current commercial processing method	If the overall cost is 30%–50% higher than the current commercial processing method
	Scalability	The ability to increase the overall # of components being produced with a certain material, and the ability to produce dimensionally larger components	Zero concerns in terms of time delay/additional required equipment/ for scaling up	1–3 concerns in terms of time delay/additional required equipment/ for scaling up	3–5 concerns in terms of time delay/additional required equipment/for scaling up	5–7 concerns in terms of time delay/additional required equipment/for scaling up	Almost impossible to scale up
	Production Method Technological Readiness Level (TRL)	The already qualified processing techniques receive a score of 5, and the ones still in the process a 3, and completely new processes receive 1	The processes with TRL between 7 and 9	The processes with TRL between 5 and 7	The processes with TRL between 3 and 5	The processes with TRL between 1 and 3	First report on the process
	Raw Material Supply	Precursor availability in the United States	If all the raw materials required for the process are manufactured and supplied in the United States. Also, the supplier/manufacturer is cheapest among the available sources internationally.	If all the raw materials required for the process are manufactured and supplied in the United States. Also, the supplier/manufacturer is not cheapest among the available sources internationally.	If all the raw materials required for the process are not manufactured in the United States but the supplier is based in the United States	If all the raw materials required for the process are not manufactured in the United States but can be shipped internationally	If all the raw materials required for the process are not manufactured in the United States but cannot be shipped internationally

Table 2-4. Materials scoring criteria for the manufacturability of new materials (continued).

Category	Criteria	Evaluation	Score Reference				
			5	4	3	2	1
Manufacturability	**Flexibility Of Manufacturing**	# of methods which can be used to manufacture material	If the material can be manufactured via 100% of the available processing techniques	If the material can be manufactured via 80% of the available processing techniques	If the material can be manufactured via 60% of the available processing techniques	If the material can be manufactured via 40% of the available processing techniques	If the material can be manufactured via 20% of the available processing techniques
	Conventional Machining	Need for drilling, joining, welding, riveting, etc.	A ready-to-go part can be directly manufactured without any postprocessing	A ready-to-go part can be directly manufactured with negligible postprocessing	Multiple subparts need to be manufactured with minimal postprocessing but require joining/welding/riveting	Multiple subparts need to be manufactured with significant postprocessing but require joining/welding/riveting	Parts with reasonable size scale cannot be manufactured
	Near Net Shaping (Complexity Of Shape)	How complex of a shape can the manufacturing process of a material make?	Not limited by the complexity of the design	Somewhat limited by the complexity of the design	Limited but few complex geometries can be achieved	Only simple geometries can be achieved	Only 1D/2D geometries are possible

2.3 A NOTE FOR APPLICATION

The following sections are intended to compile the information on the properties and manufacturing technologies for the three groups of materials—AM ODS alloys, composite materials with refractories, and HEAs—and to present and describe the application results of the decision criteria matrix. As mentioned in this section, applying the decision criteria matrix needed to use many possible means to compensate for the lack of existing properties data and uncertainties in processing, including the data in the known knowledgebase for similar materials or the variants from traditional manufacturing methods, newly produced experimental data, and postulated knowledge from these experiences.

3. OXIDE DISPERSON–STRENGTHENED ALLOYS AND DOWNSELECTION

3.1 PRODUCTION OF FERRITIC AND AUSTENITIC OXIDE DISPERSION–STRENGTHENED ALLOYS

In the production of ferritic ODS alloys, the high-chromium ferritic alloy 14YWT powder from ORNL's inventory was used. The 14YWT powder was a prealloyed powder with a nominal composition of Fe–14Cr–3W–0.4Ti (wt %) and a nominal powder size of approximately 44 μm produced by argon gas atomization at Allegheny Technologies Incorporated. To introduce nano-oxide particles in the material, an additional oxygen source was needed for the alloy powder. The 14YWT powder was mixed with oxide powders (Y_2O_3 and Fe_2O_3) to three different combinations: 0.3 wt % Y_2O_3 was added to all three mixtures, and different amounts of Fe_2O_3 powder (0, 0.1, and 0.3 wt %) were added to the 14YWT alloy powder–Y_2O_3 mixture to compensate for the loss of oxygen content in processing and the inefficient, nonuniform distribution of oxygen within the materials.

The DED method was used to consolidate the powder mixtures. The local melting and rapid cooling nature of the DED additive process is used as a rapid solidification–cooling method that is needed to produce a microstructure without overgrown oxide particles. Some key processing parameters (after optimization) include a stepover size of 2 mm, a layer height of 0.75 mm, a laser spot size of 2.5 mm, a power of 1,020 W, a beam feed rate of 750 mm/min, and a powder flow rate of 5.4 g/min. Under these conditions, 29 mini blocks of approximately 38 × 12.7 × 12.7 mm were produced for three powder mixtures. The final step of the production process was controlled hot rolling. Part of the mini blocks were hot-rolled after annealing at 700°C or 800°C for 10 min. These annealing temperatures were chosen for processing because limited coarsening of the steel microstructures, including oxide particles, was expected. This TMT consisted of multiple annealing–rolling steps, and the final thickness of the rolled coupons was approximately 5 mm, which introduced a heavy deformation of approximately 60% to the alloys. These rolled coupons were sent to the machine shop to extract miniature tensile and fracture specimens. The face-normal directions of these specimens coincide with the build direction in the AM process and with the thickness reduction direction in hot rolling. The materials with three different oxide additions and in three different TMT conditions make nine different materials in total. Table 3-1 summarizes the mixtures, AM processes, and thermomechanical processing (TMP) conditions.

Table 3-1. Materials and processing of additively manufactured ferritic ODS steels.

Material ID	Composition	AM method	TMT condition
AM-YY	Fe–14Cr–3W–0.4Ti–0.3Y_2O_3	DED	None
AM-YY-700	Fe–14Cr–3W–0.4Ti–0.3Y_2O_3	DED	Hot-rolling at 700°C for 60% reduction
AM-YY-800	Fe–14Cr–3W–0.4Ti–0.3Y_2O_3	DED	Hot-rolling at 800°C for 60% reduction
AM-YYF	Fe–14Cr–3W–0.4Ti–0.3Y_2O_3–0.1Fe_2O_3	DED	None
AM-YYF-700	Fe–14Cr–3W–0.4Ti–0.3Y_2O_3–0.1Fe_2O_3	DED	Hot-rolling at 700°C for 60% reduction
AM-YYF-800	Fe–14Cr–3W–0.4Ti–0.3Y_2O_3–0.1Fe_2O_3	DED	Hot-rolling at 800°C for 60% reduction
AM-YF	Fe–14Cr–3W–0.4Ti–0.3Y_2O_3–0.3Fe_2O_3	DED	None
AM-YF-700	Fe–14Cr–3W–0.4Ti–0.3Y_2O_3–0.3Fe_2O_3	DED	Hot-rolling at 700°C for 60% reduction
AM-YF-800	Fe–14Cr–3W–0.4Ti–0.3Y_2O_3–0.3Fe_2O_3	DED	Hot-rolling at 800°C for 60% reduction

Two austenitic alloy powders were the base materials the production of ODS alloys: stainless steel (SS) 316L and 316H powders. These powders have chemistries within the standard composition ranges:

Fe–(16–18)Cr–(10–14)Ni–(2–3)Mo–0.03(max)C and Fe–(16–18)Cr–(10–14)Ni–(2–3)Mo–(0.04–0.1)C, respectively. These alloy powders were both produced by argon gas atomization and 15–45 μm powder feedstock from Praxair. The Y_2O_3 powder was added to the alloy powders and thoroughly mixed to introduce oxygen content and/or nano-oxide particles in the AM process. The optimum or typical amount of Y_2O_3 added to the ODS base alloys is approximately 0.3 wt %. Part of the oxygen source is expected to be lost in the nanoparticle formation process because the oxygen distribution after AM is highly inhomogeneous. To compensate for this loss to inefficient microstructure sites, an amount higher than the optimum content, 0.5 wt %, was added to the two austenitic alloys. The high ductility of the austenitic SS matrix can accommodate this higher oxide amount and retain enough ductility for structural applications.

The LPBF method was used to consolidate these austenitic alloy powder–oxide powder mixtures. The mixed SS 316L + yttria and SS 316H + yttria powders were processed using a Renishaw AM250 LPBF system. The AM250 is equipped with a 400 W, ytterbium-fiber pulsed laser with a spot size of approximately 70 μm and wavelength of 1.07 μm. Six 62 mm wide, 37 mm high, and 12 mm thick plates were printed for the two powder mixtures using the following parameters: a laser power of 225 W, point distance of 65 μm, exposure time of 105 μs, hatch spacing of 100 μm, and a layer thickness of 50 μm. A standard stripe pattern linear hatch scan strategy was adopted: a stripe width of 5 mm and a scan rotation of 67° between consecutive layers. All builds were performed at RT in an inert argon atmosphere, keeping the O_2 level below 500 ppm, and using a mild steel build plate. These plates were cut into 14–17 mm high bars for convenient thermomechanical processes.

In the same way as the processing for ferritic ODS alloys, the final step of the production process involved controlled hot rolling steps. The bars were thermomechanically processed (repeatedly hot-rolled) with annealing at 700°C or 800°C for 10 min. The rolling consisted of multiple annealing–rolling steps, and the final thickness of the rolled coupons was approximately 5 mm. This height reduction corresponds to a plastic strain of 70%. Miniature tensile and fracture specimens were machined from these coupons. The face-normal directions of these specimens coincide with the build direction in the AM processes, which is the same as the thickness reduction direction in hot rolling. The two alloys in three different TMT conditions make six different materials in total, as summarized in Table 3-2.

Table 3-2. Materials and processing of additively manufactured austenitic ODS steels.

Material ID	Composition	AM method	TMT condition
AM-316L	316L	LPBF	None
AM-316L-700	316L	LPBF	Hot-rolling at 700°C for 70% reduction
AM-316L-800	316L	LPBF	Hot-rolling at 800°C for 70% reduction
AM-316H	316H	LPBF	None
AM-316H-700	316H	LPBF	Hot-rolling at 700°C for 70% reduction
AM-316H-800	316H	LPBF	Hot-rolling at 800°C for 70% reduction

3.2 MECHANICAL TESTING

Two types of mechanical testing specimens were machined for property evaluations, as shown in Figure 3-1. The first type was the SS-J2 tensile specimen, which has a 1.2 mm wide, 0.5 mm thick, and 5 mm long gage section; a total length of 16 mm; and a head width of 4 mm. The second type was a miniature fracture bend bar side-grooved (MBS) that can be precracked and fracture-tested under the three-point bend (TPB) loading mode. It is a rectangular bar with nominal dimensions of 14 mm in length × 4 mm width × 2.5 mm thickness. At the middle of the bar, a 1 mm deep electrical discharge machined notch is introduced, and 20% deep grooves are machined at both sides of the specimen.

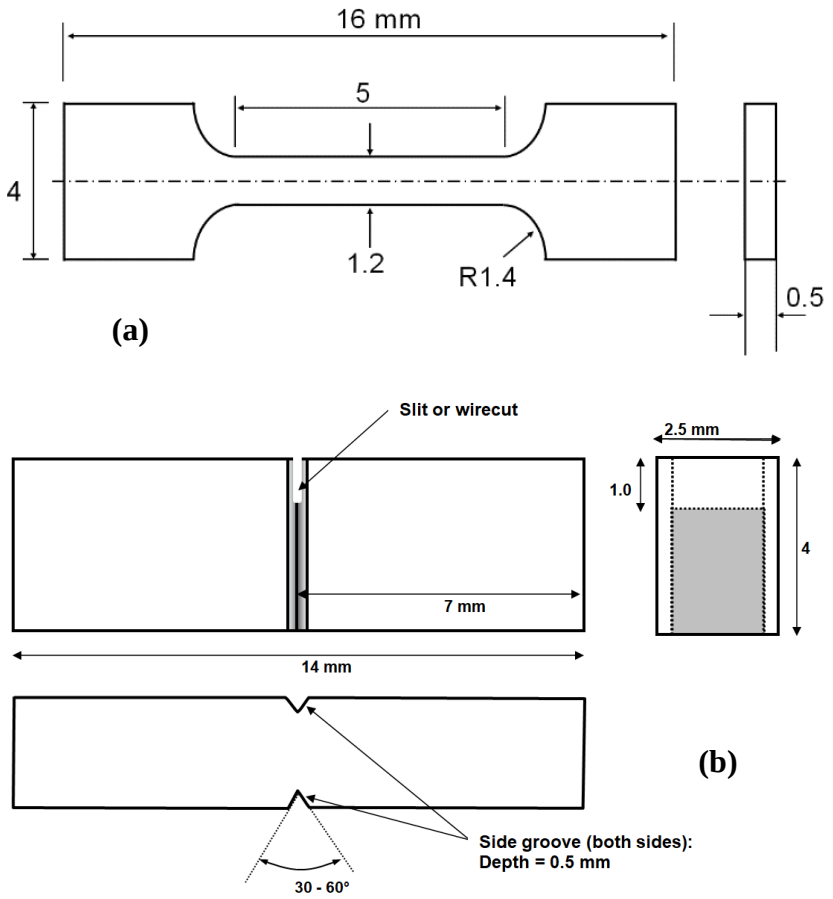

Figure 3-1. Miniature mechanical testing specimen designs:(a) SS-J2 tensile specimen and (b) three-point bend bar specimen.

Uniaxial tensile testing for SS-J2 specimens was performed by using an electromagnetic mechanical testing system at a nominal strain rate of 1×10^{-3} s^{-1} (displacement rate = 0.3 mm/min) by using shoulder-loading grip sets [30]. The loading direction coincided with the rolling direction. Raw data or load-displacement data up to failure were recorded and used to determine the common engineering strength and ductility parameters, including YS, ultimate tensile strength (UTS), uniform elongation (UE), and total elongation (TE). Unless specified otherwise, tensile testing and data analysis were performed by following the standard testing procedure in ASTM International's ASTM E8/8M and E21.

Fracture toughness testing in TPB mode was also performed using the electromagnetic mechanical testing system. The span of the TPB loading was 12.5 mm. A streamlined procedure was created, from precracking to static fracture testing to fracture toughness calculation, which was established for miniature fracture testing by the lead author [11, 10, 77]. The procedure was applied to the fracture toughness testing of the 14 mm long miniature specimens. The omission of the externally attached clip gage for displacement measurements and the use of the self-guiding, cradle-type specimen grip both enabled high-efficiency processing in this project. A simplified fracture resistance (*J*-integral) vs. crack growth resistance (*J*–*R*) curve calculation procedure was established by adopting the load–displacement curve normalization method with a slight modification that separates the displacement measurements into elastic and plastic components. Before the static fracture (*J*–*R*) testing, every single-edged MBS specimen was fatigue-precracked to create a sharp crack tip extending from the 1 mm deep machined notch to an approximately 1.8 mm total depth, or 45% of the specimen thickness. Static fracture tests were performed

in compressive bend loading mode at a displacement speed of approximately 0.005 mm/s (0.3 mm/min). Monotonic load vs. displacement data were recorded at a typical data acquisition rate of 5 Hz during the static testing. These data were used to generate *J*–*R* curves and determine fracture toughness values (J_Q and K_{JQ}). The *J*–*R* curves were constructed from the load–displacement curve data and optical measurements of the crack lengths using the curve normalization method, which was modified in this case for the miniature specimens.

Except for a few special techniques used for the miniature specimen, the fracture testing and calculation practices used in the project followed the ASTM Standard Test Methods E1820 and E399. The following special techniques were used. (1) The testing does not use any attached gage for displacement measurement. To calculate the load–displacement curve, the linear displacement component, including pure elastic displacement and machine load-line compliance, was removed, and the elastic displacement was reconstructed using the theoretical equation. (2) An iterative calculation method was used to meet the final crack length physically measured, which is an ultimate criterion defined in the curve normalization method. (3) Precracking was based on the reading of displacement amplitude only. Fatigue cracking length was considered achieved when the displacement amplitude changed by a defined amount under a given load amplitude.

3.3 MECHANICAL PROPERTIES OF FERRITIC OXIDE DISPERSION–STRENGTHENED ALLOYS

The test results for the newly produced additively manufactured ferritic and austenitic ODS alloys are summarized in the following subsections and are used in later sessions as the input for mechanical properties to apply the decision criteria for the downselection of the AM ODS materials. In the following subsections, the engineering strength parameters (YS and UTS) and ductility parameters (UE and TE) are presented and compared among the processing routes. Fracture toughness data are also presented for the ferritic ODS alloys. These comparisons may lead to the downselection of a more feasible alloy and processing route within the ODS materials.

The YS and UTS data for the ferritic ODS alloys are compared in **Error! Reference source not found.**, w hich displays the strength data of nine different materials conditions. Because the ferritic ODS alloys exhibit YS typically around 800 MPa, which is approximately twice that of non-ODS ferritic–martensitic alloys (400–500 MPa), the value can be a criterion for screening processing routes. Notably, the AM-YF material (14YWT + $0.3Y_2O_3$ + $0.3F_2O_3$) in all three conditions (as-built condition and after 700°C and 800°C TMT) exhibits YS and UTS higher than 800 MPa. The AM-YY material (14YWT + $0.3Y_2O_3$) also displays decent strength in the as-built condition, but the strength in the 700°C TMT condition only exhibits high enough strength for the criterion. The AM-YYF material (14YWT + $0.3Y_2O_3$ + $0.1F_2O_3$) in all conditions exhibits strengths less than 800 MPa. These strength data indicate that the amount of oxygen in the powder mixture matters, and the precipitation of oxide particles is incomplete in the AM and subsequent TMP process.

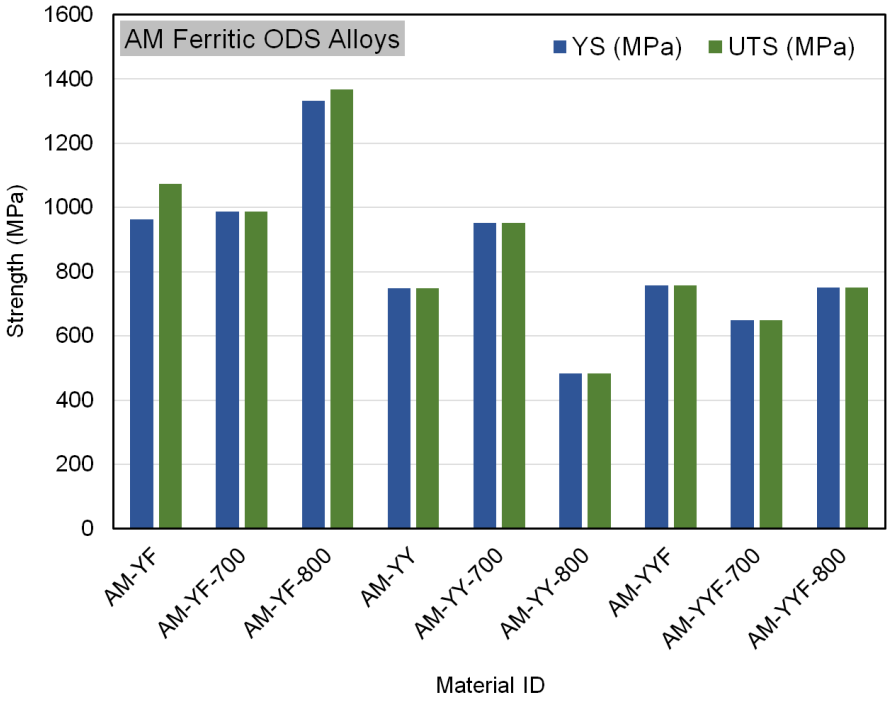

Figure 3-2. Tensile strength of additively manufactured ferritic ODS alloys.

The ductility data (UE and TE) display a much simpler comparison, as shown in **Error! Reference s ource not found.**3-3, because many of the ferritic ODS alloys produced for this research exhibit embrittlement or zero ductility. The AM-YF in the as-built condition demonstrates a significant ductility for such a high-strength (~1 GPa) material. Both UE and TE are approximately 5%, and achieving the 5% UE is a particularly meaningful result for the strength level. The same alloy after the 800°C TMT also displays some ductility, but its limited ductility might originate from small inelastic deformation around the yield strain range, which is often observed in near-embrittled materials. Therefore, these comparisons of the strength and ductility parameters among the processing routes and oxide contents made it obvious that the AM-YF ferritic ODS is the most feasible for an acceptable mechanical function as a structural material.

Error! Reference source not found. compares the fracture toughness data (in MPa√m) of AM ferritic O DS materials. All nine different fratcure toughness values are within a relatively narrow range of 18–33 MPa√m. These relatively low fracture toughness values indicate that the test temperature (room temperature) is near the lower tail of the brittle-to-ductile transition range. The upper-shelf fracture toughness of ferritic ODS alloys is typically higher than 100 MPa√m. Demonstrating a proper level of fracture toughness (>100 MPa√m) is essential to a structural material for thick-component applications. A structural material with fracture toughness less than 100 MPa√m may not show stable crack growth at high tempeatures. Therefore, the application of the ferritic ODS alloys as presented should be limited to the components requiring high strength only.

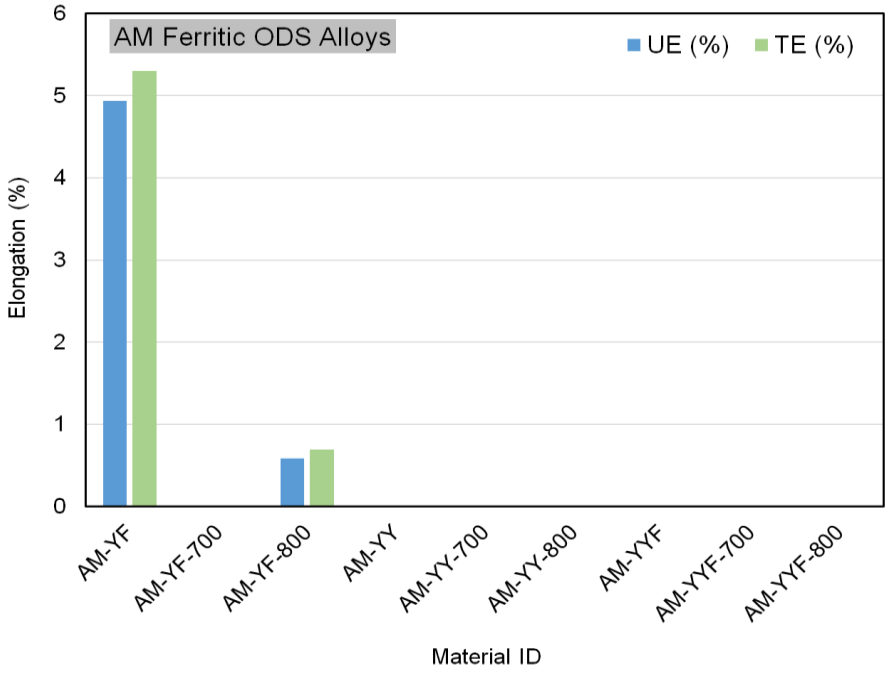

Figure 3-3. Tensile ductility of additively manufactured ferritic ODS alloys (with nil-ductility of embrittled materials).

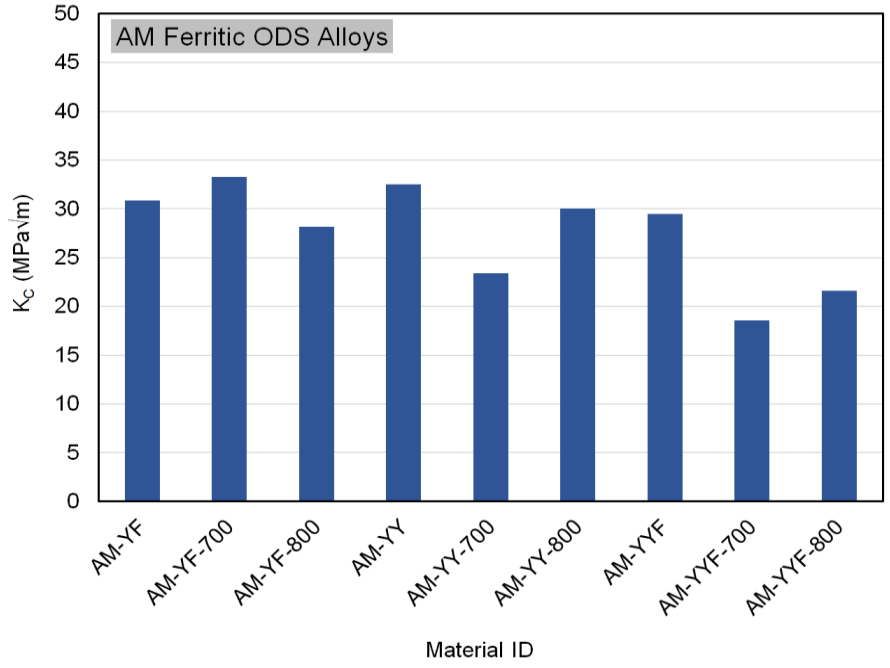

Figure 3-4. Fracture toughness (K_C) of additively manufactured ferritic ODS alloys.

3.4 MECHANICAL PROPERTIES OF AUSTENITIC OXIDE DISPERSION–STRENGTHENED ALLOYS

The tensile test results for the two austenitic ODS (316L and 316H) alloys are presented in **Error! R eference source not found.** and **Error! Reference source not found.**, respectively, for their RT strength

and ductility data. Compared with the test results for the ferritic ODS alloys, the strength of additively manufactured austenitic ODS alloys is generally lower, but their ductility is much higher. Overall, these austenic ODS alloys are more feasible for the engineering applications requiring high mechanical safety margins.

If the same strength criterion of 800 MPa is applied, then the AM 316L-700 is the only material that satisfies the criterion, as shown in **Error! Reference source not found.**. The AM 316H-700 and AM 3 16L-800 nearly meet the criterion because their YS valus are slighly lower than 800 MPa, but their UTS values are above 900 MPa. Considering that the wrought 316L and 316H steels in the annealed condition have a YS and UTS of approximately 200 MPa and 500 MPa, respectively, the strengths of these additively manufactured ODS variants of the same alloys are remarkable. The as-built ODS materials, with material IDs AM 316L and AM 316H, also exhibit much higher strengths compared with the wrought materials. However, their strengths are only slightly (20%–30%) higher than those of the AM 316L without oxide strengthening. The strength of 316H with a higher carbon content (typically within 0.04–0.1 wt %) is slighty lower than that of 316L with a limited amount of carbon content (<0.03 wt %) in all processing conditions. Such a small difference in strength might not significantly affect other mechanical behavior; however, the role of carbon content in strengthening the additively manufactured materials should be a fundamental topic to explore.

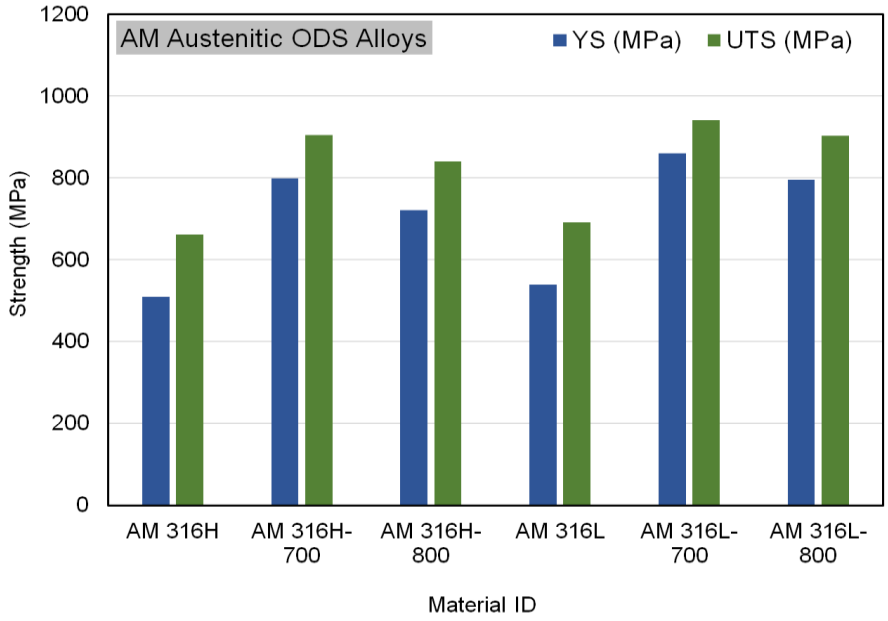

Figure 3-5. Tensile strength of additively manufactured austenitic ODS alloys.

Error! Reference source not found. compares the ductility data of the additively manufactured a ustenitic ODS alloys. First, the ODS 316L in the as-built condition demonstrates the highest ductility among the materials tested: UE is higher than 30%, and TE is higher than 40%. The ODS 316H in the as-built condition exhibits the next-highest ductility. The AM ODS alloys after 700°C and 800°C TMTs have relatively lower ductilities as the strength of those increased by the TMTs. Overall, the ductility of the additively manufactured austenitic ODS alloys is significant (all UE > 6%), and no embrittlement is observed within the material conditions tested. Another notable aspect observed is the size of necking ductility (TE-UE). Significant necking ductility is important because it is a key element to prevent any catastrophic crack growth in any structure under loading. A minimum of 7% necking ductility was observed in the additively manufactured austenitic ODS steels that were tested.

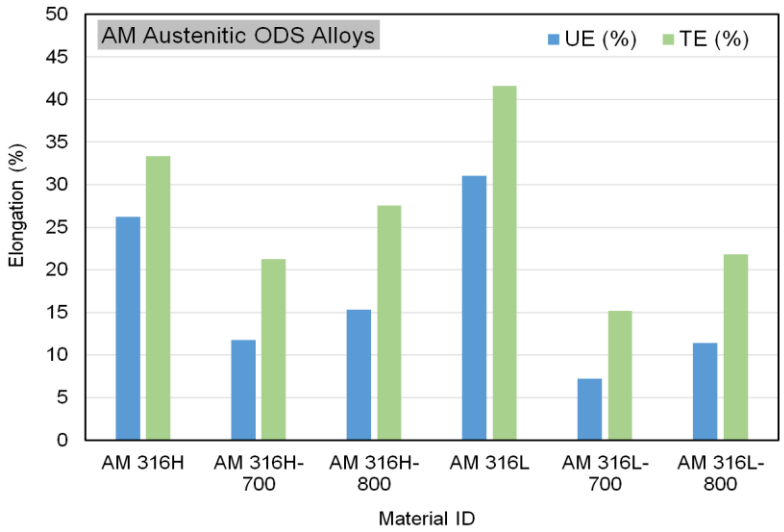

Figure 3-6. Tensile ductility of additively manufactured austenitic ODS alloys.

Figure presents the fracture toughness data of additively manufactured austenitic ODS materials. The as-printed 316L alloy demonstrates an outstanding fracture toughness at 227 MPa√m, whereas the fratcure toughness of all others is much lower and within a narrow range of 130–170 MPa√m. In the 316L alloy, both of the postbuild treatments reduced fracture toughness to the same degree. This result is different from the behavior of the 316H alloy that exhibits slight increases in fracture toughness from 156 MPa√m, much lower than 227 MPa√m, after the same postbuild treatments. Although the fracture toughness measurements, except for that of the as-printed ODS 316L alloy, are not considered high enough for the structures under high stress, no materials show any evidence of embrittlement, and these ODS materials with fracture toughness values above 100 MPa√m are considered feasible for general structural applications. Furthermore, these fracture toughness data indicate that the test temperature (RT) is in the upper-shelf range or near the upper-shelf range of the temperature transition curve of the materials. Therefore, compared with the ferritic ODS materials, the application of the austenitic ODS alloys processed via AM and postbuild TMT can be much more feasible in various conditions.

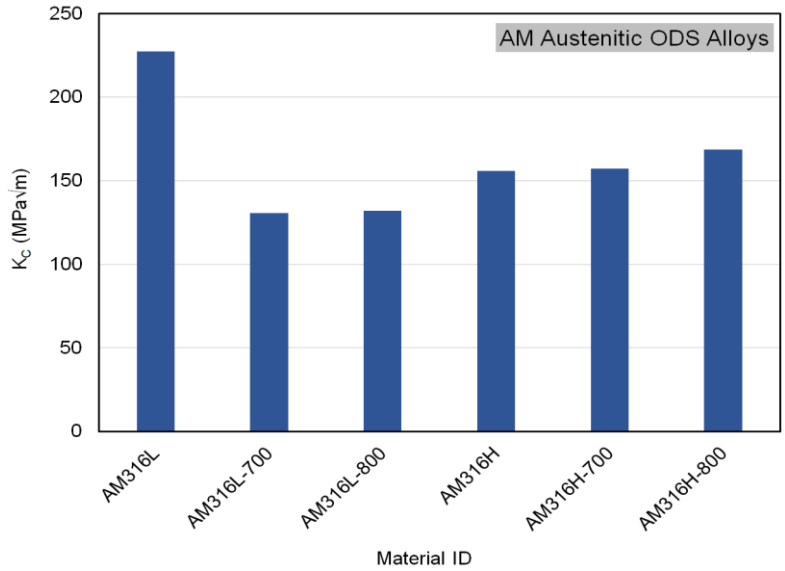

Figure 3-7. Fracture toughness (K_C) of additively manufactured austenitic ODS alloys.

3.5 SCORES FOR ADDITIVE MANUFACTURING OXIDE DISPERSION–STRENGTHENED ALLOYS

Table and 3-4 list the decision criteria in four groups that are chosen as materials evaluation items for downselecting the new materials. The numbers listed in the last two columns are the corresponding scores for the additively manufactured ferritic and austenitic ODS steels, and those given in the middle column are the reasons for deciding these scores. The scores given to the materials range from 1 to 5, and the detailed criteria matrix used to decide these scores are tabulated in the previous subsection.

Table 3-3. Application space and environmental compatibility criteria and scores for ODS materials

Category	Criteria	Reason for Scoring	Ferritic ODS Steels	Austenitic ODS Steels
Application Space	Applicability to Different Reactor Types	The ferritic or ferritic–martensitic steels are suited for many generation IV reactors. For some radioactivation and nuclear transmutation reasons, the austenitic steels are disadvantaged for a few reactor types.	4	3
	Other Industry Experience	Both ferritic and austenitic ODS alloys are new to any industrial applications.	1	1
	Data Availability	Significant data are available for the ferritic ODS alloys but not for the austenitic alloys.	3	2
	Code and Standards Availability	No availability of codes and standards for production, material qualification, and implementation of any ODS materials	1	1
	Component Versatility	Potential application of ODS materials may be limited to some function-critical components such as reactor core components.	3	3
Environmental Compatibility	Radiation Resistance	Nanostructured ODS materials have high radiation resistance such as low swelling and relatively lower degradation in mechanical properties.	4	4
	Elemental Transmutation	The ferritic Fe–Cr alloys will show very limited transmutation in irradiation, while some elements (such as Ni) in the austenitic Fe–Cr–Ni alloy can be transmutant.	4	3
	High-Temperature Oxidation Resistance	Oxidation in the austenitic alloys is highly limited up to 600°C. The oxidation resistance of ferritic alloys is relatively lower.	3	4
	Neutronics Compatibility	Negative impact to the neutron economy is acceptable for both alloy groups, but the higher Ni content in austenitic alloys gives some negative impact.	4	3
	Coolant Compatibility and Corrosion Resistance	The ferritic Fe–Cr alloys show corrosion resistance in many coolant environment, while the austenitic Fe–Cr–Ni alloys can provide higher resistance.	3	4

Table 3-4. Physical and mechanical properties and manufacturability criteria and scores for ODS materials

Category	Criteria	Reason for Scoring	Ferritic ODS Steels	Austenitic ODS Steels
Physical and Mechanical Properties	Thermal Conductivity	The thermal conductivity of both ferritic and austenitic ODS alloys may be maintained at 10–50 W/(m·K), although the value of austenitic alloys is near the lower end in irradiation.	3	3
	Thermal Capacity	Most generation IV reactors are operated at below $0.5T_M$ (melting point) of the steels (1,400°C–1,500°C).	4	4
	Tensile Properties	Both alloys can achieve a high strength >1 GPa, while the ferritic ODS alloys lose ductility for the gain in strength.	3	4
	Creep Performance	Creep rate is minimal in these alloys, and no creep rupture is expected in the load and temperature ranges of reactors.	4	4
	Fatigue	Both ODS alloys are high-strength materials, and the loads in most reactors are well below their fatigue limits.	4	4
	Fracture Toughness	Austenitic ODS alloys may retain high fracture toughness (>100 MPa√m) in most reactor types. However, the fracture toughness of ferritic ODS alloys depends strongly on the manufacturing route.	2	4
	Microstructural Dependency	The properties of both alloys have medium-level sensitivity to their microstructures.	3	3
	Scope for Microstructural Enhancement	Microstructure can be easily controlled for desirable properties within advanced processing means. Limitation may exist in mass production.	4	4
Manufacturability	Reproducibility/ Consistency	A high degree of reproducibility and consistency in product quality can be achieved with the AM and postbuild TMT route, which is only for small ODS alloy products. The ferritic ODS alloys are more sensitive to the production parameters.	3	4
	Process Complexity	A few postbuild processing steps are needed in addition to the conventional manufacturing routes.	3	3
	Cost	The overall cost for additively manufactured ODS alloys is estimated to be higher (10%–30%) than the traditional processing methods.	2	2
	Scalability	Both ODS alloys and their manufacturing processes have a good potential for the mass production of small-size components but not for the production of large components.	2	2
	Production Method Technology Readiness Level (TRL)	Manufacturing processes for both ODS alloys should be with the mid-TRL between 3 and 5. Note that there is some experience in tube (fuel cladding) fabrication.	3	3
	Raw Material Supply	Raw materials are easily available in the United States.	4	4

Table 3-4. Physical and mechanical properties and manufacturability criteria and scores for ODS materials (continued)

Category	Criteria	Reason for Scoring	Ferritic ODS Steels	Austenitic ODS Steels
Manufacturability	Flexibility of Manufacturing	All steps but the AM in the manufacturing routes can be conventional or a combined manufacturing method.	4	4
	Conventional Machining	Multiple steps and subparts will be needed for manufacturing of any ODS alloy components. However, little joining may be needed in some austenitic alloy components.	3	4
	Near Net Shaping (Complexity of Shape)	Ferritic ODS steels may be used for only simple geometries such as plate and tube. Much more complex components can be provided with the austenitic ODS alloys for their uniquely high ductility.	2	4

3.6 CONCLUDING REMARKS ON THE EVALUATION OF OXIDE DISPERSION–STRENGTHENED ALLOYS

As listed in these two tables, many of the decision criteria are scored the same for the AM ferritic and austenitic ODS alloys. However, the austenitic alloys generally have higher corrosion resistance and significantly better ductility. Furthermore, these two edges in the properties lead to additional favorable decisions or better scores for the austenitic ODS materials. These ferritic and austenitic ODS materials got total scores of 83 and 88, respectively, out of a possible 135, which correspond to the average scores of 3.07 and 3.26 for the ferritic ODS alloys and austenitic ODS alloys, respectively. Although these scores are not significantly different to make them discernable, the austenitic ODS alloys were selected to be the primary materials group in the future research on ODS materials in the AMMT Program.

4. COMPOSITES/REFRACTORIES AND DOWNSELECTION

4.1 COMPOSITE MATERIALS FOR NUCLEAR ENERGY APPLICATIONS

The advantage of composites is the beneficial combination of properties from the constituent materials that can be selected for nuclear applications. Composite materials can be tailored to have improved properties compared with those of the constituent materials [36-38]. By combining a refractory metal layer with a ceramic matrix composite substrate, a composite material can be obtained with higher toughness, improved corrosion resistance and chemical compatibility, and the ability to retain its structural properties at high temperatures [39]. Therefore, composites are anticipated to greatly benefit the nuclear industry as generation IV, modular, space, and microreactor concepts are developed and implemented. The proposed composite matrix materials, carbon (graphite) and SiC, have been investigated and used broadly by the nuclear industry for some time. More recently, fiber-reinforced composites of these materials (C/C and SiC/SiC) have gained traction because they increase the overall strength and toughness of the ceramic matrix material, maintaining these properties at elevated temperatures (>1,000°C). Since the 1990s, SiC/SiC has been seen as a candidate for fusion applications [41].

Today, ceramic composites are promising materials solutions for high-temperature reactors (HTRs) such as the very high-temperature reactor (VHTR), the molten salt reactor (MSR) and the gas-cooled fast reactor (GFR) [40]. Ceramic composites are attractive because of their low thermal expansion, high-temperature performance, lightweight nature, and resistance to radiation [9]. These composite materials

have widespread applications in other industries, as well, namely the aerospace and automotive industries. Within a reactor, composites may be used for control rod sleeves, guide tubes, upper core restraint structures, upper plenum shrouds, hot gas duct insulation modules, fuel cladding, heat pipes, and within heat exchangers [41,77,78]. Specifically, SiC is also seen as an ATF cladding and has been used as a layer in fuel architectures such as TRISO fuels [79-81]. Furthermore, these composites are lightweight, which is beneficial for the emerging modular, micro-, and space reactor applications and concepts.

Despite the impetus of development, several challenges must still be addressed for widespread adoption of composites in nuclear reactors. Corrosion (i.e., oxidation) and erosion of C/C composites is a concern at high temperatures because of reactions with oxygen and hydrogen impurities in coolant fluids [40, 82, 83]. Similarly, SiC/SiC composites are often porous, which can lead to accelerated corrosion and loss of hermeticity. Ceramic matrix composites accommodate strain by cracking but arresting the cracks with the fibers. These cracks lead to an accelerated corrosion pathway [84]. The application of a protective coating layer on these composites is seen as a promising solution, reducing corrosion, erosion, and burn-off [40, 85,86]. With these coatings, there are compatibility concerns with the composite because of thermally and irradiation-induced diffusion; additionally, there is an inherent difficulty with coating the internal length of the tubing [78,87]. Furthermore, it is difficult to join and form complex shapes while maintaining hermeticity with composites [86].

Composites are clearly a desirable and sought-after material type that would greatly benefit the nuclear industry; however, several challenges must still be addressed for these materials to be widely adopted. Furthermore, ceramic composites still require code qualification and associated design rules for use as nuclear structural materials [9]. These factors make ceramic composites—and, therefore, coated ceramic composites—prime candidates for research and development through the AMMT Program.

Each proposed composite material in this study uses either a SiC/SiC or C/C backbone. The properties of the composites largely depend on the underlying backbone. The coating will be very thin (nm–μm scale) and thus contribute minimally to the structural and neutronic properties, mainly affecting surface properties, such as compatibility with reactor coolants. Concerns still exist regarding the effects of radiation on the coating layers because transmutation could lead to activation and long-lived isotopes, and radiation could lead to embrittlement or differential swelling in the coating and backbone material. Because the properties of the composite depend more heavily on the SiC/SiC or C/C backbone, it is intuitive to first discuss the performance of SiC/SiC and C/C without a refractory coating to provide a basis for the refractory-coated composites. Therefore, after a brief discussion on the fabrication of these composites, an evaluation of C/C and SiC/SiC is given prior to evaluation of the coated composites.

The SiC/SiC and C/C composites are produced in a similar manner [40, 88]. Generally, SiC or C fibers are produced and then woven, or laid, into a pattern. This pattern or structure is known as the fiber architecture or preform. The ceramic matrix—in this case, either carbon in the form of graphite or SiC—is densified around the fiber preform. For SiC/SiC, an interphase material is formed on the fiber prior to densification to assist in bonding the fibers and the matrix. This interphase is deposited through chemical vapor deposition (CVD), thermal treatment, or polymer pyrolysis. The matrix for SiC/SiC is formed through several methods, including CVD, CVI, forced CVI, reaction sintering, liquid phase sintering, and others [88]. A newer method of matrix formation is known as the nanopowder infiltration and transient eutectic (NITE) process [88]. For C/C composites, the matrix material is densified through impregnation of a resin and subsequent pyrolysis, CVI, or impregnation and pyrolysis with a pitch instead of a resin [40].

In general, thin films or coatings are deposited by CVD, physical vapor deposition (PVD), or solution methods. All of these methods are applicable for refractory metals (i.e., Zr, Mo, and W) [89-91]. During a CVD process, reactants in the form of vapors or gases are introduced into a chamber held at a certain

pressure and temperature, where they chemically react to form the desired coating. PVD processes directly vaporize a target of the coating material, forming a vapor. The vapor is then deposited directly onto the substrate material. Solution methods generally involve applying a solution containing the necessary reactants to a substrate. Each method can result in different microstructures and has its own advantages and drawbacks. Generally, CVD is slower than the rest but results in the most conformal coatings and ability to coat complex shapes. It is difficult to coat the inside of a tube while obtaining uniform thickness with CVD methods. PVD is faster but requires line of sight to coat a material, making it much more difficult to coat complex shapes. It is also difficult to coat the inside of tubes without somehow placing the target inside of the tube. Solution methods often result in the thickest coatings, but the microstructure tends to be porous and noncrystalline. Coating complex shapes with solution methods is also difficult because careful control of the reaction rate and viscosity of the solution is required, or the solution may drip from the component prior to reaction.

Notably, specific compatibility concerns exist for coatings deposited on other materials. These are worth noting because incompatibilities between the substrate and coating will lead to failure of the coating: cracking, spallation (and, subsequently, particles present in a reactor), or delamination. These issues can ultimately lead to premature failure of a component that relied on the protective coating. The first concern is the coefficient of thermal expansion (CTE). CTE mismatch will cause cracking, buckling, and/or delamination of a coating from a substrate because of differential rates of thermal expansion or residual stresses from the deposition process. The next concern is the chemical compatibility of the substrate and coating. An element present in one material might diffuse to the other component, changing material properties or leading to delamination. Oxidation or carburization might also occur along interfaces, affecting coating adhesion. In coated systems, each layer must be chemically compatible with the layers it is touching. Other properties, such as surface finish (roughness), may also affect the coating process and coating adherence. Surface roughness may increase or decrease adherence; it may also lead to a shadowing effect, resulting in masking during PVD processes and, therefore, nonuniform coatings. The effects of radiation on the materials must also be synergistic, or the difference in responses could lead to failure at the interface.

4.2 EVALUATION OF BACKBONE COMPOSITES CARBON FIBER–REINFORCED CARBON AND SILICON CARBIDE FIBER–REINFORCED SILICON CARBIDE

In this section, the evaluations of the uncoated composites and coated composite systems are given. These materials are C/C; SiC/SiC; zirconium-, molybdenum-, and tungsten-coated C/C (Zr/C-C, Mo/C-C, and W/C-C, respectively); and zirconium-, molybdenum-, and tungsten-coated SiC/SiC (Zr/SiC–SiC, Mo/SiC-SiC, and W/SiC-SiC, respectively). Each material was evaluated against the criteria in the decision criteria matrix and given a score. The following section gives the justification for each score. Because the materials have the same backbones, several of their justifications are the same. Although this is repetitive, the justifications are given in this way for easy reference. The tabulated scores are given on the next page in Table 4-1.

Table 4-1. Scorecard for coated and noncoated refractory composite materials

Criteria		C/C	W/ C-C	Mo/ C-C	Zr/ C-C	SiC/SiC	W/ SiC-SiC	Mo/ SiC-SiC	Zr/ SiC-SiC
Application Space	Applicability to Different Reactor Types	3	4	4	4	4	4	4	4
	Other Industry Experience	5	3	3	3	4	3	3	3
	Data Availability	4	4	3	2	5	4	2	2
	Code and Standards Availability	3	3	3	3	3	3	3	3
	Component Versatility	5	5	5	5	5	5	5	5
Environmental Compatibility	Radiation Resistance	1	1	1	1	3	3	3	3
	Elemental Transmutation	4	4	3	4	4	4	3	4
	High-Temperature Oxidation Resistance	3	4	3	4	5	4	3	4
	Neutronics Compatibility	3	3	3	3	5	4	4	5
	Coolant Compatibility and Corrosion Resistance	3	3	3	3	4	3	3	3
Physical and Mechanical Properties	Thermal Conductivity	3	3	3	3	3	3	3	3
	Thermal Capacity	5	5	5	4	5	5	5	4
	Tensile Properties	4	4	4	4	3	3	3	3
	Creep Performance	3	3	3	3	5	5	5	5
	Fatigue	3	3	3	3	3	3	3	3
	Fracture Toughness	1	1	1	1	1	1	1	1
	Microstructural Dependency	2	2	2	2	2	2	2	2
	Scope for Microstructural Enhancement	4	4	4	4	4	4	4	4
Manufacturability	Reproducibility/Consistency	3	3	3	3	3	3	3	3
	Process Complexity	3	3	3	3	3	3	3	3
	Cost	3	3	3	3	3	3	3	3
	Scalability	4	4	4	4	4	4	4	4
	Production Method TRL	5	5	5	5	5	5	5	5
	Raw Material Supply	5	3	4	4	4	3	4	4
	Flexibility of Manufacturing	5	5	5	5	5	5	5	5
	Conventional Machining	3	3	3	3	3	3	3	3
	Near Net Shaping (Complexity of Shape)	4	3	3	3	4	3	3	3
Overall Scores		94	91	90	89	102	95	93	94

4.3 RATIONALES FOR SCORING BACKBONE COMPOSITE CARBON FIBER–REINFORCED CARBON

The C/C composites were given a total score of 94 out of a possible 135 (or 3.48 out of 5 on average) based on the decision criteria matrix. This value is the sum of the cumulative scores for application space (20 out of a possible 25), environmental compatibility (14 out of a possible 25), physical and mechanical properties (25 out of a possible 40), and manufacturability (35 out of a possible 45).

4.3.1 Rationale for Application Space Scores

Applicability to Different Reactor Types: 3/5. The C/C is seen as a material that could be used in VHTRs, MSRs, and GFRs, giving it a score of 3 for applicability to different reactor types [40,92].

Component Versatility: 5/5. The C/C has foreseen application as a control rod, upper core restraint block, heat exchanger material, and even as a buffer bond in fuel cladding, resulting in a score of 5 for component versatility [40].

Other Industry Experience: 5/5. The C/C composites have been extensively studied and have widespread use in multiple other industries. They have been used for rocket nozzles, reentry parts, and brake discs, resulting in a score of 5 for other industry experience [93].

Data Availability: 4/5. With regards to data availability, the variety of fibers and weave patterns affect the material properties; the lack of high-dose, high-temperature testing options, however, leave a gap in the understanding of irradiation effects on C/C composites [40]. Therefore, C/C composites are given a 4 for data availability.

Code and Standards Availability: 3/5. A score of 3 was given for code and standards availability because the American Society of Mechanical Engineers (ASME) *Boiler Presser Vessel Code* covers design and construction rules for high-temperature reactor components with ceramic composites under Section III, Division 5, Subsection HH [77].

4.3.2 Rationale for Environmental Compatibility

Radiation Resistance: 1/5. The C/C composites are given a score of 1 for radiation resistance because they are known to exhibit swelling exceeding 1% volumetric change at doses approximately 10 dpa [84,94,95]. The extent of the swelling and dimensional changes is dependent on their fiber type and architecture. Notably, C/C composites maintain their physical properties better than typical graphite. Also, the Wigner effect can cause unwanted heating and energy release in graphite materials.

Elemental Transmutation: 4/5. Production of hydrogen and helium because of transmutation and resultant embrittlement is a concern in C/C composites [96]. However, graphite has been used for several decades in nuclear reactors. Therefore, the negative effects of transmutation are expected to be minimal. The C/C composites are given a score of 4 for elemental transmutation.

High-Temperature Oxidation Resistance: 3/5. In oxidizing environments, carbon will oxidize at temperatures ≥450°C, warranting a score of 3 for high-temperature oxidation resistance [93].

Neutronics Compatibility: 3/5. The C/C is given a score of 3 for neutronics compatibility because carbon, in the form of graphite, is a known neutron moderator. This characteristic is important to consider, but C/C composites may be substituted for in-core graphite components to increase the strength/structural properties of the graphite moderator.

Coolant Compatibility and Corrosion Resistance: 3/5. C/C composites are expected to be used in gas reactors (helium) and MSRs (molten salts) and therefore are seen as compatible for these coolant types, resulting in a score of 3 [40].

4.3.3 Rationale for Physical and Mechanical Properties

Thermal Conductivity: 3/5. The thermal conductivity of C/C composites generally decreases with increasing temperature and dose. The values are dependent upon the fibers used and their architecture; values range from approximately 27 to 200 W/(m·K), resulting in a thermal conductivity score of 3 [40,96].

Thermal Capacity: 5/5. The C/C has an excellent thermal capacity, scoring 5/5. Carbon does not melt but rather sublimes around 3,895 K. The outlet temperature of a VHTR is 1,000°C, which represents approximately one-third of the sublimation temperature of graphite.

Tensile Properties: 4/5. The C/C composites have demonstrated tensile strength falling between 23 and 1,100 MPa depending on fiber type and architecture. Typical values fall closer to 150 MPa, resulting in a score of 4 for tensile properties [40,84,93,96].

Creep Performance: 3/5. Graphite is known to creep with neutron irradiation, and C/C composites have been demonstrated to experience >1% volumetric change at doses approximately 10 dpa [95,97]. However, no rupture is expected because graphite has been used in the suggested reactor types before. Therefore, C/C composites score 3/5 on creep performance.

Fatigue: 3/5. Fiber-reinforced composites are designed to resist crack propagation. Although they might not have the same fatigue resistance of metal alloys, ceramic matrix composites (CMCs) are anticipated to have satisfactory fatigue resistance. Thus, the score for fatigue is 3/5.

Fracture Toughness: 1/5. The C/C composites have demonstrated fracture toughness values ranging from 0.52 to 5.1 MPa$\sqrt{m}$. This value depends on their fiber architecture and matrix fabrication technique, resulting in a 1/5 for fracture toughness [98].

Microstructural Dependency: 2/5. The properties of a C/C composite are dependent on the arrangement, type, and treatment of the fibers used. The fibers are made through different processing routes and have different structures. The microstructures are reasonably stable in most service environments, giving a score of 2 for microstructural dependency [40,99].

Scope for Microstructural Enhancement: 4/5. The C/C composites score 4/5 on scope for microstructural enhancement because carbon fiber microstructure can be tailored using different processing routes, and the C/C composite microstructure is similarly controlled by various densification processes and fiber architecture [40,93,99].

4.3.4 Rationale for Manufacturability

Reproducibility/Consistency: 3/5. The C/C formation process is established and reproducible. Several parameters must be controlled to produce the fibers and the composites [40,93,99]. These parameters include pressure, temperature, gas flow rate, and carburizing environment, resulting in a score of 3 for reproducibility/consistency.

Process Complexity and Flexibility of Manufacturing: 3/5. The processing steps to make carbon fibers include thermosetting, carbonizing, graphitizing, surface treatment, and finally, epoxy sizing. The C/C CMCs are made by weaving or laying the fibers into the desired architecture or preform, then preforming densification of the carbon matrix around the fibers. This process can be accomplished through CVI, liquid phase impregnation, hot isostatic impregnation, and more. The C/Cs may be graphitized through thermal treatment after formation, as well [40,93,99]. Although five preprocessing steps (fiber

production) and one postprocessing step (graphitization) are required, a score of 3 is chosen because fibers are commercially available; thus, preprocessing could be circumvented.

Cost: 3/5. The current commercial processing method is the main method under evaluation. Carbon is an abundant material, and therefore, the cost of production is expected to be relatively moderate, resulting in a score of 3/5 for cost.

Scalability: 4/5. The C/C materials have been fabricated into large components such as rocket nozzles, and large numbers of C/C composites for use as brake discs have been fabricated simultaneously. The main concern is the ability to create fiber architectures of adequate size and shape, giving C/C composites a score of 4/5 for salability.

Production Method Technology Readiness Level (TRL): 5/5. The C/C CMCs are commercially produced by several companies; the processes for creating C/C CMCs is established, resulting in a TRL of 9 and a production method TRL score of 5.

Raw Material Supply: 5/5. The C/C materials are widely manufactured in the United States, resulting in a score of 5. The availability of carbon as a raw material is not a concern [40,93,99]. Relatively complex shapes can be made from C/C, but the machining of C/C can be complex.

Conventional Machining: 3/5. Turning and thread cutting are problematic because the fibers create an uneven cutting force and cause high tool wear. Furthermore, joining C/C materials to form a more complex part, especially sealed tubes, can be difficult [99-101]. Additive manufacturing of carbon fiber–reinforced polymers is a growing field, but C/C composites are currently limited by the complexity of the fiber weave pattern or architecture that can be formed. These factors result in a score of 3.

Near Net Shaping: 4/5. The densification methods can accommodate complex weaves, resulting in a score of 4 [102].

4.4 RATIONALES FOR SCORING BACKBONE COMPOSITE SILICON CARBIDE FIBER–REINFORCED SILICON CARBIDE

The SiC/SiC composites were given a total score of 102 out of a possible 135 (or 3.78 out of 5 on average) based on the decision criteria matrix. This value is the sum of the cumulative scores for application space (21out of a possible 25), environmental compatibility (21 out of a possible 25), physical and mechanical properties (26 out of a possible 40), and manufacturability (34 out of a possible 45).

4.4.1 Rationale for Application Space Scores

Applicability to Different Reactor Types: 4/5. The SiC/SiC has foreseen application in GFR, VHTR, LWR (ATF cladding), SFR (fuel-assembly body), and lead-cooled fast reactor (LFR, fuel cladding) applications [41,77,84,92,103].

Other Industry Experience: 4/5. It is used extensively in the aerospace industry and has increasing use in the automotive industry [93].

Data Availability: 5/5. Studies on SiC/SiC and its behavior in radiation have been performed since the 1970s [41].

Code and Standards Availability: 3/5. The ASME *Boiler Pressure Vessel Code*, under Section III, Division 5, Subsection HH, covers design and construction rules for high-temperature reactor components with ceramic composites [77].

Component Versatility: 5/5. Within a reactor, composites may be used for control rod sleeves, guide tubes, upper core restraint structures, upper plenum shrouds, hot gas duct insulation modules, fuel cladding, heat pipes, and within heat exchangers [41,77,79,80]. Specifically, SiC is also seen as an ATF cladding and has been used as a layer in fuel architectures such as TRISO fuels.

4.4.2 Rationale for Environmental Compatibility

Radiation Resistance: 3/5. Swelling in SiC/SiC falls between 0.8% and 2% for doses >10 dpa but does not increase up to doses of 100 dpa [114].

Elemental Transmutation: 4/5. The SiC suffers significant transmutation under fusion reactor conditions; within a fission reactor spectrum, the effects are expected to be an order of magnitude less. This transmutation is expected to cause degradation to the material but not pose challenges with decay heat, radiation, or the production of volatile species [105,106].

High-Temperature Oxidation Resistance: 5/5. The SiC will form a passive SiO_2 layer at lower temperatures; it transitions to an active oxidation regime at temperatures >1,250°C [107].

Neutronics Compatibility: 5/5. The SiC has been used in TRISO fuel particles and is seen as an ATF candidate, as well as a candidate for in-core materials of a GFR. Its effective neutron absorption cross section (neutron absorption cross section per unit of yield strength) is 10% of a zirconium alloy's [79,80,84,103].

Coolant Compatibility and Corrosion Resistance: 4/5. The SiC/SiC is a candidate material in ATF for LWRs (H_2O) and gas-cooled reactors (helium) and has demonstrated acceptable compatibility in a Pb–Li system. Also, SiC is a candidate material for MSRs but does corrode in molten salts; further tests are needed [108,109].

4.4.3 Rationale for Physical and Mechanical Properties

Thermal Conductivity: 3/5. Crystalline SiC has a thermal conductivity as high as 480 W/(m·K), but SiC/SiC has a lower thermal conductivity (5–50 W/[m·K]) [106,110,111].

Thermal Capacity: 5/5. The melting temperature (T_m) for SiC is approximately 2,730 K. The VHTR may have an outlet temperature of 1,000°C (1,273 K), which is approximately 0.47 T_m.

Tensile Properties: 3/5. The SiC/SiC yield strength is between 100 and 225 MPa [112].

Creep Performance: 5/5. The SiC has limited thermal creep <1,400°C [110].

Fatigue: 3/5. Fiber-reinforced composites are designed to resist crack propagation. Although they might not have the same fatigue resistance of metal alloys, CMCs are anticipated to have satisfactory fatigue resistance. The SiC/SiC has been shown to have a static fatigue limit stress of approximately 70 MPa and cyclic fatigue limit stress of approximately 140 MPa MPa [113].

Fracture Toughness: 1/5. The SiC/SiC has a fracture toughness of K_IC = 3.2–5.5 MPa√m [114].

Microstructural Dependency: 2/5. The properties of SiC/SiC depend on the fiber microstructure and weave pattern used. The most recent generation of fibers lead to more tolerant/stable properties in anticipated service environments [41].

Scope for Microstructural Enhancement: 4/5. The SiC fibers are required to have a certain microstructure to be radiation-tolerant. Production methods for these fibers are established. Techniques such as CVI, the NITE process, and MI can be used to form the matrix [41].

4.4.4 Rationale for Manufacturability

Reproducibility/Consistency: 3/5. The SiC/SiC can be formed through several techniques and has been made for some time. It is reproducible and consistent but requires control over several parameters. The process parameters that must be controlled from start to finish include temperature, gas flow rate, pressure, and chemical stoichiometry [41,88,106].

Process Complexity: 3/5. The SiC/SiC CMCs are produced by first weaving SiC fibers into a fiber architecture/preform, then coating the preform with an interphase material (C, O, N, or SiC), and finally densifying a matrix material around the coated preform [41,88,106,107]. Three steps are involved in the formation of SiC/SiCs. The fibers are formed by melt-spinning, curing, and ceramizing a polymer, making a total of three preprocessing steps but no significant postprocessing steps.

Cost: 3/5. The current commercial processing method is the main method under evaluation. Silicon and carbon are abundant materials; therefore, the cost of production is expected to be relatively moderate.

Scalability: 4/5. Some concern exists for large and long tubing, but in general, SiC CMCs may be fabricated into larger parts on a larger scale. Components such as brake discs, rocket nozzles, and scaled boiling water reactor (BWR) channel boxes have been fabricated [41].

Production Method TRL: 5/5. Several SiC fabrication methods are established, and commercial companies are producing SiC/SiC parts [107].

Raw Material Supply: 4/5. The SiC/SiC is given a 4 because raw material is available in the United States, but the United States is not the lead producer of silicon. Silicon and silicates are >25% of Earth's crust, indicating that the raw materials are abundant. The US Geological Survey 2023 mineral commodity summary indicates that the United States produced 310,000 metric tons of silicon in 2022. China is the main producer of silicon, at 70% of the world's supply [115]. Several US-based companies produce SiC/SiC composites and SiC fibers [107].

Flexibility of Manufacturing: 5/5. The SiC/SiC CMCs can be produced through CVI, MI, Reaction Sintering (RS), Liquid Phase Sintering (LPS), Polymer Infiltration and Pyrolysis PIP, and NITE methods [41,88,106,107].

Conventional Machining: 3/5. The SiC/SiC CMCs can be fabricated into a ready-to-go part with negligible postprocessing [41,86,106]. However, some challenges are associated with joining SiC/SiC CMCs, and conventional cutting/drilling techniques can be difficult because SiC is a very hard material. Mechanical fasteners and joints have been fabricated for SiC/SiC CMCs. It is difficult/not well-established how to join SiC parts together.

Near Net Shaping (Complexity of Shape): 4/5. 3D printing of SiC to achieve near net shaping is possible, but other methods of making SiC/SiC composites are limited to the weave pattern that can be formed [116,117].

4.5 RATIONALES FOR SCORING COATED SYSTEM TUNGSTEN-COATED CARBON FIBER–REINFORCED CARBON

The W/C-C composite was given a total score of 91 out of a possible 135 (or 3.37 out of 5 on average) based on the decision criteria matrix. This value is the sum of the cumulative scores for application space (19 out of a possible 25), environmental compatibility (15 out of a possible 25), physical and mechanical properties (25 out of a possible 40), and manufacturability (32 out of a possible 45).

4.5.1 Rationale for Application Space Scores

Applicability to Different Reactor Types: 4/5. Refractory alloys are seen as candidate materials for GFRs (in-core), LFRs (cladding and out-of-core structural), and MSRs (in-core) [103,118]. There is some concern that tungsten will react with molten salts and steam. Refractory metals are also seen as candidate materials for heat pipe linings for space reactors.

Other Industry Experience: 3/5. Tungsten-coated C/C composites are not widely used, but C/C composites are used in a plethora of applications. Tungsten-coated C/C is of interest for fusion reactors.

Data Availability: 4/5. Tungsten-coated C/C has been extensively studied for fusion environments because it is seen as a promising candidate for first wall applications [119].

Code and Standards Availability: 3/5. The ASME *Boiler Pressure Vessel Code*, under Section III, Division 5, Subsection HH, covers design and construction rules for high-temperature reactor components with ceramic composites [77].

Component Versatility: 5/5. Coated C/C composites will be applicable to many of the same applications as the uncoated composites. The main difference is their compatibility with the coolant/process environment. Therefore, refractory-coated composites are candidate materials for in-core structural, cladding, and out-of-core structural materials [103,118].

4.5.2 Rationale for Environmental Compatibility

Radiation Resistance: 1/5. The C/C composites are known to exhibit swelling exceeding 1% volumetric change at doses approximately 10 dpa. The extent of the swelling and dimensional changes is dependent on their fiber type and architecture [84,94,95]. Notably, C/C composites maintain their physical properties better than typical graphite. Also, the Wigner effect can cause unwanted heating and energy release in graphite materials. Refractory alloys such as tungsten and molybdenum may experience swelling and embrittlement for low-dpa and low–operating temperature conditions [120]. The chief concern in a coated application is that this swelling and embrittlement may induce dimensional changes in the coating, leading to delamination from the C/C composite. Although these concerns exist for the alloys, the response to radiation of the composite is expected to be more important because the structural properties of the material depend on the composite backbone.

Elemental Transmutation: 4/5. In addition to the transmutation concerns of C/C, the tungsten coating can also transmute. Transmutation of tungsten (^{184}W and ^{186}W) to rhenium and subsequently rhenium to osmium can affect the microstructural, physical, and mechanical properties of tungsten. This process could degrade the coating adhesion and hermiticity [120,121].

High-Temperature Oxidation Resistance: 4/5. Tungsten oxidation increases above 650°C. Below 500°C, tungsten forms a stable WO_3 compound in oxidizing environments [122,123].

Neutronics Compatibility: 3/5. Carbon, in the form of graphite, is a known neutron moderator. This characteristic is important to consider, but C/C composites may be substituted for in-core graphite components to increase strength/structural properties of the graphite moderator. Tungsten alloys have 35× the neutron absorption cross section of zirconium. However, in a layered composite approach, the coating will be thin, and its effect on the neutronics of a reactor are expected to be negligible [79,80,84,103].

Coolant Compatibility and Corrosion Resistance: 3/5. Refractory metals are seen as compatible with liquid metal coolants (i.e., Pb, Li). They are also proposed for applications in MSRs and GFRs [118,124]. However, there is concern that they will oxidize because of oxygen impurities at the temperatures of the high-temperature gas reactor (HTGR). Therefore, they are given a score of 3, representing moderate but potential compatibility with various coolants.

4.5.3 Rationale for Physical and Mechanical Properties

Thermal Conductivity: 3/5. Tungsten maintains at least 84 W/(m·K) at temperatures up to 500°C and doses of 5.8 dpa [125]. Tungsten is also known for its high operating temperatures. However, the thermal conductivity of the entire layered composite will depend on the C/C backbone, as well—with its values ranging from 27 to 200 W/(m·K) [96].

Thermal Capacity: 5/5. Tungsten has a melting point of 3,414°C. The VHTR outlet temperature of 1,000°C represents 0.29 T_m [126].

Tensile Properties: 4/5. The C/C composites have demonstrated tensile strength falling between 23 and 1,100 MPa depending on fiber type and architecture. Typical values fall closer to 150 MPa, resulting in a score of 4 for tensile properties [40,84,93,96].

Creep Performance: 3/5. Graphite is known to creep with neutron irradiation, and C/C composites have been demonstrated to experience >1% volumetric change at doses approximately 10 dpa [95,97]. However, no rupture is expected because graphite has been used in the suggested reactor types before. Therefore, C/C composites score 3/5 on creep performance.

Fatigue Resistance: 3/5. Fiber-reinforced composites are designed to resist crack propagation. Although they might not have the same fatigue resistance of metal alloys, CMCs are anticipated to have satisfactory fatigue resistance (3/5).

Fracture Toughness: 1/5. The C/C composites have demonstrated fracture toughness values ranging from 0.52 to 5.1 MPa√m. This value depends on their fiber architecture and matrix fabrication technique [98].

Microstructural Dependency: 2/5. The properties of a C/C composite are dependent on the arrangement, type, and treatment of the fibers used. The fibers are made through different processing routes and have different structures. The microstructures are reasonably stable in most service environments [40,99]. Tungsten, as with other refractory metals, will form WC when in the presence of carbon. This carbide is expected to embrittle the tungsten coating [124].

Scope for Microstructural Enhancement: 4/5. The C/C composites score 4/5 on scope for microstructural enhancement because the carbon fiber microstructure can be tailored using different processing routes, and the C/C composite microstructure is similarly controlled by various densification processes and fiber architecture [40,93,99]. Refractory coating microstructure is also somewhat tailorable—different deposition techniques and parameters often lead to different microstructures and, therefore, different properties.

4.5.4 Rationale for Manufacturability

Reproducibility/Consistency: 3/5. The C/C formation process is established and reproducible. Several parameters must be controlled to produce the fibers and the composites [40,93,99]. These factors include pressure, temperature, gas flow rate, and carburizing environment. In addition to the composite substrate, deposition of the coating can require control of the temperature, pressure, and gas flow rates. Because the coating process is similar to the matrix densification process, no additional process variables must be controlled, resulting in a score of 3 for reproducibility/consistency.

Process Complexity: 3/5. Once the C/C composite is produced, the refractory layer can be deposited onto it. Although this step adds complexity to the overall process, adding a CVD, PVD, or solution-based deposition method to the process, it does not add any additional pre- or postprocessing steps. Therefore, a score similar to that of the composite backbone is given.

Cost: 3/5. CVD, PVD, atomic layer deposition (ALD), and solution methods are the main methods to apply thin coatings of refractory metals. These methods represent the current commercial processing method; therefore, a score of 3 is given.

Scalability: 4/5. The C/C materials have been fabricated into large components such as rocket nozzles, and large numbers of C/C composites for use as brake discs have been fabricated simultaneously [40,93,99]. The main concern is the ability to create fiber architectures of adequate size and shape. With regards to coatings, PVD methods require high vacuum levels and line of sight. CVD methods also often require a vacuum. Both methods can require high temperatures to deposit the coating. The creation of a large furnace and vacuum system that can accommodate large and numerous parts is a concern. Still, these factors leave the layered composites with three scalability concerns, giving this category a score of 4.

Production Method: TRL 5/5. Tungsten coating techniques and C/C fabrication methods are established and working. The rank of a 7–8 TRL is given because methods are established for coating, but systems for tubes need development/work.

Raw Material Supply: 3/5. The C/C composites can be easily produced in the United States, but the availability of tungsten within the United States depends largely on scrap and imports. The US Geological Survey (USGS) estimates that 80% of the world's tungsten production occurs within China, and no domestic production of tungsten has happened since 2015 [127].

Flexibility of Manufacturing: 5/5. CVD, PVD, electroplating, and more will produce coatings of refractory metals. These methods represent the main methods of thin film coating [91].

Conventional Machining: 3/5. Refractory coatings can be deposited on components after they are assembled. Therefore, the conventional machining score is dominated by that of the composite backbone.

Near Net Shaping: 3/5. Although C/C scored a 4 in this category, the formation of quality coatings can be difficult on complex parts. This difficulty is because PVD methods require line of sight, and CVD processes are diffusion-limited and therefore need the vapor to reach all parts of a component equally. Thus, although relatively complex parts can be fabricated out of C/C, refractory-coated C/C is given a 3.

4.6 RATIONALES FOR SCORING COATED SYSTEM MOLYBDENUM-COATED CARBON FIBER–REINFORCED CARBON

The Mo/C-C composite was given a total score of 89 out of a possible 135 (or 3.3 out of 5 on average) based on the decision criteria matrix. This value is the sum of the cumulative scores for application space

(18 out of a possible 25), environmental compatibility (13 out of a possible 25), physical and mechanical properties (25 out of a possible 40), and manufacturability (33 out of a possible 45).

4.6.1 Rationale for Application Space Scores

Applicability to Different Reactor Types: 4/5. Refractory alloys are seen as candidate materials for GFRs (in-core), LFRs (cladding and out-of-core structural), and MSRs (in-core) [103,118].

Other Industry Experience: 3/5. The C/C composites are used in a plethora of applications. The application of a hermetic metal seal to a composite material has applications outside of the nuclear industry (e.g., for heat pipes) [128].

Data Availability: 3/5. The Mo/C-C is not an explicitly well-studied material; however several studies have been performed using a Mo–Si–W system to enhance the corrosion resistance of C/C composites, and the Mo–C system is well-studied [78,128,129].

Code and Standards Availability: 3/5. The ASME *Boiler Pressure Vessel Code*, under Section III, Division 5, Subsection HH, covers design and construction rules for high-temperature reactor components with ceramic composites [77].

Component Versatility: 5/5. Coated C/C composites will be applicable to many of the same applications as the uncoated composites. The main difference is their compatibility with the coolant/process environment. Therefore, refractory-coated composites are candidate materials for in-core structural, cladding, and out-of-core structural materials [103,118].

4.6.2 Rationale for Environmental Compatibility

Radiation Resistance: 1/5. The C/C composites are known to exhibit swelling exceeding 1% volumetric change at doses approximately 10 dpa. The extent of the swelling and dimensional changes is dependent on their fiber type and architecture [84,94,95]. Notably, C/C composites maintain their physical properties better than typical graphite. Also, the Wigner effect can cause unwanted heating and energy release in graphite materials. Refractory alloys such as tungsten and molybdenum may experience swelling and embrittlement for low-dpa and low–operating temperature conditions [120]. The chief concern in a coated application is that this swelling and embrittlement may induce dimensional changes in the coating, leading to delamination from the C/C composite. Although these concerns exist for the alloys, the response to radiation of the composite is expected to be more important because the structural properties of the material depend on the composite backbone.

Elemental Transmutation: 3/5. In addition to the transmutation concerns of C/C, ^{98}Mo can transmute (n, γ) to ^{99}Tc, which is a long-lived isotope ($t_{1/2}$ = 200,000 years). The isotope ^{94}Mo can also transmute (n,p) to ^{94}Nb ($t_{1/2}$ = 20,000 years). These isotopes pose a concern as long-lived radioactive species [121]. Transmutation of molybdenum to other elements will likely affect microstructural, physical, and mechanical properties.

High-Temperature Oxidation Resistance: 3/5. Molybdenum enters a vitalization regime (forming MoO_3) in the range of 500°C–700°C, depending on the partial pressure of oxygen available. Below 450°C, molybdenum forms a passivating oxide [130].

Neutronics Compatibility: 3/5. Carbon, in the form of graphite, is a known neutron moderator. This characteristic is important to consider, but C/C composites may be substituted for in-core graphite components to increase strength/structural properties of the graphite moderator. Molybdenum alloys have

10× the neutron absorption cross section of zirconium [103]. However, in a layered composite approach, the coating will be thin, and its effect on the neutronics of a reactor are expected to be negligible.

Coolant Compatibility and Corrosion Resistance: 3/5. Refractory metals are seen as compatible with liquid metal coolants (i.e., Pb, Li). They are also proposed for applications in MSRs and GFRs [118,124]. However, there is concern that they will oxidize because of oxygen impurities at the temperatures of the HTGR. Therefore, they are given a score of 3, representing moderate but potential compatibility with various coolants.

4.6.3 Rationale for Physical and Mechanical Properties

Thermal Conductivity: 3/5. Molybdenum has an excellent thermal conductivity of 138 W/(m·K) at 25°C [126]. However, the thermal conductivity of the entire layered composite will depend on the C/C backbone, as well, with values ranging from 27 to 200 W/(m·K).

Thermal Capacity: 5/5. Molybdenum has a melting temperature of 2,622°C [126]. The VHTR outlet temperature of 1,000°C represents 0.38 T_m.

Tensile Properties: 4/5. The C/C composites have demonstrated tensile strength falling between 23 and 1,100 MPa depending on fiber type and architecture. Typical values fall closer to 150 MPa, resulting in a score of 4 for tensile properties [40,84,93,96].

Creep Performance: 3/5. Graphite is known to creep with neutron irradiation, and C/C composites have been demonstrated to experience >1% volumetric change at doses approximately 10 dpa [95,97]. However, no rupture is expected because graphite has been used in the suggested reactor types before. Therefore, C/C composites score 3/5 on creep performance.

Fatigue Resistance: 3/5. Fiber-reinforced composites are designed to resist crack propagation. Although they might not have the same fatigue resistance of metal alloys, CMCs are anticipated to have satisfactory fatigue resistance (3/5).

Fracture Toughness: 1/5. The C/C composites have demonstrated fracture toughness values ranging from 0.52 to 5.1 MPa√m. This value depends on their fiber architecture and matrix fabrication technique [98].

Microstructural Dependency: 2/5. The properties of a C/C composite are dependent on the arrangement, type, and treatment of the fibers used. The fibers are made through different processing routes and have different structures. The microstructures are reasonably stable in most service environments [40,99]. Molybdenum will carburize, forming Mo_2C, in the presence of carbon [78]. This formation leads to embrittlement of the molybdenum, which could lead to cracking of the coating. It is possible that this Mo_2C layer may also improve oxidization resistance.

Scope for Microstructural Enhancement: 4/5. The C/C composites score 4/5 on scope for microstructural enhancement because the carbon fiber microstructure can be tailored using different processing routes, and the C/C composite microstructure is similarly controlled by various densification processes and fiber architecture [40,97,99]. Refractory-coating microstructure is also somewhat tailorable—different deposition techniques and parameters often lead to different microstructures and, therefore, different properties.

4.6.4 Rationale for Manufacturability

Reproducibility/Consistency: 3/5. The C/C formation process is established and reproducible. Several parameters must be controlled to produce the fibers and the composites [40,93,99]. These factors include pressure, temperature, gas flow rate, and carburizing environment. In addition to the composite substrate, deposition of the coating can require control of the temperature, pressure, and gas flow rates. Because the coating process is similar to the matrix densification process, no additional process variables must be controlled, resulting in a score of 3 for reproducibility/consistency.

Process Complexity: 3/5. Once the C/C composite is produced, the refractory layer can be deposited onto it. Although this step adds complexity to the overall process, adding a CVD, PVD, or solution-based deposition method to the process, it does not add any additional pre- or postprocessing steps. Therefore, a score similar to that of the composite backbone is given.

Cost: 3/5. CVD, PVD, ALD, and solution methods are the main methods to apply thin coatings of refractory metals. These methods represent the current commercial processing method; therefore, a score of 3 is given.

Scalability: 4/5. The C/C materials have been fabricated into large components such as rocket nozzles, and large numbers of C/C composites for use as brake discs have been fabricated simultaneously [40,93,99]. The main concern is the ability to create fiber architectures of adequate size and shape. With regards to coatings, PVD methods require high vacuum levels and line of sight. CVD methods also often require a vacuum. Both methods can require high temperatures to deposit the coating. The creation of a large furnace and vacuum system that can accommodate large and numerous parts is a concern. Still, these issues leave the layered composites with three scalability concerns, giving them a score of 4.

Production Method TRL: 5/5. Molybdenum coating techniques and C/C fabrication methods are established and working. The rank of 7–8 TRL indicates that methods are established for coating, but systems for tubes need development/work.

Raw Material Supply: 4/5. The 2022 mine production of molybdenum in the United States amounted to 42,000 metric tons, ranking third behind China and Chile [127].

Flexibility of Manufacturing: 5/5. CVD, PVD, electroplating, and more will produce coatings of refractory metals. These methods represent the main methods of thin film coating [91].

Conventional Machining: 3/5. Refractory coatings can be deposited on components after they are assembled. Therefore, the conventional machining score is dominated by that of the composite backbone.

Near Net Shaping (Complexity of Shape): 3/5. Although C/C scores a 4, the formation of quality coatings can be difficult on complex parts. This difficulty is because PVD methods require line of sight, and CVD processes are diffusion-limited and therefore need the vapor to reach all parts of a component equally. Thus, although relatively complex parts can be fabricated out of C/C, refractory-coated C/C is given a 3.

4.7 RATIONALES FOR SCORING COATED SYSTEM ZIRCONIUM-COATED CARBON FIBER–REINFORCED CARBON

The Zr/C-C composite was given a total score of 89 out of a possible 135 (or 3.3 out of 5 on average) based on the decision criteria matrix. This value is the sum of the cumulative scores for application space

(17 out of a possible 25), environmental compatibility (15 out of a possible 25), physical and mechanical properties (24 out of a possible 40), and manufacturability (33 out of a possible 45).

4.7.1 Rationale for Application Space Scores

Applicability to Different Reactor Types: 4/5. Refractory alloys are seen as candidate materials for GFRs (in-core), LFRs (cladding and out-of-core structural), and MSRs (in-core) [103,118].

Other Industry Experience: 3/5. The C/C composites are used in a plethora of applications. The application of a hermetic metal seal to a composite material has applications outside of the nuclear industry (e.g., for heat pipes) [128].

Data Availability: 2/5. Limited literature is available for zirconium coatings on C/C composites. Studies have been performed on the interaction of zirconium cladding with carbon in the context of a small modular reactor, and studies have been performed using zirconium-based coatings on SiC-coated C/C composites [131,132].

Code and Standards Availability: 3/5. The ASME *Boiler Pressure Vessel Code*, under Section III, Division 5, Subsection HH, covers design and construction rules for high-temperature reactor components with ceramic composites [77].

Component Versatility: 5/5. Coated C/C composites will be applicable to many of the same applications as the uncoated composites. The main difference is their compatibility with the coolant/process environment. Therefore, refractory-coated composites are candidate materials for in-core structural, cladding, and out-of-core structural materials [103,118].

4.7.2 Rationale for Environmental Compatibility

Radiation Resistance: 1/5. The C/C composites are known to exhibit swelling exceeding 1% volumetric change at doses approximately 10 dpa. The extent of the swelling and dimensional changes is dependent on their fiber type and architecture [84,94,95]. Notably, C/C composites maintain their physical properties better than typical graphite. Also, the Wigner effect can cause unwanted heating and energy release in graphite materials. Zirconium has been extensively used in thermal reactors; therefore, its radiation resistance is not a concern in these energies. However, fast neutrons will damage zirconium [133]. Still, the underlying composite response to radiation is deemed more significant than the zirconium coating.

Elemental Transmutation: 4/5. Most isotopes of zirconium are stable or have short half-lives (days) or extremely long half-lives ($>10^6$ years). The most concerning isotope is ^{93}Zr ($t_{1/2}$ = 1.53.× 10^6 years), but it has low specific activity and low energy emission [134]. Therefore, the transmutation of zirconium is expected to have negligible effects, and the effects of transmutation on the composite are expected to dominate.

High-Temperature Oxidation Resistance: 4/5. Zirconium forms a passive oxide scale at low temperatures. Zirconium will experience breakaway oxidization between 700°C and 800°C in the right environments [135]. Consequently, the maximum temperatures (in air) of zirconium alloys are limited to approximately 600°C. Therefore, zirconium is given a 4.

Neutronics Compatibility: 3/5. Carbon, in the form of graphite, is a known neutron moderator. This characteristic is important to consider, but C/C composites may be substituted for in-core graphite components to increase strength/structural properties of the graphite moderator. Zirconium is the

preeminent cladding material used in reactors today, largely because of its ideal neutron cross sections. A coating of zirconium will have minimal effects on the neutronics performance of a reactor.

Coolant Compatibility and Corrosion Resistance: 3/5. Refractory metals are seen as compatible with liquid metal coolants (i.e., Pb, Li). They are also proposed for applications in MSRs and GFRs [118,124]. However, there is concern that they will oxidize because of oxygen impurities at the temperatures of the HTGR. Therefore, they are given a score of 3, representing moderate but potential compatibility with various coolants.

4.7.3 Rationale for Physical and Mechanical Properties

Thermal Conductivity: 3/5. Zirconium has a thermal conductivity of 22.7 W/(m·K) at 25°C [126]. The thermal conductivity of the entire layered composite will depend on the C/C backbone, as well, with values ranging from 27 to 200 W/(m·K).

Thermal Capacity: 4/5. Zirconium has a melting point of 1,854°C [126]. The VHTR outlet temperature of 1,000°C represents approximately 0.54 T_m.

Tensile Properties: 4/5. The C/C composites have demonstrated tensile strength falling between 23 and 1,100 MPa depending on fiber type and architecture. Typical values fall closer to 150 MPa, resulting in a score of 4 for tensile properties [40,84,93,96].

Creep Performance: 3/5. Graphite is known to creep with neutron irradiation, and C/C composites have been demonstrated to experience >1% volumetric change at doses approximately 10 dpa [95,97]. However, no rupture is expected because graphite has been used in the suggested reactor types before. Therefore, C/C composites score 3/5 on creep performance.

Fatigue Resistance: 3/5. Fiber-reinforced composites are designed to resist crack propagation. Although they might not have the same fatigue resistance of metal alloys, CMCs are anticipated to have satisfactory fatigue resistance (3/5).

Fracture Toughness: 1/5. The C/C composites have demonstrated fracture toughness values ranging from 0.52 to 5.1 MPa√m. This value depends on their fiber architecture and matrix fabrication technique [98].

Microstructural Dependency: 2/5. The properties of a C/C composite are dependent on the arrangement, type, and treatment of the fibers used. The fibers are made through different processing routes and have different structures. The microstructures are reasonably stable in most service environments [40,99]. Zirconium is expected to form ZrC in the presence of carbon, such as that in C/C composites. The ZrC itself has high temperature stability and good oxidation resistance but may lead to embrittlement of the coating.

Scope of Microstructural Enhancement: 4/5. The C/C composites score 4/5 on scope for microstructural enhancement because carbon fiber microstructure can be tailored using different processing routes, and the C/C composite microstructure is similarly controlled by various densification processes and fiber architecture [40,93,99]. Refractory-coating microstructure is also somewhat tailorable; different deposition techniques and parameters often lead to different microstructures and, therefore, different properties.

4.7.4 Rationale for Manufacturability

Reproducibility/Consistency: 3/5. The C/C formation process is established and reproducible. Several parameters must be controlled to produce the fibers and the composites [40,93,99]. These factors include pressure, temperature, gas flow rate, and carburizing environment. In addition to the composite substrate, deposition of the coating can require control of the temperature, pressure, and gas flow rates. Because the coating process is similar to the matrix densification process, no additional process variables must be controlled, resulting in a score of 3 for reproducibility/consistency.

Process Complexity: 3/5. Once the C/C composite is produced, the refractory layer can be deposited onto it. Although this step adds complexity to the overall process, adding a CVD, PVD, or solution-based deposition method to the process, this does not add any additional pre- or postprocessing steps. Therefore, a score similar to that of the composite backbone is given.

Cost: 3/5. CVD, PVD, ALD, and solution methods are the main methods to apply thin coatings of refractory metals. These methods represent the current commercial processing method; therefore, a score of 3 is given.

Scalability: 4/5. The C/C materials have been fabricated into large components such as rocket nozzles, and large numbers of C/C composites for use as brake discs have been fabricated simultaneously [40,93,99]. The main concern is the ability to create fiber architectures of adequate size and shape. With regards to coatings, PVD methods require high vacuum levels and line of sight. CVD methods also often require a vacuum. Both methods can require high temperatures to deposit the coating. The creation of a large furnace and vacuum system that can accommodate large and numerous parts is a concern. Still, these issues leave the layered composites with three scalability concerns, giving them a score of 4.

Production Method TRL: 5/5. Zirconium coating techniques and C/C fabrication methods are established and working. The rank of 7–8 TRL indicates that methods are established for coating, but systems for tubes need development/work.

Raw Material Supply: 4/5. The United States produced <100,000 metric tons of zirconium in 2022. The world's leading producers of zirconium were Australia, Senegal, and South Africa [127].

Flexibility of Manufacturing: 5/5. CVD, PVD, electroplating, and more will produce coatings of refractory metals. These methods represent the main methods of thin film coating [91].

Conventional Machining: 3/5. Refractory coatings can be deposited on components after they are assembled. Therefore, the conventional machining score is dominated by that of the composite backbone.

Near Net Shaping (Complexity of Shape): 3/5. Although C/C scores 4, the formation of quality coatings can be difficult on complex parts. This difficulty is because PVD methods require line of sight, and CVD processes are diffusion-limited and therefore need the vapor to reach all parts of a component equally. Thus, although relatively complex parts can be fabricated out of C/C, refractory-coated C/C is given a 3.

4.8 RATIONALES FOR SCORING COATED SYSTEM TUNGSTEN-COATED SILICON CARBIDE FIBER–REINFORCED SILICON CARBIDE

The W/SiC-SiC composite was given a total score of 95 out of a possible 135 (3.52/5 on average) based on the decision criteria matrix. This value is the sum of the cumulative scores for application space (19 out of a possible 25), environmental compatibility (18 out of a possible 25), physical and mechanical properties (26 out of a possible 40), and manufacturability (32 out of a possible 45).

4.8.1 Rationale for Application Space Scores

Applicability to Different Reactor Types: 4/5. Refractory alloys are seen as candidate materials for GFRs (in-core), LFRs (cladding and out-of-core structural), and MSRs (in-core) [113,118]. There is some concern that tungsten will react with molten salts and steam. Refractory metals are also seen as candidate materials for heat pipe linings for space reactors.

Other Industry Experience: 3/5. Tungsten-coated SiC/SiC is not widely used, but extensive experience with SiC/SiC exists in the aerospace industry [128]. The application of a hermetic metal seal to a composite material has applications outside of the nuclear industry (e.g., for heat pipes).

Data Availability: 4/5. The W/SiC-SiC composite has been studied as first wall materials for fusion reactors [136,137].

Code and Standards Availability: 3/5. The ASME *Boiler Pressure Vessel Code*, under Section III, Division 5, Subsection HH, covers design and construction rules for high-temperature reactor components with ceramic composites [77].

Component Versatility: 5/5. Coated SiC/SiC composites will be applicable to many of the same applications as the uncoated composites. The main difference is their compatibility with the coolant/process environment. Therefore, refractory-coated composites are candidate materials for in-core structural, cladding, and out-of-core structural materials [113,118].

4.8.2 Rationale for Environmental Compatibility

Radiation Resistance: 3/5. The SiC/SiC swelling falls between 0.8% and 2% for doses >10 dpa but does not increase up to doses of 100 dpa. Refractory alloys such as tungsten and molybdenum may experience swelling and embrittlement for low-dpa and low–operating temperature conditions. The chief concern in a coated application is that this swelling and embrittlement may induce dimensional changes in the coating, leading to delamination from the SiC/SiC composite. Although these concerns exist for the alloys, the response to radiation of the composite is expected to be more important because the structural properties of the material depend on the composite backbone [114,120].

Elemental Transmutation: 4/5. In addition to the transmutation concerns of SiC/SiC, the tungsten coating can also transmute. Transmutation of tungsten (^{184}W and ^{186}W) to rhenium and subsequently rhenium to osmium can affect microstructural, physical, and mechanical properties of tungsten. This formation could degrade the coating adhesion and hermiticity [120,121].

High-Temperature Oxidation Resistance: 4/5. Tungsten oxidation increases above 650°C, with cracking and spallation occurring around 750°C. Below 500°C, tungsten forms a stable WO_3 compound in oxidizing environments [122,123].

Neutronics Compatibility: 4/5. The SiC has been used in TRISO fuel particles and is seen as an ATF candidate, as well as a candidate for in-core materials of a GFR. Its effective neutron absorption cross section is 0.10 compared with a zirconium alloy's. Tungsten alloys have 35× the neutron absorption cross section of zirconium. However, in a layered composite approach, the coating will be thin, and its effect on the neutronics of a reactor are expected to be negligible [79,80,84,113].

Coolant Compatibility and Corrosion Resistance: 3/5. Refractory metals are seen as compatible with liquid metal coolants (i.e., Pb, Li). They are also proposed for applications in MSRs and GFRs [118,124]. However, there is concern that they will oxidize because of oxygen impurities at the temperatures of the

HTGR. Therefore, they are given a score of 3, representing moderate but potential compatibility with various coolants.

4.8.3 Rationale for Physical and Mechanical Properties

Thermal Conductivity: 3/5. Tungsten maintains ≥84 W/(m·K) at temperatures up to 500°C up to doses of 5.8 dpa. However, SiC has a lower thermal conductivity (5–50 W/[m·K]) [125,138].

Thermal Capacity: 5/5. Tungsten has a melting point of 3,414°C. The VHTR outlet temperature of 1,000°C represents 0.29 T_m [126].

Tensile Properties: 3/5. The SiC/SiC YS falls between 100 and 225 MPa [44].

Creep Performance: 5/5. The SiC material has limited thermal creep at <1,400°C [138].

Fatigue: 3/5. Fiber-reinforced composites are designed to resist crack propagation. Although they might not have the same fatigue resistance of metal alloys, CMCs are anticipated to have satisfactory fatigue resistance. The SiC/SiC has been shown to have a static fatigue limit stress of approximately 70 MPa and cyclic fatigue limit stress of approximately 140 MPa [113].

Fracture Toughness: 1/5. The SiC/SiC has a fracture toughness of K_IC = 3.2–5.5 MPa√m [114].

Microstructural Dependency: 2/5. Carbon will diffuse between tungsten and SiC, forming WC and tungsten silicides, which weaken the material. Furthermore, the properties of SiC/SiC depend on the fiber microstructure and weave pattern used. The most recent generation of fibers lead to more tolerant/stable properties in anticipated service environments [124,139].

Scope for Microstructural Enhancement: 4/5. The SiC fibers are required to have a certain microstructure to be radiation-tolerant. Production methods for these fibers are established. Techniques such as CVI, the NITE process, and MI can be used to form the matrix. Refractory-coating microstructure is also somewhat tailorable; different deposition techniques and parameters often lead to different microstructures and, therefore, different properties [109].

4.8.4 Rationale for Manufacturability

Reproducibility/Consistency: 3/5. The SiC/SiC can be formed through several techniques and has been made for some time. It is reproducible and consistent but requires control over several parameters. The process parameters that must be controlled from start to finish include temperature, gas flow rate, pressure, and chemical stoichiometry [41,88,106]. In addition to the composite substrate, deposition of the coating can require control of the temperature, pressure, and gas flow rates. Because the coating process is similar to the matrix densification process, no additional process variables must be controlled.

Process Complexity: 3/5. Once the SiC/SiC composite is produced, the refractory layer can be deposited onto it. Although this step adds complexity to the overall process, adding a CVD, PVD, or solution-based deposition method to the process, it does not add any additional pre- or postprocessing steps. Therefore, a score similar to that of the composite backbone is given.

Cost: 3/5. CVD, PVD, ALD, and solution methods are the main methods to apply thin coatings of refractory metals. These methods represent the current commercial processing method; therefore, a score of 3 is given.

Scalability: 4/5. Some concern exists for large and long tubing, but in general, SiC CMCs may be fabricated into larger parts on a larger scale. Components such as brake discs, rocket nozzles, and scaled BWR channel boxes have been fabricated [41,93,95]. With regards to coatings, PVD methods require high vacuum levels and line of sight. CVD methods also often require a vacuum. Both methods can require high temperatures to deposit the coating. The creation of a large furnace and vacuum system that can accommodate large and numerous parts is a concern. Still, these issues leave the layered composites with three scalability concerns, giving them a score of 4.

Production Method TRL: 5/5. Tungsten coating techniques and SiC fabrication methods are established and working. The rank of 7–8 TRL indicates that methods are established for coating, but systems for tubes need development/work.

Raw Material Supply: 3/5. The availability of tungsten within the United States depends largely on scrap and imports. The USGS estimates that 80% of the world's tungsten production occurs within China, and no domestic production of tungsten has happened since 2015 [127].

Flexibility of Manufacturing: 5/5. CVD, PVD, electroplating, and more will produce coatings of refractory metals [91]. These methods represent the main methods of thin film coating.

Conventional Machining: 3/5. Refractory coatings can be deposited on components after they are assembled. Therefore, the conventional machining score is dominated by that of the composite backbone.

Near Net Shaping (Complexity of Shape): 3/5. Although SiC/SiC scores 4, the formation of quality coatings can be difficult on complex parts. This difficulty is because PVD methods require line of sight, and CVD processes are diffusion-limited and therefore need the vapor to reach all parts of a component equally. Thus, although relatively complex parts can be fabricated out of SiC/SiC, refractory-coated SiC/SiC is given a 3.

4.9 RATIONALES FOR SCORING COATED SYSTEMMOLYBDENUM-COATED SILICON CARBIDE FIBER–REINFORCED SILICON CARBIDE

The Mo/SiC-SiC composite was given a total score of 92 out of a possible 135 (3.41 out of 5 on average) based on the decision criteria matrix. This value is the sum of the cumulative scores for application space (17 out of a possible 25), environmental compatibility (16 out of a possible 25), physical and mechanical properties (26 out of a possible 40), and manufacturability (33 out of a possible 45).

4.9.1 Rationale for Application Space Scores

Applicability to Different Reactor Types: 4/5. Refractory alloys are seen as candidate materials for GFRs (in-core), LFRs (cladding and out-of-core structural), and MSRs (in-core) [113,118]. Refractory metals are also seen as candidate materials for heat pipe linings for space reactors.

Other Industry Experience: 3/5. Molybdenum-coated SiC/SiC is not widely used, but extensive experience with SiC/SiC exists in the aerospace industry. The application of a hermetic metal seal to a composite material has applications outside of the nuclear industry (e.g., for heat pipes) [128].

Data Availability: 2/5. Molybdenum-coated SiC/SiC is not widely used or studied. The Mo–C system has been studied, and the interactions of SiC with molybdenum have been studied. The Mo–Si (and Mo–Si–W) systems have been investigated as anticorrosion layers, as well [78,128,129,141].

Code and Standards Availability: 3/5. The ASME *Boiler Pressure Vessel Code*, under Section III, Division 5, Subsection HH, covers design and construction rules for high-temperature reactor components with ceramic composites [77].

Component Versatility: 5/5. Coated SiC/SiC composites will be applicable to many of the same applications as the uncoated composites. The main difference is their compatibility with the coolant/process environment. Therefore, refractory-coated composites are candidate materials for in-core structural, cladding, and out-of-core structural materials [103,118].

4.9.2 Rationale for Environmental Compatibility

Radiation Resistance: 3/5. Swelling of SiC/SiC falls between 0.8% and 2% for doses >10 dpa but does not increase up to doses of 100 dpa. Refractory alloys such as tungsten and molybdenum may experience swelling and embrittlement for low-dpa and low–operating temperature conditions. The chief concern in a coated application is that this swelling and embrittlement may induce dimensional changes in the coating, leading to delamination from the SiC/SiC composite. Although these concerns exist for the alloys, the response to radiation of the composite is expected to be more important because the structural properties of the material depend on the composite backbone [114,120].

Elemental Transmutation: 3/5. In addition to the transmutation concerns of SiC/SiC, ^{98}Mo can transmute (n, γ) to ^{99}Tc, which is a long-lived isotope ($t_{1/2}$ = 200,000 years). The ^{94}Mo isotope ecan also transmute (n,p) to ^{94}Nb ($t_{1/2}$ = 20,000 years). These isotopes pose a concern as long-lived radioactive species [121]. Transmutation of molybdenum to other elements will likely affect microstructural, physical, and mechanical properties.

High-Temperature Oxidation Resistance: 3/5. Molybdenum enters into a volatilization regime (forming MoO_3) in the range of 500°C–700°C, depending on the partial pressure of oxygen available. Below 450°C, molybdenum forms a passivating oxide [130].

Neutronics Compatibility: 4/5. The SiC composite has been used in TRISO fuel particles and is seen as an ATF candidate, as well as a candidate for in-core materials of a GFR [79,80,84]. Its effective neutron absorption cross section is 0.10 compared with zirconium alloys. Molybdenum alloys have 10× the neutron absorption cross section of zirconium [103]. However, in a layered composite approach, the coating will be thin, and its effect on the neutronics of a reactor are expected to be negligible.

Coolant Compatibility and Corrosion Resistance: 3/5. Refractory metals are seen as compatible with liquid metal coolants (i.e., Pb, Li). They are also proposed for applications in MSRs and GFRs [118,124]. However, there is concern that they will oxidize because of oxygen impurities at the temperatures of the HTGR. Therefore, they are given a score of 3, representing moderate but potential compatibility with various coolants.

4.9.3 Rationale for *Physical and Mechanical Properties*

Thermal Conductivity: 3/5. Molybdenum has an excellent thermal conductivity of 138 W/(m·K) at 25°C [126]. However, the thermal conductivity of the entire layered composite will depend on the SiC/SiC backbone, as well, with values ranging from 5 to 50 W/(m·K).

Thermal Capacity: 5/5. Molybdenum has a melting temperature of 2,622°C [126]. The VHTR outlet temperature of 1,000°C represents 0.38 T_m.

Tensile Properties: 3/5. The SiC/SiC YS falls between 100 and 225 MPa [112].

Creep Performance: 5/5. The SiC, which will dominate the creep performance of the Mo/SiC-SiC composite, has limited thermal creep at <1,400°C [138].

Fatigue: 3/5. Fiber-reinforced composites are designed to resist crack propagation. Although they might not have the same fatigue resistance of metal alloys, CMCs are anticipated to have satisfactory fatigue resistance. The SiC/SiC has been shown to have a static fatigue limit stress of approximately 70 MPa and cyclic fatigue limit stress of approximately 140 MPa [113].

Fracture Toughness: 1/5. The SiC/SiC has a fracture toughness of K_IC = 3.2–5.5 MPa√m [114].

Microstructural Dependency: 2/5. The properties of SiC/SiC depend on the fiber microstructure and weave pattern used. The most recent generation of fibers lead to more tolerant/stable properties in anticipated service environments [41]. Molybdenum will carburize, forming Mo_2C, in the presence of carbon [78]. This formation leads to embrittlement of the molybdenum, which could lead to cracking of the coating [124]. It is possible that this Mo_2C layer may also improve oxidization resistance.

Scope for Microstructural Enhancement: 4/5. The SiC fibers are required to have a certain microstructure to be radiation-tolerant. Production methods for these fibers are established. Techniques such as CVI, the NITE process, and MI can be used to form the matrix [41]. Refractory-coating microstructure is also somewhat tailorable; different deposition techniques and parameters often lead to different microstructures and, therefore, different properties.

4.9.4 Rationale for Manufacturability

Reproducibility/Consistency: 3/5. The SiC/SiC can be formed through several techniques and has been made for some time. It is reproducible and consistent but requires control over several parameters. The process parameters that must be controlled from start to finish including temperature, gas flow rate, pressure, and chemical stoichiometry [41,88,106]. In addition to the composite substrate, deposition of the coating can require control of the temperature, pressure, and gas flow rates. Because the coating process is similar to the matrix densification process, no additional process variables must be controlled.

Process Complexity: 3/5. Once the SiC/SiC composite is produced, the refractory layer can be deposited onto it. Although this step adds complexity to the overall process, adding a CVD, PVD, or solution-based deposition method to the process, it does not add any additional pre- or postprocessing steps. Therefore, a score similar to that of the composite backbone is given.

Cost: 3/5. CVD, PVD, ALD, and solution methods are the main methods to apply thin coatings of refractory metals. These methods represent the current commercial processing method; therefore, a score of 3 is given.

Scalability: 4/5. Some concern exists for large and long tubing, but in general, SiC CMCs may be fabricated into larger parts on a larger scale. Components such as brake discs, rocket nozzles, and scaled BWR channel boxes have been fabricated [41,93,140]. With regards to coatings, PVD methods require high vacuum levels and line of sight. CVD methods also often require a vacuum. Both methods can require high temperatures to deposit the coating. The creation of a large furnace and vacuum system that can accommodate large and numerous parts is a concern. Still, these issues leave the layered composites with three scalability concerns, giving them a score of 4.

Production Method TRL: 5/5. Molybdenum coating techniques and SiC fabrication methods are established and working. The rank of 7–8 TRL indicates that methods are established for coating, but systems for tubes need development/work.

Raw Material Supply: 4/5. The 2022 mine production of molybdenum in the United States amounted to 42,000 metric tons, ranking third behind China and Chile [127].

Flexibility of Manufacturing: 5/5. CVD, PVD, electroplating, and more will produce coatings of refractory metals [91]. These methods represent the main methods of thin film coating.

Conventional Machining: 3/5. Refractory coatings can be deposited on components after they are assembled. Therefore, the conventional machining score is dominated by that of the composite backbone.

Near Net Shaping (Complexity of Shape): 3/5. Although SiC/SiC scores 4, the formation of quality coatings can be difficult on complex parts. This difficulty is because PVD methods require line of sight, and CVD processes are diffusion-limited and therefore need the vapor to reach all parts of a component equally. Thus, although relatively complex parts can be fabricated out of SiC/SiC, refractory-coated SiC/SiC is given a 3.

4.10 RATIONALES FOR SCORING COATED SYSTEM ZIRCONIUM-COATED SILICON CARBIDE FIBER–REINFORCED SILICON CARBIDE

The Zr/SiC-SiC composite was given a total score of 94 out of a possible 135 (3.48 out of 5 on average) based on the decision criteria matrix. This value is the sum of the cumulative scores for application space (17 out of a possible 25), environmental compatibility (19 out of a possible 25), physical and mechanical properties (25 out of a possible 40), and manufacturability (33 out of a possible 45).

4.10.1 Rationale for Application Space Scores

Applicability to Different Reactor Types: 4/5. Refractory alloys are seen as candidate materials for GFRs (in-core), LFRs (cladding and out-of-core structural), and MSRs (in-core) [103,118]. Refractory metals are also seen as candidate materials for heat pipe linings for space reactors.

Other Industry Experience: 3/5. Zirconium-coated SiC/SiC is not widely used, but extensive experience with SiC/SiC exists in the aerospace industry. The application of a hermetic metal seal to a composite material has applications outside of the nuclear industry (e.g., for heat pipes) [128].

Data Availability: 2/5. Limited literature is available for zirconium coatings on SiC/SiC composites. Studies have been performed on the interaction of zirconium cladding with carbon in the context of a small modular reactor, and studies have been performed using zirconium-based coatings on SiC-coated C/C composites [131,132]. Furthermore, the wettability of zirconium on SiC has also been studied [141].

Code and Standards Availability: 3/5. The ASME *Boiler Pressure Vessel Code*, under Section III, Division 5, Subsection HH, covers design and construction rules for high-temperature reactor components with ceramic composites [77].

Component Versatility: 5/5. Coated SiC/SiC composites will be applicable to many of the same applications as the uncoated composites. The main difference is their compatibility with the coolant/process environment. Therefore, refractory-coated composites are candidate materials for in-core structural, cladding, and out-of-core structural materials [103,118].

4.10.2 Rationale for Environmental Compatibility

Radiation Resistance: 3/5. Swelling of SiC/SiC falls between 0.8% and 2% for doses >10 dpa but does not increase up to doses of 100 dpa [104]. Zirconium has been extensively used in thermal reactors;

therefore, its radiation resistance is not a concern in these energies. However, fast neutrons will damage zirconium [133]. Still, the underlying composite response to radiation is deemed more significant than the zirconium coating.

Elemental Transmutation: 4/5. Most isotopes of zirconium are stable or have short half-lives (days) or extremely long half-lives (>10^6 years). The most concerning isotope is ^{93}Zr ($t_{1/2}$ = 1.53 × 10^6 years), but it has low specific activity and low energy emission [134]. Therefore, the transmutation of zirconium is expected to have a negligible effect, and the effects of transmutation on the composite are expected to dominate.

High-Temperature Oxidation Resistance: 4/5. Zirconium forms a passive oxide scale at low temperatures. Zirconium will experience breakaway oxidization between 700°C and 800°C in the right environments [135]. Consequently, the maximum temperatures (in air) of zirconium alloys are limited to approximately 600°C. Therefore, zirconium is given a 4.

Neutronics Compatibility: 5/5. The SiC has been used in TRISO fuel particles and is seen as an ATF candidate, as well as a candidate for in-core materials of GFR [79,80,84]. Its effective neutron absorption cross section is 0.10 compared with a zirconium alloy's. Zirconium is the preeminent cladding material used in reactors today largely because of its ideal neutron cross sections. A coating of zirconium will have minimal effects on the neutronics performance of a reactor.

Coolant Compatibility and Corrosion Resistance: 3/5. Refractory metals are seen as compatible with liquid metal coolants (i.e., Pb, Li). They are also proposed for applications in MSRs and GFRs [118,124]. However, there is concern that they will oxidize because of oxygen impurities at the temperatures of the HTGR. Therefore, they are given a score of 3, representing moderate but potential compatibility with various coolants.

4.10.3 Rationale for Physical and Mechanical Properties

Thermal Conductivity: 3/5. Zirconium has a thermal conductivity of 22.7 W/(m·K) at 25°C [126]. However, the thermal conductivity of the entire layered composite will depend on the SiC/SiC backbone, as well, with values ranging from 5 to 50 W/(m·K).

Thermal Capacity: 4/5. Zirconium has a melting point of 1,854°C [126]. The VHTR outlet temperature of 1,000°C represents approximately 0.54 T_m.

Tensile Properties: 3/5. The SiC/SiC YS falls between 100 and 225 MPa [112].

Creep Performance: 5/5. The SiC, which will dominate the creep performance of the Mo/SiC-SiC composite, has limited thermal creep at <1,400°C [138].

Fatigue: 3/5. Fiber-reinforced composites are designed to resist crack propagation. Although they might not have the same fatigue resistance of metal alloys, CMCs are anticipated to have satisfactory fatigue resistance. The SiC/SiC has been shown to have a static fatigue limit stress of approximately 70 MPa and cyclic fatigue limit stress of approximately 140 MPa [113].

Fracture Toughness: 1/5. The SiC/SiC has a fracture toughness of K_IC = 3.2–5.5 MPa√m [114].

Microstructural Dependency: 2/5. The properties of SiC/SiC depend on the fiber microstructure and weave pattern used. The most recent generation of fibers lead to more tolerant/stable properties in anticipated service environments [41]. It is anticipated that zirconium will also form ZrC, leading to

embrittlement of the coating layer, when in contact with SiC. The ZrC itself has high temperature stability and good oxidation resistance.

Scope for Microstructural Enhancement: 4/5. The SiC fibers are required to have a certain microstructure to be radiation-tolerant. Production methods for these fibers are established. Techniques such as CVI, the NITE process, and MI can be used to form the matrix [41]. Refractory-coating microstructure is also somewhat tailorable; different deposition techniques and parameters often lead to different microstructures and, therefore, different properties.

4.10.4 Rationale for Manufacturability

Reproducibility/Consistency: 3/5. The SiC/SiC can be formed through several techniques and has been made for some time. It is reproducible and consistent but requires control over several parameters. The process parameters that must be controlled from start to finish include temperature, gas flow rate, pressure, and chemical stoichiometry [41,88,116]. In addition to the composite substrate, deposition of the coating can require control of the temperature, pressure, and gas flow rates. Because the coating process is similar to the matrix densification process, no additional process variables must be controlled.

Process Complexity: 3/5. Once the SiC/SiC composite is produced, the refractory layer can be deposited onto it. Although this step adds complexity to the overall process, adding a CVD, PVD, or solution-based deposition method to the process, it does not add any additional pre- or postprocessing steps. Therefore, a score similar to that of the composite backbone is given.

Cost: 3/5. CVD, PVD, ALD, and solution methods are the main methods to apply thin coatings of refractory metals. These methods represent the current commercial processing method; therefore, a score of 3 is given.

Scalability: 4/5. Some concern exists for large and long tubing, but in general, SiC CMCs may be fabricated into larger parts on a larger scale. Components such as brake discs, rocket nozzles, and scaled BWR channel boxes have been fabricated [41,93,140]. With regards to coatings, PVD methods require high vacuum levels and line of sight. CVD methods also often require a vacuum. Both methods can require high temperatures to deposit the coating. The creation of a large furnace and vacuum system that can accommodate large and numerous parts is a concern. Still, these issues leave the layered composites with three scalability concerns, giving them a score of 4.

Production Method TRL: 5/5. Zirconium coating techniques and SiC fabrication methods are established and working. The rank of 7–8 TRL indicates that methods are established for coating, but systems for tubes need development/work.

Raw Material Supply: 4/5. The United States produced <100,000 metric tons of zirconium in 2022. The world's leading producers of zirconium were Australia, Senegal, and South Africa [127].

Flexibility of Manufacturing: 5/5. CVD, PVD, electroplating, and more will produce coatings of refractory metals [91]. These methods represent the main methods of thin film coating.

Conventional Machining: 3/5. Refractory coatings can be deposited on components after they are assembled. Therefore, the conventional machining score is dominated by that of the composite backbone.

Near Net Shaping (Complexity of Shape): 3/5. Although SiC/SiC scores 4, the formation of quality coatings can be difficult on complex parts. This difficulty is because PVD methods require line of sight, and CVD processes are diffusion-limited and therefore need the vapor to reach all parts of a component

equally. Thus, although relatively complex parts can be fabricated out of SiC/SiC, refractory-coated SiC/SiC is given a 3.

4.11 CONCLUDING REMARKS ON THE EVALUATION OF COMPOSITES

Ultimately, W/SiC-SiC has the highest score (95/135) of all coated composites. The scoring for each coated composite was extremely close, with the scores varying by only three points. In general, this result makes sense because most properties of the refractory-coated composite materials depend upon the properties of the backbone composites themselves. Because there are only two backbone composites, there is significant overlap in the scoring of these materials. Furthermore, because the metal coatings are all refractory metals, their properties are also similar.

The most significant variances in scoring can be linked to the criteria of data availability, elemental transmutation, thermal capacity, and a small variance in raw material supply. Tungsten-coated SiC/SiC is a material of great interest to the fusion community. Therefore, it has been widely studied and received a higher score than the other refractory coatings. Both tungsten and molybdenum are expected to transmute to different elements in the presence of neutron irradiation. Molybdenum, however, will transmute to ^{99}Tc and ^{94}Nb, both of which are long lived isotopes, thus leading to a lower score based on the decision criteria matrix. Zirconium has the lowest melting temperature of all materials considered. For this evaluation, a reactor operating temperature of 1,000°C was assumed, corresponding with the outlet temperature of the VHTR. This temperature was chosen because refractories and composites are candidate materials for the VHTR. A temperature of 1,000°C represents 0.54 T_m for zirconium, which is the highest fraction of T_m for any of the materials. Finally, the manufacturability for all coated composites is very similar. This result is because the production process for composites is very similar, relying on similar techniques to produce C/C and SiC/SiC CMCs and the coatings. The main variation here is in the raw material supply. Tungsten is not produced in the United States, whereas molybdenum and zirconium are. The United States is not, however, the leading producer of any of these materials.

Based on the results of the evaluation using the decision criteria matrix, it is recommended that tungsten-coated SiC-SiC be pursued for further development under the AMMT Program. Because of their similar scoring, should time and resources allow, continued pursuit of all refractory-coated composites would also be beneficial.

4.12 BULK REFRACTORY ALLOYS

4.12.1 Bulk Refractory Alloys for Nuclear Energy Applications: Preliminary Results and Challenges

Refractory metals are attractive materials for nuclear reactors because they have high temperature stability, high wear resistance, good compatibility with liquid metal coolants, and good thermal conductivity at elevated temperatures. The difficulty in conventional manufacturing and shaping of these types of alloys can be overcome by developing AM techniques, making additively manufactured refractory alloys an important material for consideration under the AMMT Program. The Sigma metal AM team at LANL has performed several initial studies using the EOS M290 LPBF machine to enable further investigation into refractory alloys under the AMMT Program. These initial studies on the LPBF of refractories have been performed for a number of programs and summarized here for the benefit of AMMT. Some of these initial studies and challenges are highlighted prior to discussion of the evaluation of new refractory alloys using the decision criteria matrix.

Initial studies have included single weld tracks to determine fully dense processing parameters and surface roughness parameters. Single weld tracks are a development method used to determine bulk

parameters by determining the desired depth, width, morphology, and detail of a sufficient weld. A sufficient weld provides full density parts because of its ability to penetrate 2–3 layers of thicknesses deep while exhibiting an accommodating width that prevents a lack of fusion between adjacent passes. This method has repeatedly proven successful in testing a wide range of varying parameters simultaneously, obtaining rapid results, creating minimal material waste, having minimal required experimentation, and giving a conservative estimate of the weld geometry. Single weld track maps, as shown in Figure 4-1a, allow AM operators to quickly determine selected parameters that provide an operating window, shown in Figure 4-1b, to fabricate density cubes and/or parallelograms and measure the density to determine the final processing parameters. Surface roughness is dependent on the upskin and downskin parameters. Contour parameters also come into play when performing thin wall optimization.

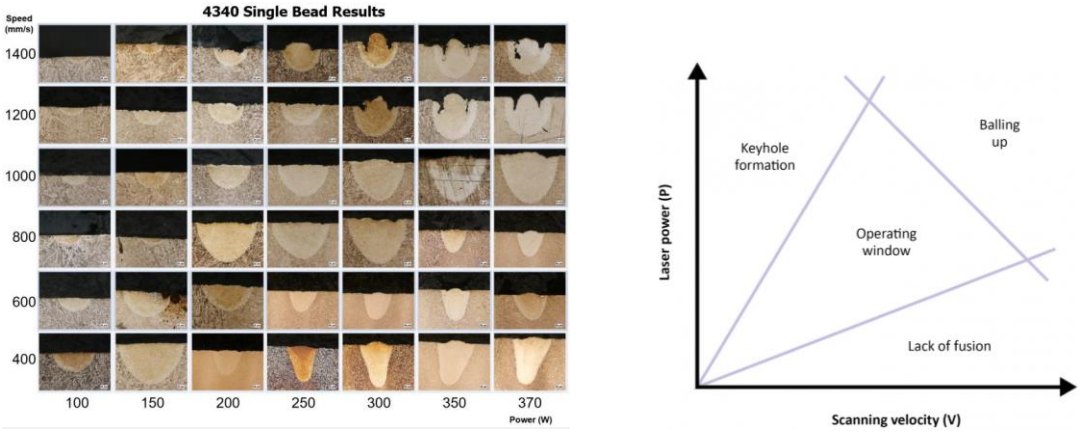

Figure 4-1. (a) Single weld tracks for 4340 (figure courtesy of Matthew Ryder, Worcester Polytechnic Institute) and (b) showing how varying parameters provide an operating window to determine the optimal bulk processing parameters.

Fully developed refractory metals include tantalum, tungsten, and a molybdenum alloy (TZM). Each has a melting point of 3,020°C, 3,422°C, and 2,623°C, respectively. Tantalum and tungsten have been used as nuclear reactor control rods because of their ability to withstand and/or exhibit a high temperature and hardness, excellent heat and electrical conductivity, corrosive resistance, and low thermal capacity. Tantalum was the first refractory metal the LANL team attempted to fabricate using the LPBF process. Bulk tantalum was successfully accomplished with a low porosity of 0.0108%, as shown in Figure 4-2.

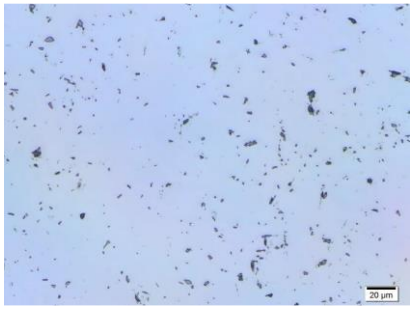

Figure 4-2. Tantalum microstructure showing porosity.

Following tantalum was the tungsten development, which proved to be more challenging because of the higher melting temperature. Insufficient fusion occurred between layers, which worsened as the *z*-height was increased. The single weld tracks were useful in narrowing down the operating window, yet it was determined that higher preheating, multiple scans, and/or in situ heat treatment were needed to

accommodate for the material differences. **Error! Reference source not found.** shows the fabricated d ensity blocks and the lack of fusion because of inadequate processing parameters.

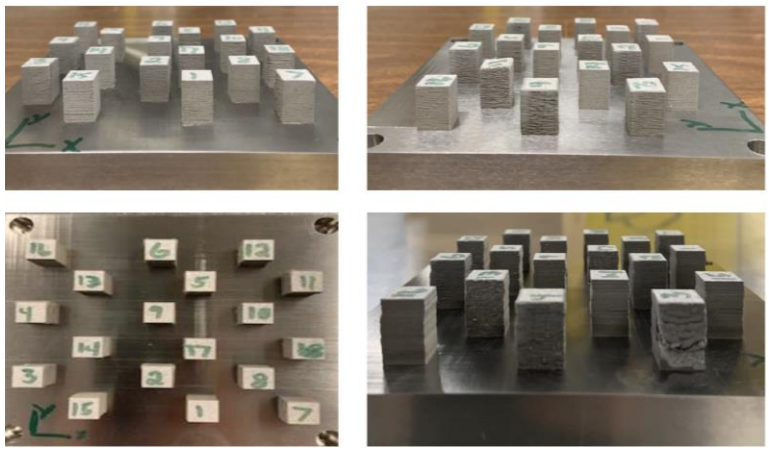

Figure 4-3. Tungsten density blocks using parameters from the operating window. Lack of fusion visible on the sides of block #3.

TZM is a material of interest for the microreactor program, where it would be used as the structural core. Metals 391 and grade 316L SS are currently approved materials for the microreactor. The operating temperature for both approved materials is approximately 800°C. In comparison, TZM provides a higher operating temperature of 1,600°C. TZM would increase the efficiency of the microreactor because of the greater thermal gradient. The latest development work has been for the W–Ni–Fe alloy, which is a good consideration for future LPBF refractory metals because of the familiarity with similar materials. With a high melting temperature of greater than 3,400°C, W–Ni–Fe is suitable for high-temperature environments, as well as providing good radiation shielding, making it a good candidate for microreactors. As shown in **Error! Reference source not found.**, initial studies have taken place in r egard to the fabrication of W–Ni–Fe using AM. With those initial studies of single beads, density cubes and tensile bars showed significant lack of fusion and fell well-short of the density that is achieved using AM. Significantly more time and effort would need to be invested into this alloy to ensure that fabrication can produce the desired properties.

Many processing difficulties were identified while fabricating refractory metals using LPBF. Those difficulties include preheating temperatures, limiting operating temperatures, hot cracking, porosity, and residual stresses. These lessons learned can be applied to future materials to prevent such issues, saving the operators and customers time and funding. It also brought the realization that system modifications will be needed to accommodate the higher fabricating temperatures. This ability will ensure a better as-built part that also exhibits the advantages of additively manufactured metals such as achieved complex geometry and higher strength.

4.12.2 Discussion and Evaluation of Potential Bulk Refractory Alloys

Other metals that are being considered because of the processing similarity to the aforementioned alloys are W–Ni–Fe, C-103, and Ta–W. One key point to keep in mind is the expense of these metals. The costs implies that there needs to be a justification for the greater application. Many powder vendors require a minimum order amount for purchasing. This amount typically ranges from 50 to 250 kg. C-103 and Ta–W are two materials for which powder is being sold by HC Stark. HC Stark is developing fabrication trials on an EOS M290 to study the feasibility of fabrication. When this study is completed, their results, parameters, and mechanical properties will be available, thus decreasing the amount of time needed to develop this alloy. Alloy C-103 has been used by several laboratories and companies around the United

States, including NASA. Pathways are available to get parameters and properties that are needed to fabricate parts that yield the desired properties.

Table 4-2 and Table list properties of C-103 and Ta–W alloys. Out of the refractory alloy considerations previously mentioned, it is of interest to perform development work on the Ta–W alloy because of the success the Sigma AM team has achieved with additively manufacturing these substances separately. The thermal needs and thermal gradients during the fabrication process are known, and a baseline parameter set to work off to determine full bulk density has been established. This knowledge, along with the results from the HC Stark feasibility of fabrication study, can lead to a fully developed material with minimal costs and research time for the rapid deployment for specific needs/cases. Development work would include the single-track welds, density cubes, and upskin and downskin parameters for surface roughness. Work on W–Ni–Fe and C-103 development would hopefully follow. More research is available on tantalum and niobium. In referencing these publications, these materials are evidently easier to manufacture and provide multiple processing parameters for various geometry thickness. Additionally, the data sets can be compared for modeling and designing purposes.

Table 4-2. Properties of tantalum tungsten alloy

Physical Properties	
Density	16.9g/cm^3
Mechanical Properties	
Hardness Vickers	245
Tensile strength ultimate	620 MPa
Tensile strength yield	482 Mpa
Elongation at break	30%
Modulus of elasticity	207 GPa
Electrical Properties	
Electrical resistivity	6 Ω·cm
Thermal Properties	
Melting point	3,030°C
Component Elements	
Tantalum	90%
Tungsten	10%

Applications include high-temperature, high-corrosion environments such as aerospace components, furnaces, and piping in nuclear plants.

Table 4-3. Properties of alloy C-103 niobium alloy

Physical Properties	
Density	8.850g/cm^3
Mechanical Properties	
Hardness Vickers	230
Tensile strength ultimate	386 MPa
Tensile strength yield	276 MPa
Elongation at break	20%
Modulus of elasticity	112 GPa
Thermal Properties	
Melting point	2,350°C
Component Elements	
Carbon	0.01%
Hafnium	9%–11%
Hydrogen	0.002%
Niobium	89%
Nitrogen	0.03%
Oxygen	0.03%
Tantalum	0.50%
Titanium	0.7%–1.3%
Tungsten	0.50%
Zirconium	0.70%

C-103 niobium alloy is well-suited for rocket and jet propulsion and jet propulsion applications utilized in spacecraft and launch vehicles. C-103 niobium alloy also has excellent resistance to high-frequency vibrations at cryogenic temperatures, which occur in many satellite applications, because of its low ductile-to-brittle transition temperature.

Table contains the scorecard for the refractory alloys W–Ta, W–Ni–Fe, TZM, and C-103. The scores were given based off literature, as well as experience and engineering judgement. Because W–Ta, W–Ni–Fe, and C-103 have not previously been manufactured through AM, each material was given a score of 3 for all criteria in the manufacturability category.

Table 4-4. Scorecard for refractory alloys

Criteria		TZM	W–Ta	W–Ni–Fe	C-103
Application Space	Applicability to Different Reactor Types	5	5	5	5
	Other Industry Experience	5	4	5	5
	Data Availability	4	1	3	4
	Code and Standards Availability	4	3	4	4
	Component Versatility	5	5	5	5
Environmental Compatibility	Radiation Resistance	4	3	4	5
	Elemental Transmutation	3	3	4	4
	High-Temperature Oxidation Resistance	3	4	5	5
	Neutronics Compatibility	3	3	3	4
	Coolant Compatibility and Corrosion Resistance	5	3	3	3
Physical and Mechanical Properties	Thermal Conductivity	5	3	3	3
	Thermal Capacity	5	3	5	5
	Tensile Properties	5	3	5	5
	Creep Performance	2	3	2	4
	Fatigue	3	3	3	4
	Fracture Toughness	3	3	3	5
	Microstructural Dependency	5	5	5	5
	Scope for Microstructural Enhancement	4	3	3	3
Manufacturability	Reproducibility/Consistency	3	3	3	3
	Process Complexity	4	3	3	3
	Cost	2	3	3	3
	Scalability	4	3	3	3
	Production Method TRL	4	3	3	3
	Raw Material Supply	4	3	3	3
	Flexibility of Manufacturing	4	3	3	3
	Conventional Machining	3	3	3	3
	Near Net Shaping (Complexity of Shape)	5	3	3	3
Overall Scores		106	87	97	105

4.13 CONCLUDING REMARKS ON THE EVALUATION OF REFRACTORY ALLOYS

Single weld studies were performed on TZM, tungsten, and tantalum to elucidate the relationship between laser power and scanning velocity and to determine fully dense processing parameters and surface roughness parameters for the LPBF AM of refractory alloys. The single weld tracks were useful in narrowing down the operating window; it was determined that different preheating, multiple scans, and/or in situ heat treatment will be needed to accommodate for material differences. Three preliminary studies performed will enable quicker processing and development of advanced refractory alloys under consideration for the AMMT project. Through evaluation using the decision criteria matrix, C-103 scored the highest out of the new refractory alloys (W–Ta, W–Ni–Fe, and C-103) with a score of 105 out of 135 (3.89 out of 5 on average). It is anticipated to have superior creep performance, fatigue, fracture toughness, and neutronics compatibility compared with W–Ta and W–Ni–Fe. Furthermore, it is more well-studied, with more data availability than the other two alloys. TZM also scored highly at 106 out of 135 (3.93 out of 5 on average), but it is currently being investigated under the microreactor program and does not need further investigation in the AMMT Program. Therefore, based on the results of the evaluation using the decision criteria matrix, it is recommended that C-103 be pursued for further development under the AMMT Program.

5. HIGH-ENTROPY ALLOYS AND DOWNSELECTION

5.1 INTRODUCTION TO HIGH-ENTROPY ALLOYS

This section defines HEAs and current manufacturing techniques applied during research and provides the classification of alloys. An extended literature survey on HEAs was performed to obtain information on a variety of alloy compositions and their key properties, and the results were reported in a separate AMMT milestone [6]. This section summarizes the key characteristics and conclusions from the literature survey activity.

HEAs are defined as alloys with five or more principal elements. The concentration of each principal element is 5%–35% [142]. In addition to the principal elements, HEAs may contain other elements in minor quantities below 5 atom %. The entropy of mixing multiple principal elements is much more pronounced in HEAs than conventional alloys, which possibly facilitates the formation of solid solution phases with less complicated crystal structures as compared with the conventional alloys. However, the presence of multi-principal elements of different groups increases the propensity for the formation of multiphase microstructures in HEAs. High mechanical strength [143], exceptional wear resistance [144], good high-temperature properties [145], and outstanding corrosion and oxidation resistance [146,147] are commonly observed in HEAs because of their unique multi-principal element compositions.

HEAs can be classified based on phase stability and mode of deformation; stable HEAs deform via dislocation slip, and metastable HEAs deform via TRIP and/or twinning-induced plasticity (TWIP) upon mechanical/thermal damage. Stable HEAs can be further classified based on the types of phases that constitute the microstructure (see Figure for classification). Moreover, the scope for application of HEAs across various industries is determined mainly by the mechanical properties and secondly by the mode of deformation, which forms the basis for this classification. A detailed literature review on HEAs summarizing different aspects such as the microstructure, phase constitution, and primary and postprocessing methods employed, including a summary of findings reported in the articles, is presented in Sections 3.4 and 3.5.

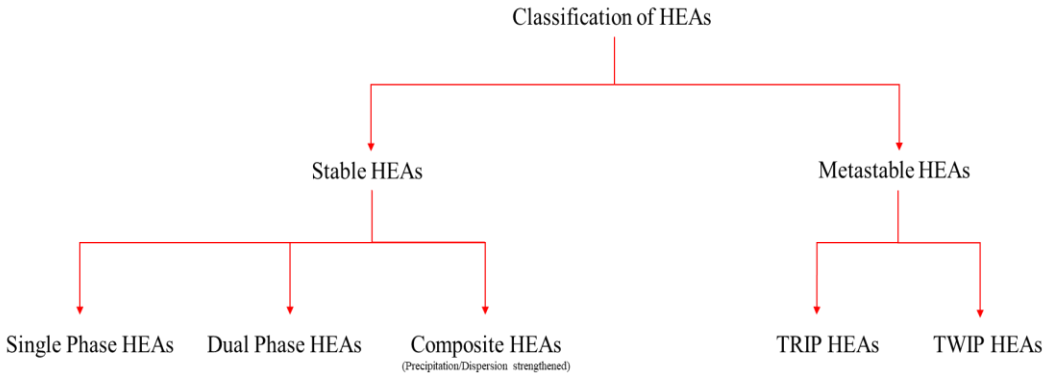

Figure 5-1. Classification of HEAs.

A variety of fabrication techniques have been used for the production of HEAs; the current state-of-the-art fabrication techniques that are employed to fabricate HEAs are discussed in the following subsections.

Solid-State Processing: This route includes a preliminary step for producing (via atomization or high-energy ball milling) either prealloyed HEA powders or individual elemental powders, which are later mixed using a ball mill or roller mixers to obtain the desired HEA compositions.

Cold Uniaxial Pressing and Sintering: The mixed/prealloyed HEA powders are filled inside a die (typically made of tool steel, H13 steel, or EN steel) and cold-pressed by two punches (from top and bottom) for a green compact. This green compact is then sintered below melting point to achieve a dense compact [148,149].

Hot Pressing: Hot pressing combines cold pressing and sintering into single step. Axial loads are applied on the heated powders so that high-density compacts can be obtained [150-152]. An advanced hot pressing, known as *hot isostatic pressing*, is also available for compacting HEA powders [153].

Spark Plasma Sintering: Spark plasma sintering is an advanced sintering process that is also known as *pulsed electric current sintering* and is used to compact powders significantly faster than the conventional sintering process. The fewer procedural steps make this process cost-, time-, and energy-efficient. Furthermore, high-density parts with limited grain growth can be obtained in this process [154-157].

ShAPE/Friction Stir Additive Processing: Friction stir additive processing is a cost-effective, deformation-based processing method that has recently been used to fabricate HEAs [158]. ShAPE is a novel technology that can potentially manufacture HEA tubes directly from powders. Although HEAs have not yet been processed using this technology, aluminum alloy tubes with significantly higher densities have been processed from the gas-atomized, prealloyed powders using this technique [75].

Conventional Liquid State Processing: HEAs are commercially manufactured through melting and casting techniques. One of the main drawbacks of the liquid state processing techniques is the evaporation of the low-melting elements. Furthermore, the slow cooling rates lead to the formation of dendritic/heterogenic microstructures, thereby requiring a postfabrication homogenization heat treatment prior to the application [159,160].

Arc Melting Process: Bulk ingots with higher densities (close to the theoretical density) can be produced via arc melting. Another advantage of the arc melting process is the low energy consumption. However, as mentioned previously, arc melting produces undesired heterogenous microstructures [159].

Vacuum Induction Melting Process: The only difference between arc melting and vacuum induction melting is that the vacuum induction melting [161,162] involves heating via electromagnetic induction as opposed to an electric arc in the arc melting process. The heating and cooling rates can be accurately

controlled for nearly homogenous microstructures in this process as compared with the arc melting process [163-165]. One of the main disadvantages of this method is the poor surface finish of the solidified products, which may need postprocessing in some cases.

Vacuum Levitation Melting Process: Vacuum levitation melting (VLM) is a novel induction melting furnace in which the raw metals are levitated in a crucible and alloyed by convective mixing by stirring while under a levitating force. VLM eliminates the contamination from the crucible, and the ingot retains a more uniform microstructure than when using the traditional arc melting technique [166-169].

Directional Solidification Process: In the directional solidification process, the melt is solidified along a narrow passage in a constrained manner to promote columnar grains, identical grain boundaries, and homogeneous microstructures. This process may even be employed after arc melting/vacuum induction melting to obtain uniformly columnar microstructures for specific applications [55,170]. The processing parameters, such as downward velocity, is shown to affect the YS of the product and thus can be tuned for enhanced mechanical performance [171].

Infiltration Process: The infiltration process falls under the category of squeeze casting and has the advantage of producing complex-shaped components with relatively lower porosities. This process has mainly been employed to fabricate HEA–oxide composites [172].

Electromagnetic Stirring: Electromagnetic stirring processes can produce high-quality ingots with minimal defects and porosity [173,174]. This process is achieved by placing the magnetic field coils (electromagnetic stirrer) around the crucibles containing the conducting metals/alloy melt, surrounding the crucibles. Three different stirring modes—vertical, horizontal, and helical—can be attained by controlling the electromagnetic field strengths [175].

Liquid State Additive Manufacturing: In addition to the typical advantages, such as design freedom, direct implementation of monolithic structures, eliminating the need for riveting/welding/joining and postprocessing, minimal failure risk, low wastage, and more, the AM processing also results in alloys with superior mechanical properties when compared with the conventionally processed counterparts [62,63,176,177]. Several different AM techniques are available for fabricating HEAs; however, powder bed fusion and DED are the most widely used techniques for manufacturing HEAs.

Powder Bed Fusion: Powder bed fusion techniques include selective laser modeling (SLM) and selective electron beam melting (SEBM). In powder bed fusion, parts are printed on a powder bed with a substrate underneath. The supporting effect of powder enables printing complex structures, such as cantilever, hollow, and complex arrays. The parts manufactured by SLM and SEBM exhibit very high dimensional accuracy with negligible surface roughness. Although the SLM equipment is simple and works in an argon environment, the SEBM equipment is quite sophisticated and needs a vacuum environment [178–181]. In most cases, the powder bed in SEBM is heated to avoid charging owing to the electron beam, which reduces the cooling rates. On the other hand, cooling rates of up to 10^4–10^5 K s^{-1} can be achieved in SLM as opposed to less than 100 K s^{-1} in the conventional casting techniques. Thus, parts with significantly finer grain and subgrain features [182,183] and enhanced mechanical properties can be produced via SLM [184].

Directed Energy Deposition: Laser engineered net shaping (LENS [63,67]), wire arc AM (WAAM) [80–83], and electron beam AM (EBAM) are the most popular DED techniques used for processing HEAs. LENS is a powder-fed technique, and WAAM and EBAM are wire-fed techniques. Also, LENS uses a laser beam in contrast to an electron beam in EBAM and electric arc in WAAM. The DED techniques typically produce parts with poor surface finish, low dimensional accuracies, and low design complexities compared with the powder bed fusion techniques. However, most DED-processed HEAs exhibit better mechanical properties than the conventionally cast counterparts.

5.2 PROMISING HIGH-ENTROPY ALLOY CANDIDATES FOR NUCLEAR APPLICATIONS

Few HEAs can be recommended based on the literature survey presented in the earlier milestone report [6]; these HEAs are as follows.

HEAs $Al_{0.3}Cu_{0.5}CrFeNi_2$, $Al_5Cr_{12}Fe_{35}Mn_{28}Ni_{20}$, and $Al_{10}Cr_{12}Fe_{35}Mn_{23}Ni_{20}$ are face-centered cubic (fcc)-based HEAs suggested by the US Nuclear Regulatory Commission (NRC) report titled *Use of High Entropy Alloys (HEAs) in Future Nuclear Applications*, published in January 2023. All the three alloys exhibit good mechanical properties at RT.

HEA $(Ni_2Co_2FeCr)_{92}Al_4Nb_4$ is a precipitation-strengthened HEA exhibiting approximately 500 MPa YS with a ductility of approximately 6% at 870°C. It is one of the few HEAs that exhibits remarkable high-temperature mechanical properties.

GRX-810 is an ODS-strengthened alloy recently developed by NASA with high-temperature (at 1,093°C) creep performance 2–3 orders of magnitude better than the current high-temperature alloys. Thus, GRX-810 is mainly a three component Ni–Co–Cr-based alloy with minor additions of other elements such as aluminum, titanium, niobium, tungsten, and carbon, and it may not be strictly classified under the category of HEAs. However, this material can be best classified as a medium-entropy alloy or an ODS alloy because of the presence of Y_2O_3 particles. *Therefore, the authors of this report recommend pursuing this material under a different work package under the AMMT Program.*

HEA $Al_{0.3}Ti_{0.2}Co_{0.7}CrFeNi_{1.7}$ is a precipitation-strengthened fcc HEA reported to exhibit a YS of approximately 1,630 MPa and good tensile ductility of approximately 15% at RT, which is significantly higher than most SSs. This HEA is also expected to have high-temperature stability up to approximately 1,100°C.

5.3 EXPERIMENTAL CHARACTERIZATION OF HIGH-ENTROPY ALLOYS

The primary objective of this work is to conduct advanced manufacturing feasibility studies on the downselected, promising HEAs based on the elaborate literature survey presented in Section 3 of this report. This study provides information to evaluate the benefits (if any) of advanced manufacturing methods that enable bulk economic manufacturing routes and may also further enhance the properties of the selected HEAs. The advanced manufacturing routes include liquid and solid-state manufacturing approaches. **Error! Reference source not found.** summarizes the experimental work executed to date in F Y 2023 and the work in progress. ShAPE is considered for the two downselected HEAs ($Al_{0.3}Ti_{0.2}Co_{0.7}CrFeNi_{1.7}$ and $Al_{10}Cr_{12}Fe_{35}Mn_{23}Ni_{20}$) because of its unique processing conditions, which result in finer microstructures with compositionally homogenous grains that would potentially enhance the mechanical properties. Additionally, the effect of solid-phase processing on the mechanical properties of a single-phase HEA can provide valuable information and potentially more economical routes to HEA adoption to the markets. It is therefore also recommended that a functional graded alloy to HEA as a final coating begin explored to determine the effect on the interlayers and interface properties. The technical details of the work completed are provided in the following sections.

5.4 DOWNSELECTED HIGH-ENTROPY ALLOY: $AL_{0.3}TI_{0.2}CO_{0.7}CRFENI_{1.7}$

5.4.1 Background

HEA $Al_{0.3}Ti_{0.2}Co_{0.7}CrFeNi_{1.7}$ is a precipitation-strengthened alloy reported to exhibit an YS of approximately 1,600 MPa with decent ductility at RT and is expected to have high-temperature stability

up to approximately 1,100°C [56]. This HEA was fabricated via two different AM techniques: DED and SLM. The evolution of the heterogeneous microstructures in the AD and subsequently annealed conditions and their tensile properties at RT have been reported previously [68,185]. However, the temperature-dependent mechanical behavior essential for nuclear applications was not yet investigated. This report provides a discussion on the microstructural differences, as well as the temperature-dependent (from RT to 500°C) nanoindentation behavior of the heterogeneous microstructures obtained via one-step annealing, post-DED, and SLM processing of HEA $Al_{0.3}Ti_{0.2}Co_{0.7}CrFeNi_{1.7}$. The differences in the nanoindentation behavior between the AD and the one-step annealed conditions of the DED and SLM-processed conditions are determined. The work in this section is presented in another publication [186].

5.4.2 Materials and Methods

This study used the Optomec LENS-750 system equipped with an IPG YLS-1500 fiber laser system (with a maximum power output of 1,500 W) for the DED and Trumpf TruPrint 1000 laser powder bed fusion system used for SLM. Prealloyed powders of HEA $Al_{0.3}Ti_{0.2}Co_{0.7}CrFeNi_{1.7}$ procured from Tosoh and shape metal deposition were used for both DED and SLM processing. The samples were provided by the University of North Texas.

The AD specimens from DED [referred to as DED(AD)] and SLM [referred to as SLM(AD)] were sectioned using the KENT USA (WSI-200) electric discharge machine. Sections from DED(AD) and SLM(AD) conditions were then individually encapsulated in a quartz tube backfilled with argon for the heat treatments (HTs) (800°C for 5 h followed by water quenching). These conditions will be hereafter referred to as DED(HT) and SLM(HT).

Scanning electron microscopy (SEM) imaging was performed on all four conditions in an FEI-Quanta Nova-Nano SEM 230. Nanoindentation tests (Hysitron Inc., Minneapolis, Minnesota, USA) were performed at RT, 250°C, and 500°C using a Sapphire Berkovich tip. The tests were carried out at a 1,000 mN load with a loading time of 5 s, holding time of 2 s, and unloading time of 5 s. A 50 μm spacing between indents was used to avoid overlap of plastic zones from adjacent indents. The high-temperature indentations were done in an Ar + H_2 atmosphere to minimize the oxidation of the samples, and the system was allowed to stabilize at each temperature for at least 15 min before performing the indentations. A minimum of 25 good indents were used for hardness calculations for statistics.

The phase fraction vs. temperature plot for HEA $Al_{0.3}Ti_{0.2}Co_{0.7}CrFeNi_{1.7}$ was simulated using Thermo-Calc software (with Thermo-Calc Software's TCS High Entropy Alloy Database [TCHEA3]).

5.4.3 Results and Discussion

The SEM backscattered images from the as-deposited [DED(AD)] and the one-step annealed conditions [DED(HT)] of the DED-processed HEA $Al_{0.3}Ti_{0.2}Co_{0.7}CrFeNi_{1.7}$ are shown in **Error! Reference source not found.**(a–c) and 5-2(d–e), respectively. The DED as-deposited condition shows a single-phase (fcc) microstructure with reasonably large, peculiar-shaped [62] grains, often with jagged grain boundaries. Additionally, some grains also exhibit solidification cells presumably arising from compositional segregation owing to the high solidification rates involved in DED processing. However, the possible formation of early-stage nanoscale $L1_2$ precipitates within the fcc matrix of the DED(AD) condition was previously observed in high-energy synchrotron x-ray diffraction results [185]. The annealing heat treatment (800°C for 5 h) conducted on the DED-processed HEA led to the partial recrystallization of fcc grains and a significant growth of the non-recrystallized fcc grains. The grain size of the non-recrystallized grains increased from approximately 81 μm in the DED(AD) to approximately 159 μm in the DED(HT) condition [185]. The annealing heat treatment also resulted in the formation of $L1_2$ precipitates with two different morphologies within the fcc matrix. The SEM images in **Error! Reference s**

ource not found.(d and e) reveal the rod-like $L1_2$ precipitates in the recrystallized fcc grains, and the SEM image in **Error! Reference source not found.**(f) shows the *equiaxed/near-spherical* $L1_2$ p recipitates in the non-recrystallized grains. The precipitation mechanism fundamentally differs between the two kinds of grains: continuous precipitation in the non-recrystallized grains and discontinuous precipitation in the recrystallized grains, leading to different morphologies for the $L1_2$ precipitates [185].

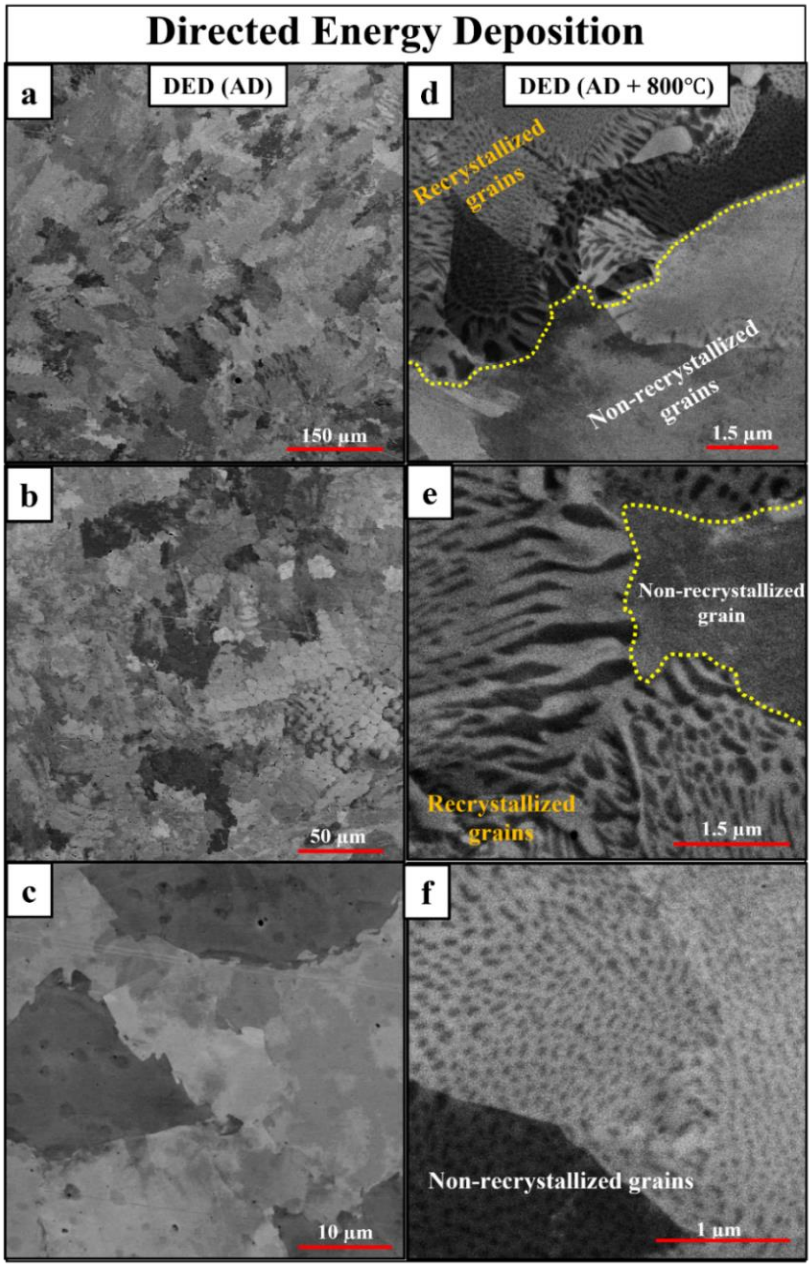

Figure 5-2. Low-, medium-, and high-magnification SEM backscattered images for (a–c) DED(AD) and (d–f) DED(HT or AD + 800°C) conditions of DED-processed HEA $Al_{0.3}Ti_{0.2}Co_{0.7}CrFeNi_{1.7}$.

The SEM backscattered images from the as-deposited [SLM(AD)] and the one-step annealed conditions [SLM(HT)] of the SLM-processed HEA $Al_{0.3}Ti_{0.2}Co_{0.7}CrFeNi_{1.7}$ are shown in Figure 5-3(a–c) and Figure 5-3(d–e), respectively. The SLM(AD) condition exhibits elongated, possibly growing epitaxially, fcc

grains with a significant fraction of solidification cells involving substantial compositional segregation [**Error! Reference source not found.**(a and b)]. Unlike the DED(AD) condition, the intercellular walls i n the SLM(AD) condition exhibited a body-centered cubic (bcc) + B2 microstructure [68]. The high-magnification SEM image of the intercellular region in **Error! Reference source not found.**(c) clearly s hows the fine-scale B2 precipitates in the darker bcc phase inside the cell wall. The SLM(AD) condition also showed early-stage nanoscale $L1_2$ precipitates within the fcc matrix [68]. The microstructures of the one-step annealed condition, SLM(HT) presented in **Error! Reference source not found.**(d–f), appears t o be identical to the DED(HT) condition [**Error! Reference source not found.**(d–f)]. However, the $L1_2$ precipitates in the SLM(HT) condition are marginally more refined than in the DED(HT) condition. The grain sizes in the as-deposited (~50 μm) and the one-step annealed conditions (~20 μm) are also lower in the case of the SLM-processed alloy as compared with the DED-processed counterpart.

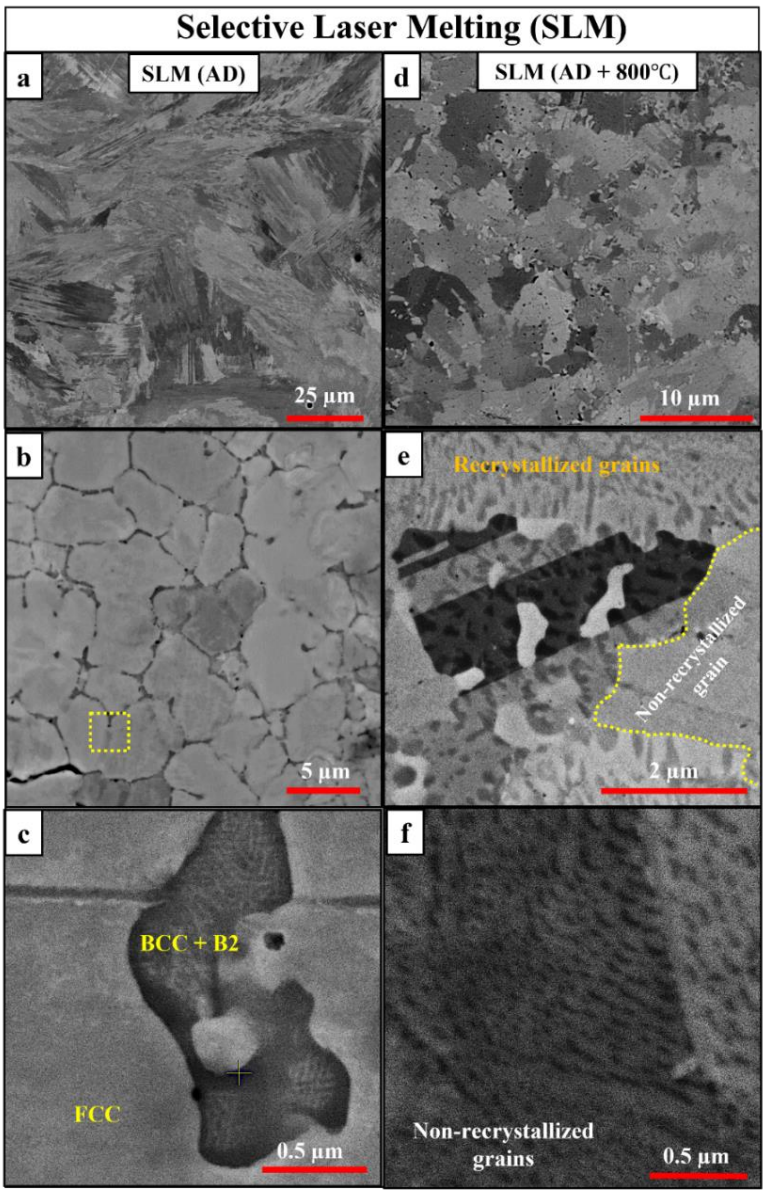

Figure 5-3. Low-, medium-, and high-magnification SEM backscattered images for (a–c) SLM(AD) and (d–f) SLM(HT or AD + 800°C) conditions of SLM-processed HEA $Al_{0.3}Ti_{0.2}Co_{0.7}CrFeNi_{1.7}$.

In short, the as-deposited conditions of DED- and SLM-processed HEAs exhibited predominantly single-phase fcc microstructure with a negligible fraction of $L1_2$ precipitates. Although the SLM(AD) condition revealed B2 + bcc microstructure in the intercellular regions between solidification cells, it is shown to have an insignificant effect on the mechanical properties owing to its low phase fraction, as well as large separation distances [68]. On the other hand, both heat-treated conditions, SLM(HT) and DED(HT), exhibited hierarchically heterogeneous microstructures at multiple length scales, *finer* recrystallized fcc grains with rod-like $L1_2$ precipitates, and *coarser* non-recrystallized fcc grains with equiaxed/spherical $L1_2$ precipitates.

Table 5-1. Nanoindentation hardness (in GPa) values for all four conditions of AM-processed HEA $Al_{0.3}Ti_{0.2}Co_{0.7}CrFeNi_{1.7}$

AM method	Condition	RT	250°C	500°C	% loss
DED	AD	4.157 ± 0.287	3.763 ± 0.212	3.197 ± 0.233	23.13↓
	AD + 800°C (HT)	4.710 ± 0.123	4.663 ± 0.183	4.387 ± 0.153	6.5↓
SLM	AD	4.116 ± 0.145	3.569 ± 0.171	3.560 ± 0.121	13.3↓
	AD + 800°C (HT)	4.654 ± 0.171	4.494 ± 0.132	4.427 ± 0.104	4.9↓

The nanoindentation tests were performed at three different temperatures—RT, 250°C, and 500°C—for all four AM-processed HEA conditions. The resultant hardness vs. temperature plot is presented in **Error! Reference source not found.**, and the corresponding hardness values are listed in Table . The p ercent loss (reduction) in hardness between the two temperatures RT and 500°C is calculated for all four conditions using the equation,

$$\%\ loss\ reduction = \frac{Hardness\ (RT) - Hardness\ (500℃)}{Hardness\ (RT)},$$

and the calculated values are listed in the last column of Error! Reference source not found.. The heat-t reated conditions [DED(HT) and SLM(HT)] exhibited remarkably higher hardness values (>4.3 GPa) at all three temperatures compared with the as-deposited conditions of this AM-processed HEA. This increase in the hardness can be attributed to the significantly higher phase fraction of the $L1_2$ precipitates in the heat-treated conditions as opposed to the much lower fractions of precipitates observed in the as-deposited conditions.

The anticipated decrease in the hardness with an increase in the temperature from RT to 500°C is observed for all four conditions, as shown in **Error! Reference source not found.**. However, the percent r eduction in the hardness values for the as-deposited conditions [23.1% for DED(AD) and 13.3% for the SLM(AD)] is substantially higher than the heat-treated conditions [6.5% for DED(HT) and 4.9% for SLM(HT)]. This large difference in the percent reduction in the hardness values can be attributed mainly to two factors: (1) relieving of stored residual stresses in the as-deposited conditions during the high-temperature testing and (2) the softer single-phase fcc microstructure compared with the harder hierarchical multiphase microstructures in the heat-treated conditions. It should be emphasized that the lower values of percent reduction in hardness with an increase in temperature in the heat-treated conditions further signify the stability of the hierarchically heterogeneous microstructures at elevated temperatures.

Although both DED and SLM as-deposited conditions showed nearly identical hardness values at RT, the SLM(AD) condition showed significantly higher hardness than the DED(AD) condition at elevated temperatures, especially at 500°C [**Error! Reference source not found.**(c)]. However, the heat-treated c onditions, DED(HT) and SLM(HT), showed practically overlapping performance at all three

temperatures, as shown in **Error! Reference source not found.** (d). The load vs. displacement (*P–h*) c urves obtained from the nanoindentation tests for all four conditions are presented in Figure . Serrated yielding behavior, also known as the Portevin–Le Chatlier (PLC) effect, was observed in the loading portion of the *P–h* curves for the DED(AD) and SLM(AD) conditions tested at 500°C, as shown in Figure (c).

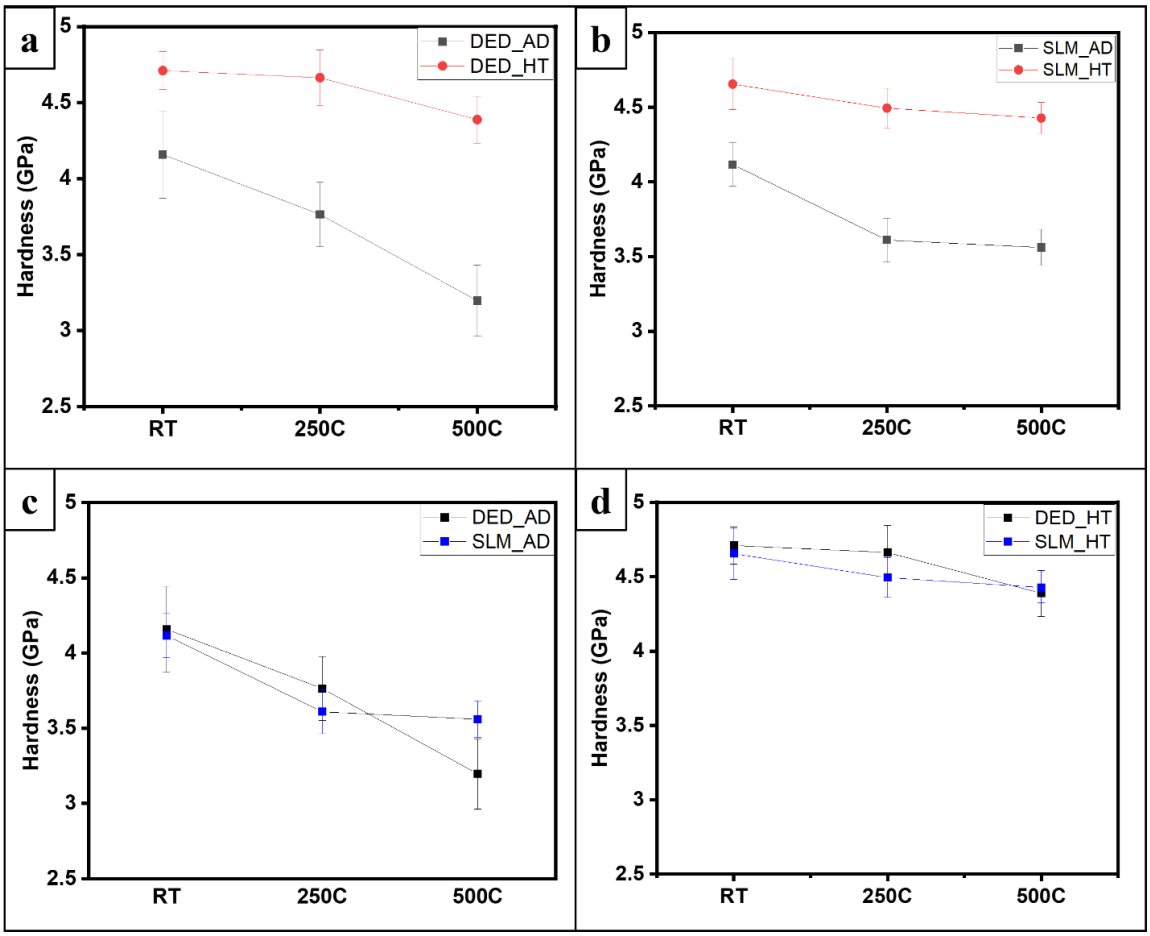

Figure 5-4. Hardness vs. temperature plots comparing (a) DED(AD) and DED(HT) conditions; (b) SLM(AD) and SLM(HT) conditions; (c) DED(AD) and SLM(AD) conditions; and (d) DED(HT) and SLM(HT) conditions of the AM-processed HEA $Al_{0.3}Ti_{0.2}Co_{0.7}CrFeNi_{1.7}$.

These perturbations or discontinuities indicate the mechanical instability of the microstructure during the deformation process. The serrated yielding behavior in metals or alloys is commonly associated with the activation of a heterogenous dislocation source and its multiplication under loading [187]. However, Schuh's [188] review on the "Nanoindentation studies of materials" additionally points out that phase transformations that occur during the nanoindentation process could also result in the serrated yielding or the PLC effect [189]. Therefore, microstructural characterization was performed on DED(AD) and SLM(AD) conditions post-nanoindentation (at 500°C), and the resultant SEM backscattered images are presented in Figures 5-6(a, b) and 5-6(c, d), respectively. Features resembling $L1_2$ precipitates were present in both conditions, demonstrating the possibility of the dynamic precipitation of the $L1_2$ phase within the fcc matrix during the nanoindentation testing at 500°C. Moreover, the phase fraction vs. temperature prediction for this HEA ($Al_{0.3}Ti_{0.2}Co_{0.7}CrFeNi_{1.7}$) presented in Figure 5-7 revealed almost 40% for the $L1_2$ phase at 500°C. It is envisaged that dynamic precipitation pins down the mobile dislocations, restoring the hardness locally during the deformation [190,191] Therefore, the serrated

yielding observed in the DED(AD) and SLM(AD) conditions during the nanoindentation loading (at 500°C) could be mainly due to the precipitation of the $L1_2$ phase within the fcc matrix.

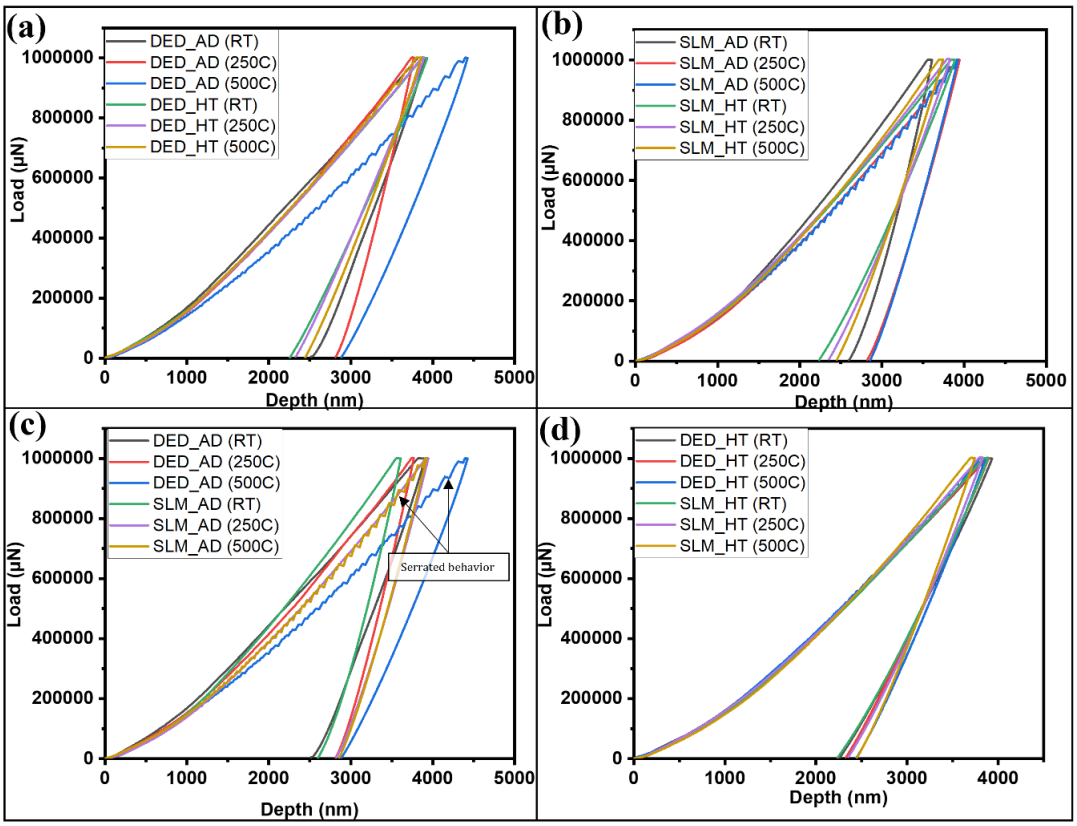

Figure 5-5. Representative load vs. displacement (*P–h*) curves as a function of temperature comparing (a) DED(AD) and DED(HT) conditions, (b) SLM(AD) and SLM(HT) conditions, (c) DED(AD) and SLM(AD) conditions, and (d) DED(HT)and SLM(HT) conditions for HEA $Al_{0.3}Ti_{0.2}Co_{0.7}CrFeNi_{1.7}$.

Notably, the same serrated behavior is not observed for SLM(AD) or DED(AD) conditions tested at RT or 250°C [**Error! Reference source not found.**(c)]. The phase fraction vs. temperature plot (in Figure 5-7) reveals no significant change in the $L1_2$ phase fraction for temperatures below 500°C. Therefore, it is intuitive that sluggish diffusion at lower temperatures makes the $L1_2$ precipitation kinetically unfavorable. Thus, no serrations were observed in the *P–h* curves for DED(AD) and SLM(AD) conditions tested at RT and 250°C. Similarly, the *P–h* curves in **Error! Reference source not found.**(d) for DED(HT) and S LM(HT) conditions did not reveal any signs of serrated yielding during nanoindentation, which again illustrates the stability of the hierarchically heterogeneous microstructures at elevated temperatures.

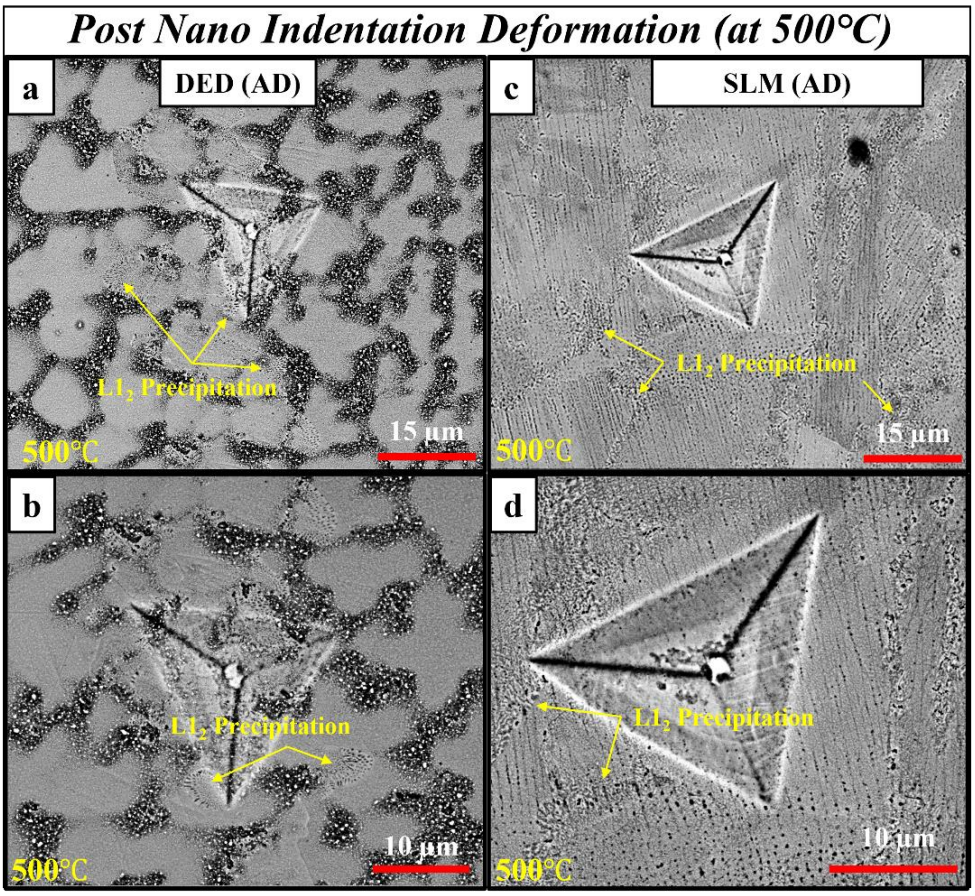

Figure 5-6. SEM backscattered images revealing the $L1_2$ precipitation post nanoindentation deformation at 500°C for (a, b) DED(AD) and (c, d) SLM(AD) conditions of the AM-processed HEA.

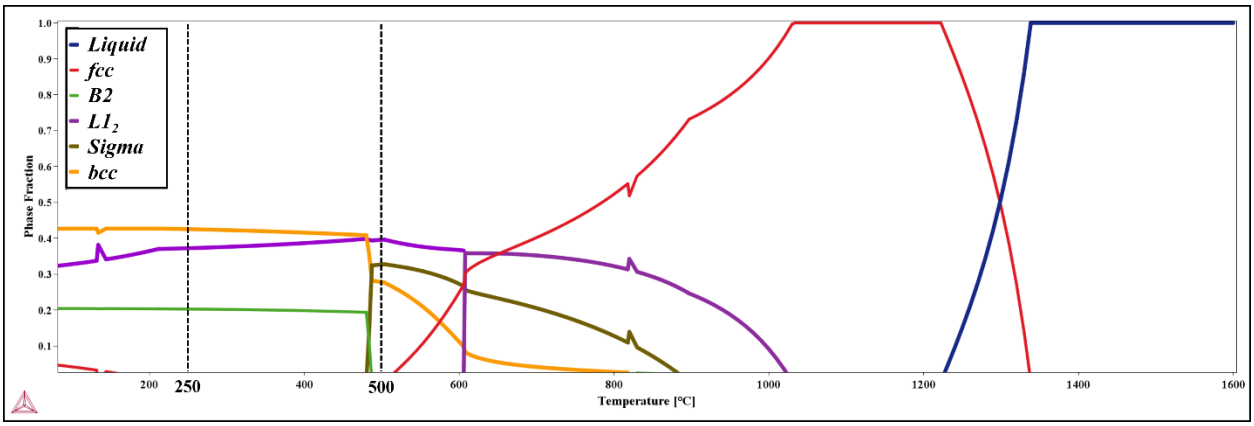

Figure 5-7. Phase fraction vs. temperature plot for HEA $Al_{0.3}Ti_{0.2}Co_{0.7}CrFeNi_{1.7}$ generated using Thermo-Calc software.

5.4.4 Summary

In summary, the temperature-dependent (from RT to 500°C) nanoindentation behavior of the DED- and SLM-processed HEA $Al_{0.3}Ti_{0.2}Co_{0.7}CrFeNi_{1.7}$ was investigated in the as-deposited and one-step annealed conditions for this study. The hierarchically heterogeneous microstructures obtained via simple, one-step

annealing of the DED- and SLM-processed HEA exhibited significantly better performance than the nearly homogeneous microstructures in the as-deposited state. The one-step annealed conditions revealed a less than 6.6% reduction in hardness values at 500°C compared with RT, and the as-deposited conditions showed a greater than 18% reduction in hardness between RT and 500°C. The one-step annealed conditions also exhibited significantly higher hardness than the as-deposited conditions owing to their multiphase (fcc + $L1_2$) microstructures, with a substantial fraction of ordered $L1_2$ precipitates. Furthermore, serrated yielding (PLC effect) indicative of microstructural instability was observed during nanoindentation deformation (at 500°C) for both SLM- and DED-processed conditions but not after the one-step annealing. Overall, the nanoindentation results signify the stability of these hierarchically heterogeneous microstructures developed via single-step annealing, exploiting the residual stresses in the AM-processed HEA $Al_{0.3}Ti_{0.2}Co_{0.7}CrFeNi_{1.7}$. The results presented in this study open strong possibilities for applications of HEAs in high-temperature nuclear reactors. ShAPE processing followed by high-temperature nanoindentation testing at 800°C is in progress.

5.5 DOWNSELECTED HIGH-ENTROPY ALLOY: $AL_{10}CR_{12}FE_{35}MN_{23}NI_{20}$

5.5.1 Background

According to the NRC report titled *Use of High Entropy Alloys (HEAs) in Future Nuclear Applications*, published in January 2023, three HEAs ($Al_{0.3}Cu_{0.5}CrFeNi_2$, $Al_5Cr_{12}Fe_{35}Mn_{28}Ni_{20}$, and $Al_{10}Cr_{12}Fe_{35}Mn_{23}Ni_{20}$) exhibited enhanced structural and functional properties over the code-certified materials. Furthermore, the report identifies AlCuCrFeNi and AlCrFeMnNi HEAs as compositional areas of interest for future studies. Among these three HEAs, $Al_{10}Cr_{12}Fe_{35}Mn_{23}Ni_{20}$ has the highest YS and UTS and therefore has been chosen for experimental work in the current work package. Cast rods of this HEA were procured from sophisticated alloys and ShAPE processing followed by nanoindentation testing is in progress.

5.6 GRADED HIGH-ENTROPY ALLOYS

5.6.1 Background

In nuclear reactor environments, in which the materials are subjected to thermal and mechanical stresses, corrosion, diffusion, and irradiation, the development of advanced coatings may prevent the materials from these degradation mechanisms. Novel materials and associated advanced manufacturing techniques for coatings, along with advanced characterization, are required to improve coatings' performances. The Fe–Co–Cr–Ni-based HEAs can present a single-phase fcc structure that demonstrates superior irradiation resistance compared with multiphase and bcc structures. Previous studies have revealed that there are significant challenges in manufacturing the single-phase HEAs with conventional casting methods.

This work uses DED AM as a coating materials development technology that allows the fabrication of graded HEAs. LENS DED is uniquely suited to tailor material properties and compositions to a specific application and features a high level of control over processing parameters that allows for microstructural and as-built optimization. The DED method can control the flow of powders during fabrication to result in a component with gradual variation of chemistry along the build direction and resulting in compositionally graded materials. This compositional variation also alters the inherent microstructure with changes in phase fraction, mechanical properties, and more. Thus, a proper design of coatings can be developed that benefits from spatial variation in properties.

5.6.2 Materials and Methods

The graded HEA composition was fabricated using DED method in a Optomec LENS MR-7 equipment at Idaho National Laboratory (INL) as part of an INL Laboratory Directed Research and Development (LDRD) project (2019–2021). The three alloy powders for mixing were 70Co–30Cr (commercially known as Stellite 21), 316L SS, and IN 718 alloy, and specimens of 10 layers of compositions were fabricated to create graded materials.

In INL's LDRD Program, microstructural characterization on graded sections of materials was performed using SEM, and compositional changes across the build were determined using energy dispersive spectroscopy (EDS) [192]. Nanoindentation was performed across the build direction to identify trends along complex sample compositions. Bulk cross sections were assessed for successful fusion and lack of macroscopic defects (e.g., unmelted particles, separation of layers) [193]. However, microscopic, inhomogeneous regions including unmelted powders and agglomerated elements (e.g., Co–Cr) were observed in optical and SEM imaging. The motivation of this work is to understand the details of such regions and adjacent HEA regions using transmission electron microscopy (TEM). A thorough understanding of such region chemistry and formation mechanisms will help to optimize printing parameters (e.g., adjust hatch spacing, energy density, potentially dynamic process parameter adjustment) to increase homogeneity and performance [194].

A Helios Hydra Plasma focused ion beam (FIB) was used to prepare the TEM lamella. A JEOL Grand Arm scanning transmission electron microscopy (STEM) with a Schottky field emission gun operated at 300 keV was used for nanoscale characterization of samples microstructure. The high-angle annular dark-field TEM/STEM imaging was used to analyze the samples. High-resolution elemental mapping was also acquired using x-ray EDS in STEM mode.

5.6.3 Results and Discussion

Figure (a) shows the schematic of the gradient HEA sample that was DED-fabricated using powders of three different off-shelf powders upon the substrate of the 316L alloy. The schematic shows the build layers with thickness in a range of 0.3–0.5 mm. The content of Co–Cr, IN718, and 316L powder varies along the build direction with each layer.

Figure (b) shows the photograph of the graded sample on the top of the substrate as marked by the yellow line.

Figure (c) shows the optical image of the substrate and the graded material, and the layers of deposition are visible in the image contrast. The microscopic pores that are commonly observed in AM materials are also visible.

Figure (d) shows the chemical map generated by EDS in SEM that clearly shows the compositional variation of primary elements, such as iron, cobalt, and chromium, along the build direction.

Figure (e) shows an enlarged optical image of the region marked in the fifth box of

Figure (c). This area contained a possible unmelted agglomeration of an iron-rich region. Furthermore, a TEM lamella was prepared in the region indicated by the green box for nanoscale analysis of the interface of the HEA and the unmelted region.

Figure (a) shows the prefinal FIB lift-out where the interface between the unmelted region and the HEA region is clearly visible and has been marked by the red line. Figure (b) shows the STEM image of the region where the small precipitates on both sides of the interface are visible. Figure (c) shows the chemical map generated by the EDS in TEM that clearly shows the cobalt compositional variation across these two regions. Apart from cobalt, iron appears to be higher in the unmelted region. So, it is possible that this region can be unmelted 316L powder. Similarly, Figure (d–g) shows the chemical maps of iron, titanium, chromium, and nickel, respectively. One of the precipitates in the HEA region has been identified as titanium-rich in Figure (e), and the unmelted part has chromium-rich precipitates, as shown in shown in Figure (f).

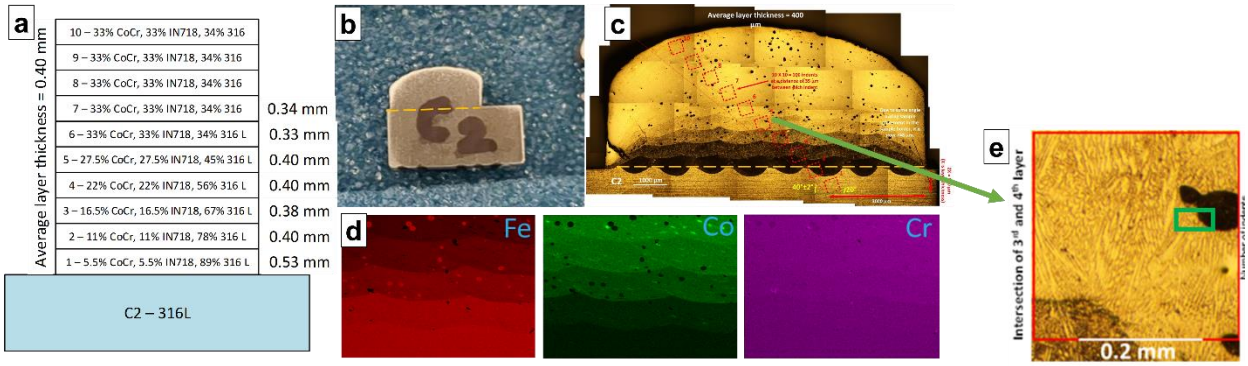

Figure 5-8. (a) A schematic of the gradient HEA composition fabrication upon the 316L substrate using the DED method; (b) the fabricated gradient material on the substrate, demarked by the yellow line; (c) the optical image of the gradient materials; (d) SEM images that show the continuous variation of iron, cobalt, and chromium with deposition thickness; and (e) an enlarged optical image showing the area of interest and the marked as region "5" in (c). The approximate area of TEM lift-out has been marked in the green box.

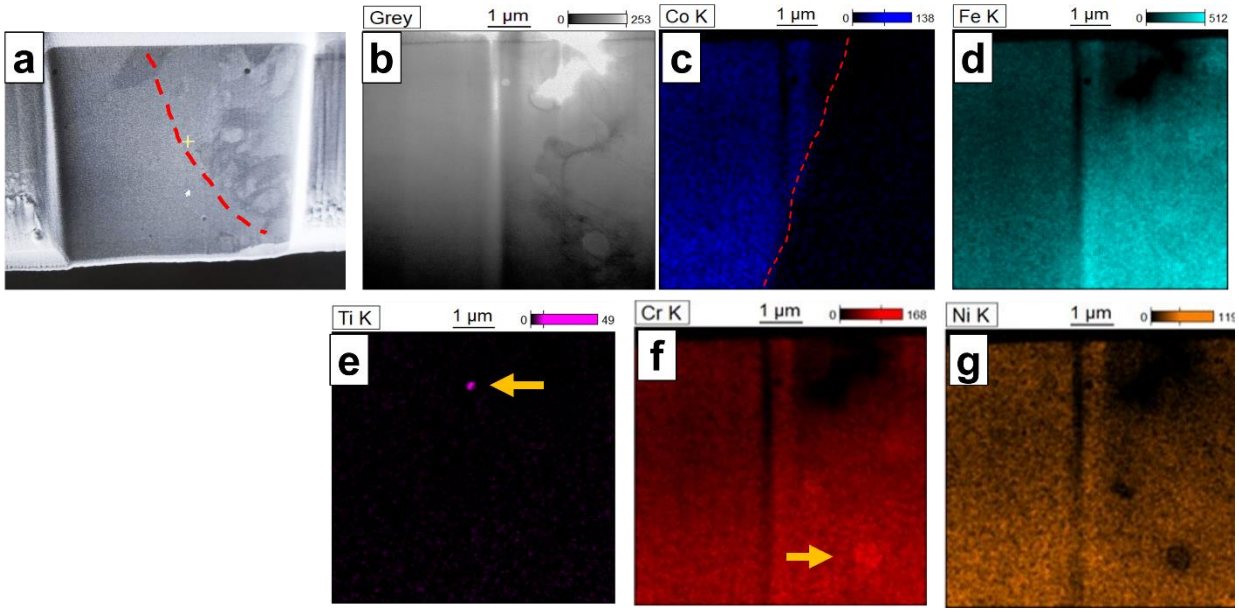

Figure 5-9. (a) Tahe FIB lift-out shows the area of interest showing the unmelted steel powder on the left side; (b) the STEM image shows the same area of interest with the interface between the HEA and the unmelted steel powder particle; and (c) the cobalt elemental map shows the interface between the two phases. The titanium map in (e) shows the titanium-rich region in HEA region, and (f) shows the chromium-rich region in unmelted steel powder particle.

Figure 3 focuses on the HEA region highlight the chemistry of the precipitate phase. The precipitate in the HEA side is further studied, and it has been identified as titanium oxide based on the strong presence of titanium and oxygen, as shown in Figure 3(c–d). Usually, titanium has been reported to form oxide readily during powder processing. But, this study did not determine whether the oxide was already present in the powder used or if it formed during processing. However, only one of such oxide particles is observed in the TEM lamella, so the volume fraction of such oxide inclusion is believed to be very low.

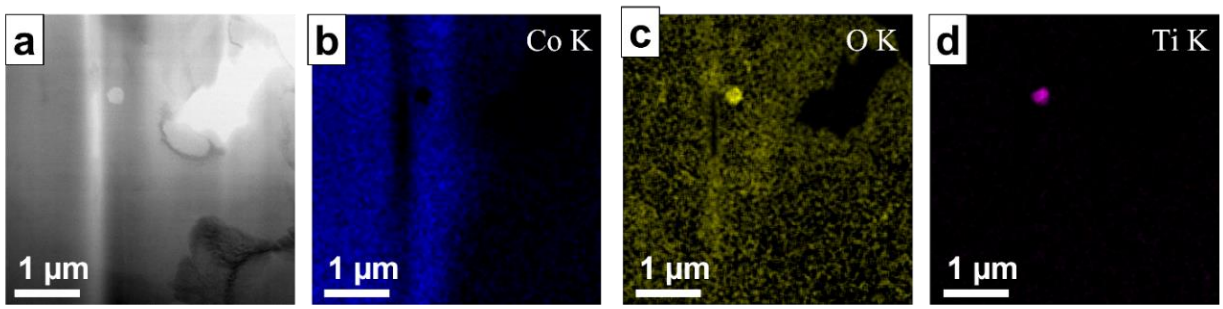

Figure 3. (a) The STEM image shows the morphology of the titanium oxide precipitate in the HEA region. (b–d) The chemical maps in the HEA region highlight the titanium and oxygen presence in the form of the precipitate.

Similarly, Figure shows the unmelted region that was further analyzed to identify the composition of precipitates present in this region. Figure (a) shows the spherical precipitate, and Figure (b–e) shows the individual chemical map in the region. The precipitate appears to be strongly rich in chromium.

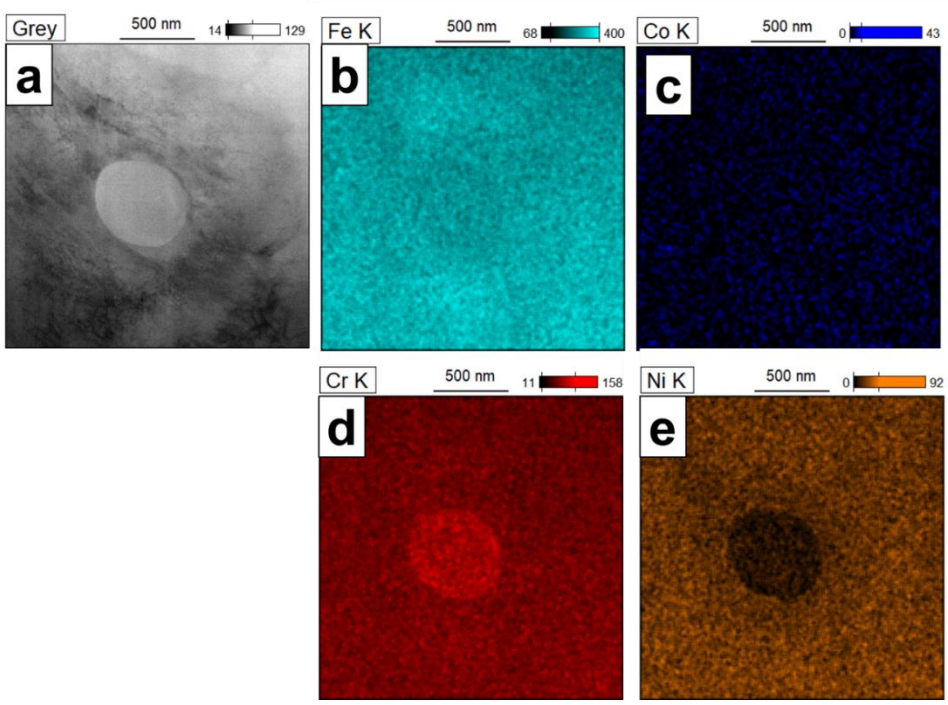

Figure 5-11. (a) The STEM image shows the morphology of the chromium-rich particle in the unmelted steel; (b–d) shows the elemental distribution in the chromium-rich region.

Figure (a) shows an SEM image of the HEA region that shows the formation of the dendritic and interdendritic regions during the solidification process. The interdendritic regions appear to be mostly a continuous channel, but there are some regions where they appear to be discontinuous. This discontinuity

is possibly due to the projection of the interdendritic channels running within the sample and not being captured in such 2D images. The same dendritic–interdendritic has been observed in TEM, as well, in the HEA region, as shown in Figure (b). Further chemical analysis in Figure (c–g) shows that the interdendritic region is mostly enriched in niobium. It also corresponds to the brighter chemical contrast of the interdendritic region shown in 5-12(a).

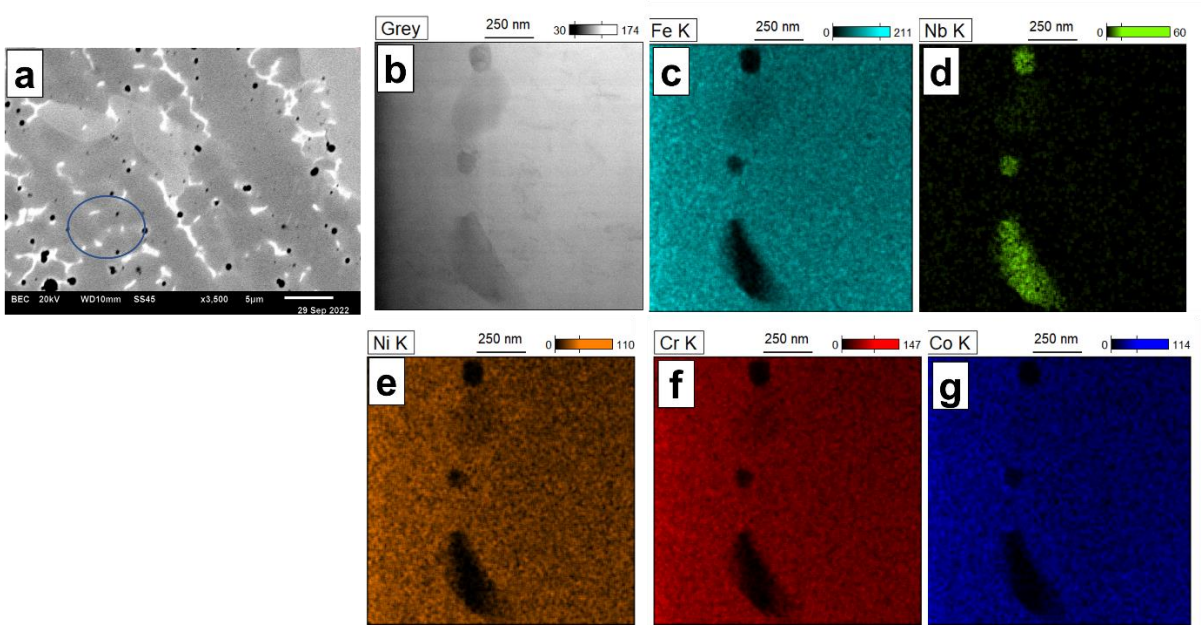

Figure 5-12. (a–b) An SEM and STEM image show the dendritic–interdendritic region formation in the HEA region; (c–g) the chemical map using STEM-EDS shows the strong presence of niobium and the absence of iron, nickel, chromium, and cobalt in the interdendritic region.

5.6.4 Summary

A novel DED fabrication of graded compositions of HEAs using common, off-the-shelf alloy powders has been studied using advanced microscopy. The main findings are as follows:

- The composition in each build layer appears to be quite homogeneous. The HEA seems to form an dendritic–interdendritic region mainly because of the presence of elements, such as niobium.
- The HEA still contains some unmelted parts of possible 316L powders. The unmelted region has been examined, and it contained nanoscale chromium-rich precipitates.
- The HEA region also contains a small fraction of titanium oxide precipitates.
- Although the microstructural examination confirms the successful fabrication of graded materials, further optimization of process parameters is needed to reduce porosity in the microstructure and undesired brittle intermetallic phases.

5.7 PRELIMINARY DECISION MATRIX RATING OF TWO DOWNSELECTED HIGH-ENTROPY ALLOYS

Based on the literature review, the preliminary experiments performed, and engineering rationale, a preliminary rating was performed on the two downselected alloys and summarized in Table, with the

associated justification in the following text. HEA $Al_{10}Cr_{12}Fe_{35}Mn_{23}Ni_{20}$ performed marginally better than HEA $Al_{0.3}Ti_{0.2}Co_{0.7}CrFeNi_{1.7}$ with a rating of 62.5 vs. 56.5.

Table 5-2. Preliminary decision matrix rating for HEAs

Criteria		$Al_{0.3}Ti_{0.2}Co_{0.7}CrFeNi_{1.7}$	$Al_{10}Cr_{12}Fe_{35}Mn_{23}Ni_{20}$
Application Space	Applicability to Different Reactor Types	3	5
	Other Industry Experience	3	3
	Data Availability	0	0
	Code and Standards Availability	0	0
	Component Versatility	2	2
Environmental Compatibility	Radiation Resistance	0	0
	Elemental Transmutation	0	0
	High-Temperature Oxidation Resistance	0	0
	Neutronics Compatibility	0	0
	Coolant Compatibility and Corrosion Resistance	0	0
Physical and Mechanical Properties	Thermal Conductivity	0	0
	Thermal Capacity	0	0
	Tensile Properties	5	5
	Creep Performance	0	0
	Fatigue	0	0
	Fracture Toughness	0	3
	Microstructural Dependency	5	5
	Scope for Microstructural Enhancement	5	5
Manufacturability	Reproducibility/Consistency	4	4
	Process Complexity	4.5	4.5
	Cost	3	3
	Scalability	5	5
	Production Method TRL	1	1
	Raw Material Supply	3	5
	Flexibility of Manufacturing	5	5
	Conventional Machining	3	3
	Near Net Shaping (Complexity of Shape)	5	4
Overall Scores		56.5	62.5

5.8 RATIONALES FOR RATINGS

5.8.1 $Al_{0.3}Ti_{0.2}Co_{0.7}CrFeNi_{1.7}$

The HEA $Al_{0.3}Ti_{0.2}Co_{0.7}CrFeNi_{1.7}$ was given a score of 56.5 out of a possible 135 (2.09 out of 5 on average) based on the decision criteria matrix. Most of the criteria scored "0," as this HEA is recently developed and has no data reported for those criteria particularly. However, some of the criteria have been

assigned a score based on limited data available in the literature. The justification for the assigned scores is provided in this section.

Applicability to Different Reactor Types (3/5): The mechanical and functional properties of HEA $Al_{0.3}Ti_{0.2}Co_{0.7}CrFeNi_{1.7}$ can be significantly tuned to withstand the environments in several reactors. Moreover, this HEA is believed to retain its structural integrity up to 1,100°C. Because no experimental data are available on the application of this HEA in any of the reactors yet, a score of 3 can been assigned based on intuition.

Other Industry Experience (3/5): HEAs are typically suitable for structural applications; thus, widespread use in various other industries is envisaged. Because no reports exist investigating the other industry applications, a score of 3 has been assigned.

Component Versatility (2/5): This HEA has foreseen application as a fuel cladding material requiring good structural integrity. Other applications may open after determining this HEA's properties in other aspects such as corrosion, irradiation resistance, and more. Therefore, only a score of 2 has been assigned.

Tensile Properties (5/5): This HEA is reported to exhibit a YS of approximately 1,630 MPa and good tensile ductility of approximately 15% at RT, which is significantly higher than most SSs. This HEA is expected to have high-temperature stability up to approximately 1,100°C; thus, a score of 5 has been assigned for tensile properties.

Microstructural Dependency (5/5): The mechanical and functional properties of this HEA are greatly dependent on the underlying microstructure; therefore, a score of 5 has been assigned.

Scope for Microstructural Enhancement (5/5): Because this HEA's properties can be significantly tuned, a score of 5 has been assigned.

Reproducibility/Consistency (4/5): This HEA has only been manufactured via casting, DED, and SLM so far. Although casting is highly reproducible and consistent, the other two laser AM techniques may not be, and this area needs further validation. Therefore, a score of 4 has been assigned.

Process Complexity (4.5/5): This HEA can be easily manufactured via casting or AM. However, AM involves a preprocessing step of producing good-quality spherical powders prior to manufacturing, which are chiefly made via the atomization process. Therefore, a score of 4.5 is assigned.

Cost (3/5): Because this HEA is not commercially produced yet, a score of 3 has been assigned because the cost would be comparable with any SSs produced commercially at the present time.

Scalability (5/5): The scalability for this HEAs is only limited by the type of processing technique employed, and no specific issues pertaining to its composition is foreseen; therefore, a score of 5 can be assigned.

Production level TRL (1/5): This HEA is not commercially produced yet, and only a handful of research articles can be found. Therefore, a score of 1 has been assigned.

Raw Material Supply (3/5): The raw material supply for casting this HEA should be no different from any SSs. However, for AM, the availability of HEA powders can be highly challenging. Therefore, a score of 3 has been assigned.

Flexibility of Manufacturing (5/5): This HEA can be manufactured via all the bulk manufacturing techniques; thus, a score of 5 has been assigned.

Conventional Machining (3/5): The part, if manufactured via casting, requires significant postprocessing but requires only minimal postprocessing when fabricated via AM. Therefore, an average score of 3 has been assigned.

Near Net Shaping (Complexity of Shape) (5/5): The fabrication of this HEA is not limited by the complexity of the design.

5.8.2 $Al_{10}Cr_{12}Fe_{35}Mn_{23}Ni_{20}$

HEA $Al_{10}Cr_{12}Fe_{35}Mn_{23}Ni_{20}$ was given a score of 62.5 out of possible 135 (2.31 out of 5 on average) based on the decision criteria matrix. Most of criteria scored "0," as this HEA is recently developed and has no data reported for those criteria particularly. However, some of the criteria have been assigned a score based on limited data available in the literature. The justification for the assigned scores is provided in this section.

Applicability to Different Reactor Types (5/5): HEA $Al_{10}Cr_{12}Fe_{35}Mn_{23}Ni_{20}$ is free from cobalt, and moreover, the properties can be greatly tuned to withstand the environments in several reactors. Despite no experimental data available on the application of this HEA in any reactors yet, the US NRC strongly recommends this HEA for future nuclear applications because of its enhanced mechanical properties and microstructural benefits. Therefore, a score of 5 has been assigned.

Other Industry Experience (3/5): HEAs are typically suitable for structural applications; thus, widespread use in various other industries is envisaged. Because there are no reports investigating the other industry application for this HEA, a score of 3 has been assigned.

Component Versatility (2/5): This HEA has foreseen application as a fuel cladding material requiring good structural integrity. Other applications may open after determining this HEA's properties in other aspects such as corrosion, irradiation resistance, and more. Therefore, only a score of 2 has been assigned.

Tensile Properties (5/5): This HEA in cold-rolled state is reported to exhibit a yield strength of approximately 1,400 MPa and decent tensile ductility of approximately 5.83% at RT, which is significantly higher than most code-certified materials. Thus, a score of 5 has been assigned for tensile properties.

Fracture Toughness (3/5): The fracture toughness of this HEA in the cold-rolled state is approximately 79 MPa√m, which is slightly lower than other code-certified materials. Therefore, a score of 3 has been assigned.

Microstructural Dependency (5/5): The mechanical and functional properties of this HEA are greatly dependent on the underlying microstructure; therefore, a score of 5 has been assigned.

Scope for Microstructural Enhancement (5/5): Because this HEA's properties can be significantly tuned, a score of 5 has been assigned.

Reproducibility/Consistency (4/5): This HEA has been manufactured via casting, which is highly reproducible and consistent. Therefore, a score of 5 has been assigned.

Process Complexity (4.5/5): This HEA can be easily manufactured via casting without any preprocessing required. Therefore, a score of 5 is assigned.

Cost (3/5): Because this HEA is not commercially produced yet, a score of 3 has been assigned because the cost would be comparable with any SSs produced commercially at present.

Scalability (5/5): The scalability for this HEA is only limited by the type of processing technique employed, and no specific issues pertaining to its composition is foreseen. Therefore, a score of 5 can be assigned.

Production level TRL (1/5): This HEA is not commercially produced yet, and only a handful of research articles can be found. Therefore, a score of 1 has been assigned.

Raw Material Supply (5/5): The raw material supply for casting this HEA should be no different from any SSs. Therefore, a score of 5 has been assigned.

Flexibility of Manufacturing (5/5): This HEA can be manufactured via all the bulk manufacturing techniques; thus, a score of 5 has been assigned.

Conventional Machining (3/5): The part, if manufactured via casting, requires significant postprocessing but requires only requires minimal postprocessing when fabricated via AM. Therefore, an average score of 3 has been assigned.

Near Net Shaping (Complexity of Shape) (4/5): The fabrication of this HEA is not limited by the complexity of the design. However, the presence of the element copper in the HEA may pose some processing challenges via laser AM. Therefore, a score of 4 has been assigned.

5.9 SUMMARY OF HIGH-ENTROPY ALLOY EVALUATION

High entropy alloys (HEAs) have the potential to serve in extreme environments of next generation nuclear reactors for temperatures up to 1,000°C for nearly 100,000 hours due to their unique phase transformation pathways and nanoscale and mesoscale microstructures.
The HEA classification used in this study performed by PNNL and the elaborate literature survey performed provide insights into the processing, microstructure, and properties of the several HEAs reported targeting different applications. Six HEAs were identified as promising for the nuclear industry focusing on the high temperature properties with Co as an alloying element in two of these alloys ($(Ni_2Co_2FeCr)_{92}Al_4Nb_4$; $Al_{0.3}Ti_{0.2}Co_{0.7}CrFeNi_{1.7}$). GRX-810 (Co-33%, Cr-29%, Re-1.5%, Al-0.3%, Ti-0.25%, Nb-0.75%, W-3%, C-0.05%, Ni-Balance), developed by NASA shows creep performance 2-3 orders of magnitude better than the current high temperature alloys, is best classified as a medium entropy alloy or an oxide dispersion strengthened (ODS) alloy due to the presence of Y_2O_3 particles and therefore, we recommend pursuing this material as part of a different AMMT work package. Most of the HEA research reviewed, used arc (73%) and vacuum melting (15%) processes as a fabrication method, with only 11% of the papers reviewed used laser based additive manufactured processes. Solid state manufacturing processes were only reported in less than 5% of the instances. The literature survey shown therefore the opportunity to explore solid phase processes as a manufacturing technique due to the grain refinement and decreased segregation properties during processes.
Two HEAs ($Al_{0.3}Ti_{0.2}Co_{0.7}CrFeNi_{1.7}$ and $Al_{10}Cr_{12}Fe_{35}Mn_{23}Ni_{20}$) was down selected for detailed experimental work using two AM processes (DED and SLM). These two alloys were also targeted for solid phase processes which is currently in progress. An advanced processing route was furthermore evaluated for fabricating functionally graded HEAs using Directed Energy Deposition (DED) and off-the-shelf metal alloy powders. This advanced processing methodology for functionally graded HEAs would

open avenues for rapidly assessing new HEA compositions at significantly cheaper costs. While the microstructural examination indicates the successful fabrication of graded materials, further investigation is needed to optimize the process parameters to reduce porosity and undesired brittle intermetallic phases and ensure complete melting of the metal alloy powders.
The temperature-dependent (from Room Temperature (RT) to 500°C) nanoindentation behavior of the DED and SLM processed $Al_{0.3}Ti_{0.2}Co_{0.7}CrFeNi_{1.7}$ HEA was investigated in the as-deposited and one-step annealed conditions for this study. The hierarchically heterogeneous microstructures obtained via simple one-step annealing of the DED and selective laser melting (SLM) -processed HEA exhibited significantly better performance than the nearly homogeneous microstructures in the as-deposited state. The one-step annealed conditions revealed less than 6.6% reduction in hardness values at 500°C compared to RT, while the as-deposited conditions showed greater than 18% reduction in hardness between RT and 500°C. The one-step annealed conditions also exhibited significantly higher hardness than the as-deposited conditions owing to their multi-phase (FCC+$L1_2$) microstructures with a substantial fraction of ordered $L1_2$ precipitates. Although this alloy was tested only up to 500C at this time, it is also expected to have high-temperature stability up to ~1100 °C, which can be verified in future work.
The research performed as part of this study, resulted in 3 conference presentations and one accepted journal publication.

6. CONCLUSION AND RECOMMENDATION

The multilaboratory collaborative research consists of the feasibility studies on new materials and relevant advanced manufacturing technologies, collection of materials properties data and knowledge through experiments and a literature survey, and the development and application of a decision criteria matrix for downselecting candidate materials and manufacturing technologies. The efforts for FY 2023 have focused on the three new material groups, including ODS materials, refractory composites, and alloys, and HEAs investigated by ORNL (work package: CT-23OR130406), LANL (CT-23LA130403), and PNNL (CT-23PN130408), respectively. A common materials evaluation criteria matrix has been developed through an intense multilaboratory effort and was applied to the evaluation and prioritization of new materials using advanced manufacturing technologies. The following sections summarize the results of the literature survey, experimental characterization, and application of the common decision criteria matrix performed by the three laboratories.

6.1 ADDITIVELY MANUFACTURED OXIDE DISPERSION–STRENGTHENED ALLOYS

The main efforts were exerted to identify an accelerated development path for ODS alloys by creatively combining AM technologies with the recent advances in ODS materials and traditional manufacturing technologies. An AM and postbuild processing route was developed for ODS ferritic (Fe–Cr alloy or 14YWT) and austenitic (Fe–Cr–Ni alloys or 316L and 316H) alloys. Basic microstructural and mechanical characterizations were performed to provide feedback to the alloy and processing design. Furthermore, multiple laboratories collaborated to create a decision criteria matrix to evaluate and downselect the new materials processed by advanced manufacturing methods. New ODS alloy processing routes combining AM processes and postbuild TMTs were designed and applied to the production of 15 variants of ferritic and austenitic ODS materials. The AM processes include DED for ferritic alloys and LPBF for austenitic alloys, and the postbuild TMTs were 700°C and 800°C controlled hot-rolling steps.

Key mechanical test results, including TS, tensile ductility, and fracture toughness data, are reported and explained. The highest strength among the ODS variants (YS > 1 GPa) was measured from a ferritic ODS alloy, and the highest ductility (TE > 40%) and fracture toughness (K_C > 200 MPa√m) were measured from austenitic ODS alloys.

Many of the decision criteria were scored the same for the AM ferritic and austenitic ODS alloys; however, the austenitic alloys generally have higher corrosion resistance and significantly better ductility, yielding a slightly higher average score than the ferritic alloys (3.26 vs. 3.07 out of 5). Therefore, the austenitic ODS alloy was downselected to be the primary materials type in the future research on ODS materials in the AMMT Program.

6.2 COMPOSITES AND REFRACTORIES

Single weld studies were performed on TZM, tungsten, and tantalum to elucidate the relationship between laser power and scanning velocity and to determine fully dense processing parameters and surface roughness parameters for the LPBF AM of refractory alloys. The single weld tracks were useful in narrowing down the operating window; it was determined that different preheating, multiple scans, and/or in situ heat treatment will be needed to accommodate for material differences. Three preliminary studies performed will enable quicker processing and development of advanced refractory alloys under consideration for the AMMT project.

Through evaluation using the decision criteria matrix, C-103 scored the highest out of the new refractory alloys (W–Ta, W–Ni–Fe, and C-103), with a score of 105 out of 135 (3.89 out of 5 on average). It is anticipated to have superior creep performance, fatigue, fracture toughness, and neutronics compatibility compared with W–Ta and W–Ni–Fe. Furthermore, it is more well-studied, with more data availability than the other two alloys. TZM also scored highly, 106 out of 135 (3.93 out of 5), but it is currently being investigated under the microreactor program and does not need further investigation in the AMMT Program. Therefore, based on the results of the evaluation using the decision criteria matrix, it is recommended that C-103 be pursued for further development under the AMMT Program.

Composites considerations were limited to a carbon fiber reinforced carbon (C/C) or silicon carbide reinforced silicon carbide (SiC/SiC) composite backbone in conjunction with a metallic (Mo, Zr, or W) liner. Ultimately, tungsten coated SiC/SiC (W/SiC-SiC) has the highest score (95/135) of all coated composites. The scoring for each coated composite was extremely close, with the scores only varying by only three points. W/SiC-SiC will maintain its structural integrity at elevated temperatures, is thought to have satisfactory neutronics properties, and sufficient compatibility liquid metal coolants (Pb, Li) and coolants used in MSRs and GFRs. It is seen as a candidate material for both in-core and out-of-core structural components. Based on the results of the evaluation using the decision criteria matrix, it is recommended that W coated SiC-SiC be pursued for further development under the AMMT program.

6.3 HIGH-ENTROPY ALLOYS

The HEA classification used in this review and the elaborate literature survey presented in this report provide insights into the processing, microstructure, and properties of the several HEAs reported targeting different applications. Based on the literature survey, six HEAs were identified as promising for the nuclear industry, focusing on the high-temperature properties with cobalt as an alloying element in two of these alloys [$(Ni_2Co_2FeCr)_{92}Al_4Nb_4$; $Al_{0.3}Ti_{0.2}Co_{0.7}CrFeNi_{1.7}$]. GRX-810, developed by NASA, shows creep performance 2–3 orders of magnitude better than the current high-temperature alloys and is best classified as a medium-entropy alloy or an ODS alloy because of the presence of Y_2O_3 particles. Therefore, the authors of this report recommend pursuing this material as part of a different AMMT work package. Although the decision matrix is not fully developed yet for the six candidate HEAs, the literature survey provides technical justification to downselect two HEAs ($Al_{0.3}Ti_{0.2}Co_{0.7}CrFeNi_{1.7}$ and $Al_{10}Cr_{12}Fe_{35}Mn_{23}Ni_{20}$) for detailed experimental work under this work package. This work package also investigated an advanced processing route for fabricating functionally graded HEAs using DED and off-the-shelf metal alloy powders. This advanced processing methodology for functionally graded HEAs would open avenues for rapidly assessing new HEA compositions at significantly cheaper costs.

Most of the HEA research used arc (73%) and vacuum melting (15%) processes as a fabrication method, with only 11% of the papers reviewed used laser-based AM processes. Solid-state manufacturing processes were only reported in less than 5% of the instances. The literature survey shows the opportunity to explore solid-phase processes as a manufacturing technique because of the grain refinement and decreased segregation properties during processes. Therefore, the inclusion of ShAPE is in progress for the two downselected HEAs ($Al_{0.3}Ti_{0.2}Co_{0.7}CrFeNi_{1.7}$ and $Al_{10}Cr_{12}Fe_{35}Mn_{23}Ni_{20}$) because of its unique processing conditions, which result in finer microstructures with compositionally homogenous grains that would potentially enhance the mechanical properties. Additionally, the effect of solid-phase processing on the mechanical properties of a single-phase HEA can provide valuable information and potentially more economical routes to HEA adoption to the markets. It is therefore also recommended that a functionally graded alloy to HEA used as a final coating be explored to determine the effect on the interlayers and interface properties.

The temperature-dependent (from RT to 500°C) nanoindentation behavior of the DED- and SLM-processed $Al_{0.3}Ti_{0.2}Co_{0.7}CrFeNi_{1.7}$ HEA was investigated in the as-deposited and one-step annealed conditions for this study. The hierarchically heterogeneous microstructures obtained via simple one-step annealing of the DED and SLM-processed HEA exhibited significantly better performance than the nearly homogeneous microstructures in the as-deposited state. The one-step annealed conditions revealed less than 6.6% reduction in hardness values at 500°C compared with RT, and the as-deposited conditions showed a greater than 18% reduction in hardness between RT and 500°C. The one-step annealed conditions also exhibited significantly higher hardness than the as-deposited conditions owing to their multiphase (fcc + $L1_2$) microstructures with a substantial fraction of ordered $L1_2$ precipitates. Furthermore, serrated yielding (PLC effect) indicative of microstructural instability was observed during nanoindentation deformation (at 500°C) for both SLM- and DED-processed conditions but not after the one-step annealing. Overall, the nanoindentation results signify the stability of these hierarchically heterogeneous microstructures developed via single-step annealing, exploiting the residual stresses in the AM-processed HEA $Al_{0.3}Ti_{0.2}Co_{0.7}CrFeNi_{1.7}$. Overall, the results presented were promising. However, applying this HEA in high-temperature nuclear reactors would require a more detailed assessment of other properties. ShAPE processing followed by high-temperature nanoindentation testing at 800°C is in progress. This HEA is also expected to have high-temperature stability up to approximately 1,100°C.

Microstructural characterization of the graded compositions of HEAs fabricated via the DED technique using common, off-the-shelf alloy powders has been performed. The results reveal homogenous compositions in each build layer. However, the graded HEAs formed dendritic–interdendritic microstructures mainly because of the presence of heavier elements, such as niobium. Few regions contained unmelted 316L powders with nanoscale, chromium-rich precipitates sparsely distributed. Additionally, titanium oxide particles were observed in the HEA matrix. Although the microstructural examination indicates the successful fabrication of graded materials, further investigation is needed to optimize the process parameters to reduce porosity and undesired brittle intermetallic phases and ensure complete melting of the metal alloy powders.

Based on the literature review, the preliminary experiments performed, and engineering rationale, a preliminary rating was performed on the two downselected alloys. HEA $Al_{10}Cr_{12}Fe_{35}Mn_{23}Ni_{20}$ performed marginally better than HEA $Al_{0.3}Ti_{0.2}Co_{0.7}CrFeNi_{1.7}$ with a rating of 62.5 vs. 56.5 (2.31 vs. 2.09 out of 5).

7. REFERENCES

[1] L.K. Mansur, A.F. Rowcliffe, R.K. Nanstad, S.J. Zinkle, W.R. Corwin, and R.E. Stoller, "Materials needs for fusion, Generation IV fission reactors and spallation neutron sources – similarities and differences," *J. Nucl. Mater.*, 329-333 (2004) 166–172.

[2] G.S. Was, D. Petti, S. Ukai, S. Zinkle, "Materials for future nuclear energy systems," *J. Nucl. Mater.*, 527 (2019) 151837.

[3] S.J. Zinkle, J.T. Busby, "Structural materials for fission & fusion energy," *Mater. Today*, 12 (2009) 12–19.

[4] T.S. Byun, D. Collins, B. Fillingim, T. Feldhausen, H. Hyer, Y.-R. Lin, D.T. Hoelzer, K. Hanson, "Downselection and Basic Properties of Additively Manufactured ODS Alloys," AMMT program report: M3CT-23OR1304061 (ORNL/TM-2023/3033), Oak Ridge National Laboratory, 2023.

[5] B. Kanies, R. Montoya, M. Brand, E. Kardoulaki, M. Beaux, D. Andersson, "Assessment of Advanced Manufacturing Techniques for Composite and Refractory Alloy Structures," AMMT program report: M3CT-23LA1304031 (LA-UR-23-29515), Los Alamos National Laboratory, 2023.

[6] M.S.K.K. Yadav, N.S. Meher, I. van Rooyen, S. Tripathi, N. Canfield, "Feasibility Study of Advanced Manufacturing Techniques and Compositions of High Entropy Alloys,," AMMT program report: M3CT-23LA1304081 (PNNL-34763), Pacific Northwest National Laboratory, 2023.

[7] L. Tan, T. S. Byun, Y. Katoh, L.L. Snead, "Stability of MX-type strengthening nanoprecipitates in ferritic steels under thermal aging, stress and ion irradiation," *Acta Mater.*, 71 (2014) 11–19.

[8] M.B. Toloczko, D.S. Gelles, F.A. Garner, R.J. Kurtz, K. Abe, "Irradiation creep and swelling from 400 to 600 C of the oxide dispersion strengthened ferritic alloy MA957," *J. Nucl. Mater.*, 212 (1994) 604–607.

[9] O. Anderoglu, T.S. Byun, M. Toloczko, S.A. Maloy, "Mechanical performance of ferritic martensitic steels for high dose applications in advanced nuclear reactors," *Metall. Mater. Transact.*, A44 (2013) 70–83.

[10] T.S. Byun, J.H. Kim, J.H. Yoon, D.T. Hoelzer, " High Temperature Fracture Characteristics of Nanostructured Ferritic Alloy (NFA)," *J. Nucl. Mater.* , 407 (2010) 78–82.

[11] T.S. Byun, J.H. Yoon, S.H. Wee, D.T. Hoelzer, S.A. Maloy, ",Fracture Behavior of 9Cr Nanostructured Ferritic Alloy with Improved Fracture Toughness," *J. Nucl. Mater.*, 449 (2014) 39–48.

[12] T.S. Byun, J.H. Yoon, D.T. Hoelzer, Y.B. Lee, S.H. Kang, S.A. Maloy, "Process Development for 9Cr Nanostructured Ferritic Alloy (NFA) with High Fracture Toughness," *J. Nucl. Mater.* , 449 (2014) 290-299.

[13] D.T. Hoelzer, "History and Outlook of ODS/NFA Ferritic Alloys for Nuclear Applications," *Trans. ANS*, 118 (2018) 1587–1590.

[14] D.T. Hoelzer, J. Bentley, M.A. Sokolov, M.K. Miller, G.R. Odette, M.J. Alinger, "Influence of particle dispersions on the high-temperature strength of ferritic alloys," *J. Nucl. Mater.*, 367–370 (2007) 166–172.

[15] X.L. Wang, C.T. Liu, U. Keiderling, A.D. Stoica, L. Yang, M.K. Miller, C.L. Fu, D. Ma, K. An, "Unusual thermal stability of nano-structured ferritic alloys," ,*J. Alloys & Compounds*, 529 (2012) 96–101.

[16] C.P. Massey, D.T. Hoelzer, P.D. Edmondson, A. Kini, B. Gault, K.A. Terrani, S.J. Zinkle, "Stability of a model Fe-14Cr nanostructured ferritic alloy after long-term thermal creep," *Scripta Mater.*, 170 (2019) 134–139.

[17] M.B. Toloczko el al., Fuel Cycle R&D Program FY 2014 milestone report, Pacific Northwest National Laboratory, 2014.

[18] K.G. Field, J. Simpson, M. N. Gussev, H. Wang, M. Li, X. Zhang, X. Chen, T. Koyanagi, K. Kane, A. Marquez Rossy, M. Balooch, and K.A. Terrani, "Handbook of Advanced Manufactured Material Properties from TCR Structure Builds at ORNL – FY19," ORNL/TM-2019/1328, Oak Ridge National Laboratory, 2019.

[19] T.S. Byun, M.N. Gussev, T.G. Lach, M.R. McAlister, J.J. Simpson, B.E. Garrison, Y. Yamamoto, C.B. Joslin, J.K. Carver, F.A. List, R.R. Dehoff, K.A. Terrani, M. Li, X. Zhang, "Mechanical Properties and Deformation Behavior of Additively Manufactured 316L Stainless Steel – FY 2020," ORNL/TM-2020/1574, Oak Ridge National Laboratory, 2020.

[20] T.S. Byun, B.E. Garrison, M.R. McAlister, X. Chen, M.N. Gussev, T.G. Lach, A. Le Coq, K. Linton, et al., "Mechanical behavior of additively manufactured and wrought 316L stainless steels before and after neutron irradiation," *J. Nucl. Mater.,* 548 (2021) 152849.

[21] B.M. Morrow, T.J. Lienert, C.M. Knapp, J.O. Sutton, M.J. Brand, R.M. Pacheco, V. Livescu, J.S. Carpenter, G.T. Gray, "Impact of Defects in Powder Feedstock Materials on Microstructure of 304L and 316L Stainless Steel Produced by Additive Manufacturing," *Metall. Mater. Trans. A,* 49 (2018) 3637–3650.

[22] T. Ronneberg, C.M. Davies, P.A. Hooper, "Revealing Relationships between Porosity, Microstructure and Mechanical Properties of Laser Powder Bed Fusion 316L Stainless Steel through Heat Treatment," *Mater. Des.,* 189 (2020) 108481.

[23] J. Birnbaum, J.C. Steuben, E.J. Barrick, A.P. Iliopoulos, J.G. Michopoulos, "Intrinsic Strain Aging, Σ3 Boundaries, and Origins of Cellular Substructure in Additively Manufactured 316L," *Addit. Manuf.,* 29 (2019) 100784.

[24] U.S. Bertoli, B.E. MacDonald, J.M. Schoenung, "Stability of Cellular Microstructure in Laser Powder Bed Fusion of 316L Stainless Steel," *Mater. Sci. Eng. A,* 739 (2019) 109–117.

[25] M. Li, X. Zhang, W.Y. Chen, F. Heidet, T.S. Byun, K.A. Terrani, "Creep Behavior of 316L Stainless Steel Manufactured by Laser Powder Bed Fusion," *J. Nucl. Mater.,* 548 (2021) 152847.

[26] T. Kurzynowski, K. Gruber, W. Stopyra, B. Kuźnicka, E. Chlebus, "Correlation between Process Parameters, Microstructure and Properties of 316 L Stainless Steel Processed by Selective Laser Melting," *Mater. Sci. Eng. A,* 718 (2018) 64–73.

[27] C. R. Brinkman, "Elevated-Temperature Mechanical Properties of an Advanced Type 316 Stainless Steel, United States," ORNL/CP-101053, Oak Ridge National Laboratory, 1999.

[28] E. Garlea, H. Choo, C.C. Sluss, M.R. Koehler, R.L. Bridges, X. Xiao, Y. Ren, B.H. Jared, "Variation of Elastic Mechanical Properties with Texture, Porosity, and Defect Characteristics in Laser Powder Bed Fusion 316L Stainless Steel," *Mater. Sci. Eng. A,* 763 (2019) 138032.

[29] T. Pinomaa, M. Lindroos, M. Walbrühl, N. Provatas, A. Laukkanen, "The Significance of Spatial Length Scales and Solute Segregation in Strengthening Rapid Solidification Microstructures of 316L Stainless Steel," *Acta Mater.,* 184 (2020) 1–16.

[30] D. Kong, X. Ni, C. Dong, L. Zhang, C. Man, X. Cheng, and X. Li, "Anisotropy in the Microstructure and Mechanical Property for the Bulk and Porous 316L Stainless Steel Fabricated via Selective Laser Melting," *Mater. Lett.,* 235 (2019) 1–5.

[31] J. Lin, F. Chen, X. Tang, J. Liu, S. Shen, and G. Ge, "Radiation-Induced Swelling and Hardening of 316L Stainless Steel Fabricated by Selected Laser Melting," *Vacuum,* 174 (2020) 109183.

[32] M. Song, M. Wang, X. Lou, R.B. Rebak, and G.S. Was, "Radiation Damage and Irradiation-Assisted Stress Corrosion Cracking of Additively Manufactured 316L Stainless Steels," *J. Nucl. Mater.,* 513 (2019) 33–44.

[33] G. Meric de Bellefon, K.M. Bertsch, M.R. Chancey, Y.Q. Wang, D.J. Thoma, "Influence of solidification structures on radiation-induced swelling in an additively-manufactured austenitic stainless steel," *J. Nucl. Mater.,* 523 (2019) 291–298.

[34] N. Sridharan, M.N. Gussev, K.G. Field,, "Performance of a ferritic/martensitic steel for nuclear reactor applications fabricated using additive manufacturing,," *J. Nucl. Mater.,* 521 (2019) 45–55.

[35] W. Zhong, N. Sridharan, D. Isheim, K.G. Field, Y. Yang, K. Terrani, L. Tan, "Microstructures and mechanical properties of a modified 9Cr ferritic-martensitic steel in the as-built condition after additive manufacturing," *J. Nucl. Mater.,* 545 (2021) 152742.

[36] M. Belmonte, "Advanced Ceramic Materials for High Temperature Applications," *Adv. Engi. Materi.,* 8 (2006) 693–703.

[37] H. Ohnabe, S. Masaki, M. Onozuka, K. Miyahara, T. Sasa, "Potential application of ceramic matrix composites to aero-engine components," *Composites Part A: Applied Science and Manufacturing,* 30 (1999) 489–496.

[38] K.K. Chawla, "Ceramic Matrix Composites," *Composite Materials*, (2019) 251–296.

[39] F. García Ferré, A. Mairov, L. Ceseracciu, Y. Serruys, P. Trocellier, C. Baumier, O. Kaïtasov, R. Brescia, D. Gastaldi, P. Vena, M. G. Beghi, L. Beck, K. Sridharan, F. Di Fonzo, "Radiation endurance in Al2O3 nanoceramics," *Scientific Reports*, 6 (2016) 33478.

[40] P. David, "Carbon/carbon materials for Generation IV nuclear reactors," in *Structural Materials for Generation IV Nuclear Reactors*, (2017) 471–493.

[41] Y. Katoh, L.L. Snead, "*Silicon carbide and its composites for nuclear applications – Historical overview*," *J. Nucl. Mater.*, (2019) 526.

[42] O. Oyelola, P. Crawforth, R. M'Saoubi, A.T. Clare, *Addit. Manuf.*, 24 (2018) 20.

[43] E.J. Pickering, A.W. Carruthers, P.J. Barron, S.C. Middleburgh, D.E.J. Armstrong, A.S. Gandy, *Entropy 2021*, 23 (2021) 98.

[44] O. El-Atwani, N. Li, M. Li, A. Devaraj, J.K.S. Baldwin, M.M. Schneider, D. Sobieraj, J. S. Wróbel, D. Nguyen-Manh, S.A. Maloy, E. Martinez, *Sci. Adv.*, 5 (2019).

[45] A.S. Gandy, B. Jim, G. Coe, D. Patel, L. Hardwick, S. Akhmadaliev, N. Reeves-McLaren, and R. Goodall, *Front. Mater.*, 6 (2019).

[46] A. Ayyagari, R. Salloom, S. Muskeri, S. Mukherjee, *Materialia*, 4 (2018) 99.

[47] A. Waseem, H.J. Ryu, *Sci. Rep.*, 7 (2017).

[48] T. Nagase, S. Anada, P.D. Rack, J.H. Noh, H. Yasuda, H. Mori, T. Egami, *Intermetallics*, 26 (2012) 122–130.

[49] T. Nagase, S. Anada, P. Rack, H. Yasuda, H, Mori, J. Noh, T. Egami, *Intermetallics*, 38 (2013) 70–79.

[50] S.Q. Xia, X. Yang, T.F. Yang, S. Liu, Y. Zhang, *JOM*, 67 (2015) 2340.

[51] T. Nagase, P. Rack, J. Noh, T. Egami, *Intermetallics*, 59 (2015) 32–42.

[52] D.J.M. King, P.A. Burr, E.G. Obbard, S.C. Middleburgh, *J. Nucl. Mater.*, 488 (2017) 70.

[53] P. Agrawal, S. Gupta, A. Dhal, R. Prabhakaran, L. Shao, R.S. Mishra, *J. Nucl. Mater.*, 574 (2023) 154217.

[54] A. Kareer, J.C. Waite, B. Li, A. Couet, D.E.J. Armstrong, A.J. Wilkinson, *J. Nucl. Mater.*, 526 (2019) 151744.

[55] B. Kombaiah, Y. Zhou, K. Jin, A. Manzoor, J.D. Poplawsky, J.A. Aguiar, H. Bei, D.S. Aidhy, P.D. Edmondson, Y. Zhang,, *ACS Appl Mater Interfaces*, 15 (2023) 3912.

[56] B. Gwalani, S. Dasari, A. Sharma, V. Soni, S. Shukla, A. Jagetia, P. Agrawal, R.S. Mishra, R. Banerjee, *Acta Mater*, 219 (2021) 117234 .

[57] Y. Zhao, Z. Chen, K. Yan, S. Naseem, W. Le, H. Zhang, W. Lu, *Materials Science and Engineering A*, 838 (2022) 142759.

[58] S. Dasari, A. Jagetia, Y.J. Chang, V. Soni, B. Gwalani, S. Gorsse, A.C. Yeh, R. Banerjee, *J. Alloys. Compd.*, 830, 154707 (2020).

[59] V. Chaudhary, N. M. Sai Kiran Kumar Yadav, S.A. Mantri, S. Dasari, A. Jagetia, R.V. Ramanujan, R. Banerjee, *J. Alloys. Compd.*, 823 (2020) 153817.

[60] W. Liu, J.N. DuPont, *Scr. Mater.*, 48 (2003) 1337.

[61] D.D. Lima, S.A. Mantri, C.V. Mikler, R. Contieri, C.J. Yannetta, K.N. Campo, E.S. Lopes, M.J. Styles, T. Borkar, R. Caram, R. Banerjee, *Mater. Des.*, 130 (2017) 8.

[62] M.S.K.K.Y. Nartu, A. Jagetia, V. Chaudhary, S.A. Mantri, E. Ivanov, N.B. Dahotre, R.V. Ramanujan, R. Banerjee, *Scr. Mater.*, 187 (2020) 30.

[63] M.S.K.K.Y. Nartu, T. Alam, S. Dasari, S.A. Mantri, S. Gorsse, H. Siller, N. Dahotre, R. Banerjee, *Materialia*, 9 (2020) 100522.

[64] V. Chaudhary, M.S.K.K.Y. Nartu, S. Dasari, S.M. Varahabhatla, A. Sharma, M. Radhakrishnan, S.A. Mantri, S. Gorsse, N.B. Dahotre, R.V Ramanujan, R. Banerjee, *Scr. Mater.*, 224 (2023) 115149.

[65] M.S.K.K.Y. Nartu, D. Flannery, S. Mazumder, S.A. Mantri, S.S. Joshi, A.V. Ayyagari, B. McWilliams, K. Cho, N.B. Dahotre, R. Banerjee, *JOM*, 1 (2021).

[66] M.S.K.K.Y. Nartu, S. Sharma, S.A. Mantri, S.S. Joshi, M.V. Pantawane, S. Mazumder, N.B. Dahotre, R. Banerjee, "in Additive Manufacturing in Biomedical Applications," *ASM International*, (2022) 130–159.

[67] M. S. K. K. Y. Nartu, A. Chesetti, S. Dasari, A. Sharma, S. A. Mantri, N. B. Dahotre, and R. Banerjee, *Materials Science and Engineering A* , 849 (2022) 143505.

[68] A. Chesetti, S. Banerjee, S. Dasari, S.M. Varahabhatla, A. Sharma, S.A. Mantri, M.S.K.K.Y. Nartu, N. Dahotre, R. Banerjee, *Additive Manufacturing Letters*, 6 (2023) 100140.

[69] C. Schneider-Maunoury, L. Weiss, P. Acquier, D. Boisselier, P. Laheurte, *Addit. Manuf.*, 17, 55 (2017).

[70] A.K. Gupta, M. Talha, *Progress in Aerospace Sciences*, 79 (2015) 1.

[71] A. Sola, D. Bellucci, V. Cannillo, *Biotechnol. Adv.*, 34 (2016) 504.

[72] B. Saleh, J. Jiang, R. Fathi, T. Al-hababi, Q. Xu, L. Wang, D. Song, A. Ma, ,*Compos. B Eng.*, 201 (2020) 108376.

[73] V. Chaudhary, M.S.K.K.Y. Nartu, S. Dasari, S.M. Varahabhatla, A. Sharma, M. Radhakrishnan, S.A. Mantri, S. Gorsse, N.B. Dahotre, R.V. Ramanujan, R. Banerjee, *Scr. Mater.*, 224 (2023) 115149.

[74] M. Radhakrishnan, M. McKinstry, V. Chaudhary, M.S.K.K.Y. Nartu, K.V.M. Krishna, R.V. Ramanujan, R. Banerjee, N.B. Dahotre, *Scr. Mater.*, 226 (2023) 115269.

[75] X. Li, T. Wang, X. Ma, N. Overman, S. Whalen, D. Herling, K. Kappagantula, *J. Manuf. Process*, 80 (2022) 108.

[76] T. Hartmann, S. Maloy, M. Komarasamy, "Materials Scorecards, Phase 2," March 2022.

[77] J.W. Geringer, Y. Katoh, S. Gonczy, T. Burchell, M. Mitchell, M. Jenkins, W.E. Windes, "Codes and standards for ceramic composite core materials for High Temperature Reactor applications," *Nuclear Engineering and Design*, 405 (2023).

[78] E. Kardoulaki, T.J. Nizolek, E.P. Luther, M. Swartz, "On the Interactions of Molybdenum and Graphite, a Promising Material System for Microreactors," *Jom*, 73 (2021) 3499–3512.

[79] K.A. Terrani, "Accident tolerant fuel cladding development: Promise, status, and challenges," *Journal of Nuclear Materials*, 501 (2018) 13–30.

[80] M.S.T. Price, "The Dragon Project origins, achievements and legacies," *Nuclear Engineering and Design*, 251 (2012) 60–68.

[81] J.M. Blocker, M.F. Browning, W.J. Wilson, V.M. Secrest, A.C. Secrest, R.B. Landrigan, J.H. Oxley, "Properties of Ceramic-Coated Nuclear-Fuel Particles," *Nuclear Science and Engineering*, 20 (1964) 153–170.

[82] J. Lee, B.A. Pint, "CORROSION IN GAS-COOLED REACTORS," US Department of Energy, ed., 2021.

[83] K. Tokunaga, N. Yoshida, N. Noda, T. Sogabe, T. Kato, "High heat load properties of tungsten coated carbon materials," *Journal of Nuclear Materials*, 258–263 (1998) 998–1004.

[84] C. Sauder, "Ceramic Matrix Composites: Nuclear Applications," *Ceramic Matrix Composites*, (2014) 609–646.

[85] J.I. Kim, W.J. Kim, D.J. Choi, J.Y. Park, W.S. Ryu, "Design of a C/SiC functionally graded coating for the oxidation protection of C/C composites," *Carbon*, 43 (2005) 1749–1757.

[86] C.H. Henager, Y. Shin, Y. Blum, L.A. Giannuzzi, B.W. Kempshall, S.M. Schwarz, "Coatings and joining for SiC and SiC-composites for nuclear energy systems," *Journal of Nuclear Materials*, 367–370 (2007) 1139–1143.

[87] M.F. Beaux, D.R. Vodnik, R.J. Peterson, B.L. Bennett, J.J. Salazar, T.G. Holesinger, G. King, S.A. Maloy, D. J. Devlin, I.O. Usov, "Chemical vapor deposition of Mo tubes for fuel cladding applications," *Surface and Coatings Technology*, 337 (2018) 510–515.

[88] A. Kohyama, "CMC for Nuclear Applications," *Ceramic Matrix Composites*, (2008) 353–384.

[89] D.J.H. Emslie, P. Chadha, J.S. Price, "Metal ALD and pulsed CVD: Fundamental reactions and links with solution chemistry," *Coordination Chemistry Reviews*, 257 (2013) 3282–3296.

[90] B.W. Lamm, D.J. Mitchell, "Chemical Vapor Deposition of Zirconium Compounds: A Review," *Coatings*, 13 (2023).

[91] S. Senderoff, G.W. Mellors, “Coherent Coatings of Refractory Metal,” *Science,* 153 (1966) 1475–1481.

[92] S.J. Zinkle, K.A. Terrani, L.L. Snead, “Motivation for utilizing new high-performance advanced materials in nuclear energy systems,” *Current Opinion in Solid State and Materials Science,* 20 (2016) 401–410.

[93] “Ceramic Matrix Composites: Fiber Reinforced Ceramics and Their Applications,” Editted by Dr.-Ing. Walter Krenkel, Wiley, May 2008.

[94] L.L. Snead, Y. Katoh, K. Ozawa, “Stability of 3-D carbon fiber composite to high neutron fluence,” *Journal of Nuclear Materials,* 417 (2011) 629–632.

[95] L.L. Snead, T.D. Burchell, Y. Katoh, “Swelling of nuclear graphite and high quality carbon fiber composite under very high irradiation temperature,” *Journal of Nuclear Materials,* 381 (2008) 55–61.

[96] D.B. Timothy, “Radiation damage in carbon–carbon composites: structure and property effects,” *Physica Scripta,* 1996 (1996) 17.

[97] T.D. Burchell, K.L. Murty, J. Eapen, “Irradiation induced creep of graphite,” *JOM,* 62 (2010) 93–99.

[98] R. Huang, F. Zeng, Y. Peng, H. Liu, Y. Gao, Q. Yang, “Influence of fiber/matrix interface on the texture evolution and fracture toughness of C/C,” *Diamond and Related Materials,* 127 (2022) 109112.

[99] T. Windhorst, G. Blount, “Carbon-carbon composites a summary of recent developments and applications,” *Materials & Design,* 18 (1997) 11–15.

[100] M. Ferraris, V. Casalegno, "Integration and Joining of Ceramic Matrix Composites," *Ceramic Matrix Composites,* (2014) 549–567.

[101] F. T. Lan, K.Z. Li, H.J. Li, Y.G. He, X.T. Shen, W.F. Cao, “Joining of carbon/carbon composites for nuclear applications,” *Journal of Materials Science,* 44 (2009) 3747–3750.

[102] N. van de Werken, H. Tekinalp, P. Khanbolouki, S. Ozcan, A. Williams, M. Tehrani, “Additively manufactured carbon fiber-reinforced composites: State of the art and perspective,” *Additive Manufacturing,* 31 (2020) 100962.

[103] C.R.F. Azevedo, “Selection of fuel cladding material for nuclear fission reactors,” *Engineering Failure Analysis,* 18 (2011) 1943–1962.

[104] Y. Katoh, T. Nozawa, C. Shih, K. Ozawa, T. Koyanagi, W. Porter, L.L. Snead, “High-dose neutron irradiation of Hi-Nicalon Type S silicon carbide composites. Part 2: Mechanical and physical properties,” *Journal of Nuclear Materials,* 462 (2015) 450–457.

[105] M.E. Sawan, Y. Katoh, L.L. Snead, “Transmutation of silicon carbide in fusion nuclear environment,” *Journal of Nuclear Materials,* 442 (2013) S370–S375.

[106] T. Noda, "Advanced SiC-SiC Composites for Nuclear Application," *Handbook of Advanced Ceramics and Composites,* (2020) 641–666.

[107] Y. Katoh, K. Ozawa, C. Shih, T. Nozawa, R.J. Shinavski, A. Hasegawa, L.L. Snead, “Continuous SiC fiber, CVI SiC matrix composites for nuclear applications: Properties and irradiation effects,” *Journal of Nuclear Materials,* 448 (2014) 448–476.

[108] C. Park, K. Noborio, R. Kasada, Y. Yamamoto, S. Konishi, “Compatibility of SiCf/SiC composite exposed to liquid Pb–Li flow,” *Journal of Nuclear Materials,* 417 (2011) 1218–1220.

[109] J.J. Lee, S.S. Raiman, Y. Katoh, T. Koyanagi, C.I. Contescu, X. Hu, Y. Yang, “Chemical compatibility of silicon carbide in molten fluoride salts for the fluoride salt-cooled high temperature reactor,” *Journal of Nuclear Materials,* 524 (2019) 119–134.

[110] K.A. Terrani, T. Lach, H. Wang, A.L. Coq, K. Linton, C. Petrie, T. Koyanagi, T.S. Byun, “Irradiation stability and thermomechanical properties of 3D-printed SiC,” *Journal of Nuclear Materials,* 551 (2021).

[111] L.L. Snead, T. Nozawa, Y. Katoh, T.S. Byun, S. Kondo, D.A. Petti, “Handbook of SiC properties for fuel performance modeling,” *Journal of Nuclear Materials,* 371 (2007) 329–377.

[112] K. Hironaka, T. Nozawa, T. Hinoki, N. Igawa, Y. Katoh, L.L. Snead, A. Kohyama, “High-temperature tensile strength of near-stoichiometric SiC/SiC composites,” *Journal of Nuclear Materials,* 307–311 (2002) 1093–1097.

[113] Y. Katoh, D.F. Wilson, C.W. Forsberg, "Assessment of silicon carbide composites for advanced salt-cooled reactors," ORNL/TM-2007/168, Oak Ridge National Laboratory, 2007.

[114] J. Delage, E. Saiz, N. Al Nasiri, "Fracture behaviour of SiC/SiC ceramic matrix composite at room temperature," *Journal of the European Ceramic Society,* 42 (2022) 3156–3167.

[115] "Mineral commodity summaries 2023", *National Minerals Information Center Report*, Reston, VA, 2023.

[116] T. Koyanagi, K. Terrani, S. Harrison, J. Liu, Y. Katoh, "Additive manufacturing of silicon carbide for nuclear applications," *Journal of Nuclear Materials,* 543 (2021).

[117] M.D. Richardson, A.T. Chumacher, A.M. Rogers, C.M. Petrie, *Large-Scale Additive Manufacturing of SiC with Process Monitoring*, Oak Ridge National Laboratory, Oak Ridge, TN, 2022.

[118] S.J. Zinkle, G.S. Was, "Materials challenges in nuclear energy," *Acta Materialia,* 61 (2013) 735–758.

[119] C. Ruset, E. Grigore, H. Maier, R. Neu, H. Greuner, M. Mayer, G. Matthews, "Development of W coatings for fusion applications," *Fusion Engineering and Design,* 86 (2011) 1677–1680.

[120] K.J. Leonard, "4.06 - Radiation Effects in Refractory Metals and Alloys," *Comprehensive Nuclear Materials*, R.J.M. Konings, ed., pp. 181-213, Oxford: Elsevier, 2012.

[121] L.R. Greenwood, F.A. Garner, "Transmutation of Mo, Re, W, Hf, and V in various irradiation test facilities and STARFIRE," *Journal of Nuclear Materials,* 212–215 (1994) 635–639.

[122] A. Warren, A. Nylund, I. Olefjord, "Oxidation of tungsten and tungsten carbide in dry and humid atmospheres," *International Journal of Refractory Metals and Hard Materials,* 14 (1996) 345–353.

[123] E.A. Gulbransen, and K.F. Andrew, "Kinetics of the Oxidation of Pure Tungsten from 500° to 1300°C," *Journal of The Electrochemical Society,* 107 (1960) 619.

[124] T. Muroga, "Refractory metals as core materials for Generation IV nuclear reactors," *Structural Materials for Generation IV Nuclear Reactors,* (2017) 415–440.

[125] J. Habainy, Y. Dai, Y. Lee, S. Iyengar, "Thermal diffusivity of tungsten irradiated with protons up to 5.8 dpa," *Journal of Nuclear Materials,* 509 (2018) 152–157.

[126] J. Rumble, editor, "CRC handbook of chemistry and physics," (2017).

[127] "Mineral commodity summaries 2022," *National Minerals Information Center Report*, Reston, VA, 2022.

[128] D.E. Glass, R.N. Shenoy, Z. Wang, M.C. Halbig, *Effectiveness of Diffusion Barrier Coatings for Mo-Re Embedded in C/SiC and C/C,* Langley Research Center, Hampton, Virginia, 2001.

[129] K.-Z. Li, D.-S. Hou, H.-J. Li, Q.-G. Fu, G.-S. Jiao, "Si–W–Mo coating for SiC coated carbon/carbon composites against oxidation," *Surface and Coatings Technology,* 201 (2007) 9598–9602.

[130] T. Nelson, E.S. Sooby, Y.J. Kim, B. Cheng, S.A. Maloy, "High temperature oxidation of molybdenum in water vapor environments," *Journal of Nuclear Materials,* 448 (2014) 441–447.

[131] G. Feng, L. Chen, X. Yao, Y. Yu, H. Li, "Design and characterization of zirconium-based multilayer coating for carbon/carbon composites against oxyacetylene ablation," *Corrosion Science,* 192 (2021) 109785.

[132] E. Kardoulaki, N. Abdul-Jabbar, D. Byler, M.M. Hassan, S. Mann, T. Coons, J. White, "Carburization Kinetics of Zircalloy-4 and Its Implication for Small Modular Reactor Performance," *Materials (Basel),* 15 (2022) 12.

[133] F. Onimus, S. Doriot, J.L. Béchade, "3.01 - Radiation Effects in Zirconium Alloys☆," *Comprehensive Nuclear Materials (Second Edition)*, R.J.M. Konings and R.E. Stoller, eds., 1–56, Oxford: Elsevier, 2020.

[134] A. Takibaev, M. Saito, V. Artisyuk, V. Apse, A. Shmelev, "Transmutation of Zirconium-93 in High-flux Blanket of Fusion Neutron Source," *Journal of Nuclear Science and Technology,* 37 (2000) 870–876.

[135] J.L. Vandegrift, P.M. Price, J.-P. Stroud, C.J. Parga, I.J. Van Rooyen, B.J. Jaques, D.P. Butt, "Oxidation behavior of Zirconium, Zircaloy-3, Zircaloy-4, Zr-1Nb, and Zr-2.5Nb in air and oxygen," *Nuclear Materials and Energy,* 20 (2019) 100692.

[136] H. Kishimoto, T. Shibayama, K. Shimoda, T. Kobayashi, A. Kohyama, "Microstructural and mechanical characterization of W/SiC bonding for structural material in fusion," *Journal of Nuclear Materials*, 417 (2011) 387–390.

[137] T. Koyanagi, Y. Katoh, T. Nozawa, L.L. Snead, S. Kondo, C.H. Henager, M. Ferraris, T. Hinoki, Q. Huang, "Recent progress in the development of SiC composites for nuclear fusion applications," *Journal of Nuclear Materials*, 511 (2018) 544–555.

[138] K.A. Terrani, T. Lach, H. Wang, A. Le Coq, K. Linton, C. Petrie, T. Koyanagi, T.S. Byun, "Irradiation stability and thermomechanical properties of 3D-printed SiC," *Journal of Nuclear Materials*, 551 (2021).

[139] Y. Du, B. Wang, Y. Zhong, T. Hinoki, "Assessment of the Potential Diffusion Barriers between Tungsten and Silicon Carbide for Nuclear Fusion Application," *Coatings*, 12 (2022) 5.

[140] K. Yueh, *SiC Composite for Fuel Structure Applications*, The Electric Power Research Institute, 2017.

[141] G.W. Liu, M.L. Muolo, F. Valenza, A. Passerone, "Survey on wetting of SiC by molten metals," *Ceramics International*, 36 (2010) 1177–1188.

[142] J.W. Yeh, S.K. Chen, S.J. Lin, J.Y. Gan, T.S. Chin, T.T. Shun, C.H. Tsau, S.Y. Chang, *Adv. Eng. Mater.*, 6 (2004) 299.

[143] B. Gwalani, S. Gorsse, D. Choudhuri, Y. Zheng, R.S. Mishra, R. Banerjee, *Scr. Mater.* 162 (2019) 18.

[144] S. Yadav, S. Sarkar, A. Aggarwal, A. Kumar, K. Biswas, *Wear*, 93 (2018) 410–411.

[145] K.R. Lim, K.S. Lee, J.S. Lee, J.Y. Kim, H.J. Chang, Y.S. Na, *J. Alloys Compd.*, 728 (2017) 1235.

[146] M.A. Melia, J.D. Carroll, S.R. Whetten, S.N. Esmaeely, J. Locke, E. White, I. Anderson, M. Chandross, J.R. Michael, N. Argibay, E.J. Schindelholz, A.B. Kustas, Mechanical and Corrosion Properties of Additively Manufactured CoCrFeMnNi High Entropy Alloy, *Additive Manufacturing*, (2019).

[147] K. Kuwabara, H. Shiratori, T. Fujieda, K. Yamanaka, Y. Koizumi, A. Chiba, *Addit. Manuf.*, 23 (2018) 264.

[148] Y. Fan, Y. Zhang, H. Guan, H. Suo, L. He, *Rare Metal Materials and Engineering*, 42 (2013) 1127.

[149] V. Shivam, J. Basu, V.K. Pandey, Y. Shadangi, and N.K. Mukhopadhyay, *Advanced Powder Technology*, 29 (2018) 2221.

[150] Z. Fu, W. Chen, H. Wen, Z. Chen, E.J. Lavernia, *J. Alloys Compd.*, 646 (2015) 175.

[151] C. Sun, P. Li, S. Xi, Y. Zhou, S. Li, X. Yang, *Materials Science and Engineering: A*, 728 (2018) 144.

[152] Z. Fu, W. Chen, H. Wen, D. Zhang, Z. Chen, B. Zheng, Y. Zhou, E.J. Lavernia, *Acta Mater.*, 107 (2016) 59.

[153] Z. Tang, O.N. Senkov, C.M. Parish, C. Zhang, F. Zhang, L.J. Santodonato, G. Wang, G. Zhao, F. Yang, P.K. Liaw, *Materials Science and Engineering: A*, 647 (2015) 229.

[154] S. Mohanty, N.P. Gurao, P. Padaikathan, K. Biswas, *Mater. Charact.*, 129 (2017) 127.

[155] A. Emamifar, B. Sadeghi, P. Cavaliere, H. Ziaei, *Powder Metall.*, 62, 61 (2019).

[156] N. Eißmann, B. Klöden, T. Weißgärber, B. Kieback, *Powder Metall.*, 60, 184 (2017).

[157] A.I. Yurkova, V.V. Cherniavsky, V. Bolbut, M. Krüger, I. Bogomol, *J. Alloys Compd.*, 786 (2019) 139.

[158] P. Agrawal, R.S. Haridas, P. Agrawal, R.S. Mishra, *Addit. Manuf.*, 60 (2022) 103282.

[159] L. Hou, J. Hui, Y. Yao, J. Chen, J. Liu, *Vacuum*, 164 (2019) 212.

[160] S. Singh, N. Wanderka, B.S. Murty, U. Glatzel, J. Banhart, *Acta Mater.*, 59 (2011) 182.

[161] Y. Liu, Y. Zhang, H. Zhang, N. Wang, X. Chen, H. Zhang, Y. Li, *J. Alloys Compd.*, 694 (2017) 869.

[162] D.G. Kim, Y.H. Jo, J.M. Park, W.M. Choi, H.S. Kim, B.J. Lee, S.S. Sohn, S. Lee, *J. Alloys Compd.*, 812 (2020) 152111.

[163] É. Fazakas, J.Q. Wang, V. Zadorozhnyy, D.V. Louzguine-Luzgin, L.K. Varga, *Materials and Corrosion*, 65 (2014) 691.
[164] Y. Du, Y. Lu, T. Wang, T. Li, G. Zhang, *Procedia Eng.*, 27 (2012) 1129.
[165] Z. Yao, "Comparison of structures and properties of arc-melted and induction-melted high entropy alloys." Master's thesis, (2016).
[166] S. qin Xia, Z. Wang, T. fei Yang, Y. Zhang, *Journal of Iron and Steel Research*, International 22 (2015) 879.
[167] S.Q. Xia, X. Yang, T.F. Yang, S. Liu, Y. Zhang, *JOM*, 67 (2015) 2340.
[168] S. Shen, F. Chen, X. Tang, J. Lin, G. Ge, J. Liu, *Journal of Nuclear Materials*, 540 (2020) 152380.
[169] S. Xia, M.C. Gao, T. Yang, P.K. Liaw, Y. Zhang, *Journal of Nuclear Materials*, 480 (2016) 100.
[170] H. Zheng, R. Chen, G. Qin, X. Li, Y. Su, H. Ding, J. Guo, H. Fu, *J. Alloys Compd.*, 787 (2019) 1023.
[171] H. Zheng, R. Chen, G. Qin, X. Li, Y. Su, H. Ding, J. Guo, H. Fu, *J. Mater. Sci. Technol.*, 38 (2020) 19.
[172] S.T. Mileiko, S.A. Firstov, N.A. Novokhatskaya, V.F. Gorban, N.P. Krapivka, *Compos. Part A Appl. Sci. Manuf.*, 76 (2015) 131.
[173] Y. Yu, F. He, Z. Qiao, Z. Wang, W. Liu, J. Yang, *J. Alloys Compd.*, 775 (2019) 1376.
[174] F. He, Z. Wang, P. Cheng, Q. Wang, J. Li, Y. Dang, J. Wang, C.T. Liu, *J. Alloys Compd.*, 656 (2016) 284.
[175] S. Deepak Kumar, J. Ghose, A. Mandal, *Sustainable Engineering Products and Manufacturing Technologies*, 25 (2019).
[176] G.T. Gray, V. Livescu, P.A. Rigg, C.P. Trujillo, C.M. Cady, S.R. Chen, J.S. Carpenter, T.J. Lienert, S.J. Fensin, *Acta Mater.*, 138 (2017) 140.
[177] M.S.K.K.Y. Nartu, S. Dasari, A. Sharma, S.A. Mantri, S. Sharma, M.V. Pantawane, B. McWilliams, K. Cho, N.B. Dahotre, R. Banerjee, *Materials Science and Engineering: A*, 821 (2021) 141627.
[178] P. Wang, P. Huang, F.L. Ng, W.J. Sin, S. Lu, M.L.S. Nai, Z.L. Dong, J. Wei, *Mater. Des.*, 168 (2019) 107576.
[179] V.V. Popov, A. Katz-Demyanetz, A. Koptyug, M. Bamberger, *Heliyon*, 5 (2019) e01188.
[180] K. Kuwabara, H. Shiratori, T. Fujieda, K. Yamanaka, Y. Koizumi, A. Chiba, *Addit. Manuf.*, 23 (2018) 264.
[181] T. Fujieda, H. Shiratori, K. Kuwabara, M. Hirota, T. Kato, K. Yamanaka, Y. Koizumi, A. Chiba, S. Watanabe, *Mater. Lett.*, 189 (2017) 148.
[182] R. Li, P. Niu, T. Yuan, P. Cao, C. Chen, K. Zhou, *J. Alloys Compd.*, 746 (2018) 125.
[183] D. Lin, L. Xu, H. Jing, Y. Han, L. Zhao, F. Minami, *Addit. Manuf.*, 32 (2020) 101058.
[184] S. Luo, P. Gao, H. Yu, J. Yang, Z. Wang, X. Zeng, *J. Alloys Compd.* 771 (2019) 387.
[185] M.S.K.K.Y. Nartu, A. Chesetti, S. Dasari, A. Sharma, S.A. Mantri, N.B. Dahotre, R. Banerjee, *Materials Science and Engineering A*, 849 (2022).
[186] M.S.K.K.Y. Nartu, S. Jha, A. Chesetti, S. Mukherjee, I. Van Rooyen, R. Banerjee, *JOM*, (2023).
[187] V. Kumar, A. Gupta, D. Lahiri, K. Balani, *J. Phys. D Appl. Phys.*, 46 (2013).
[188] C.A. Schuh, *Materials Today*, 9 (2006) 32.
[189] J. Il Jang, M.J. Lance, S. Wen, T.Y. Tsui, G.M. Pharr, *Acta Mater.*, 53 (2005) 1759.
[190] S. Banerjee, U.M. Naik, *Acta Mater.*, 44 (1996) 3667.
[191] D. Choudhuri, S.A. Mantri, T. Alam, S. Banerjee, R. Banerjee, *Scr. Mater.*, 124 (2016) 15.
[192] C. Downey, "Development of Advanced Coating Technologies Using Powder-Blown Directed Energy Deposition (DED) Additive Manufacturing for Advanced Nuclear Reactor Applications," Master's Thesis, University of Idaho, 2023.
[193] C. Downey, L. Nunez, J. Toman, M. Abdo, I.J. van Rooyen, TMS 2023 Conference Presentation, (2023).
[194] C. Downey, I.J. Van Rooyen, L. Nunez, US Patent App. 18/069,023, 2023.